Inclusive Lepton Analysis

In the previous chapter, we introduced the methods by which leptons are identified in the Mark II detector. We now turn our attention to understanding the observed lepton sample. From the discussion in Chapter 1, we expect most of the high momentum leptons to be products of heavy quark decay. We therefore describe the lepton signal in terms of its various contributions from semi-leptonic charm and bottom quark decay. The total number of leptons gives us the branching ratios for these decays averaged over the various types of charm and bottom hadrons produced at 29 GeV/c. From the lepton momentum spectrum, we infer the average hadron energy ($< z >$ of the fragmentation function). Finally, the lepton transverse momentum spectrum allows us to separate bottom and charm decays.

In addition to the leptons from charm and bottom hadron decay, we must account for a lesser contribution to the signal from background sources: non-prompt leptons and mis-identified hadrons. The amount of background is determined using the results of the previous chapter; we will find that more than 80 % of leptons above momenta of 2 GeV/c come from heavy quark decay.

The analysis procedure is quite similar to that of a previous study of inclusive leptons using one-seventh of the data [94]. The observed lepton signal is tabulated along with the expected contributions from background sources. The parameterization of the inclusive lepton fit is introduced; the Monte Carlo (p, p_t) distributions are derived along with the assumed fragmentation function parameters. The results from the fit to the data in 63 bins of (p, p_t) are presented.

The fractions of bottom, charm and background in various (p, p_t) regions are then calculated. In the final section, the inclusive lepton results obtained are compared with other measurements.

6.1 Hadronic Event Selection

The total data sample corresponds to an integrated luminosity of 195 ± 9 pb^{-1}. Hadronic events typically have larger charged particle multiplicities and larger amounts of visible energy than do non-hadronic events (such as $e^+e^- \rightarrow e^+e^-, \mu^+\mu^-, \tau^+\tau^-$, and two-photon events). With this fact in mind, the following cuts are used to select hadronic events:

Hadronic Event Cuts

1. There must be at least six charged tracks. At least five of these tracks must be fully contained in the DC (i.e. cannot go through an endcap), have momenta between 150 MeV/c and 16 GeV/c and lie within 2 cm in r and 5 cm in z of the average beam position. Each track must have at least 2 VC hits and cannot come from an identified e^+e^- pair.
2. The event vertex must lie within 4 cm in r and 10 cm in z of the DC origin.
3. The energy sum of all charged tracks must be greater than 7.25 GeV.

A total of 77,591 events pass hadronic event cuts. In these events, the thrust axis is determined from charged tracks (including any leptons). Each track used in the calculation of thrust must satisfy a number of additional cuts. (For brevity, these cuts are not given here, they may be found in Ref. 95.) In each event, there must be at least four tracks used in the calculation of thrust. In order to ensure that events are well contained in the detector, the component of the thrust axis parallel to the beam direction must be less than 0.7. After applying the above cuts, there are 65,459 events remaining. There is a background of approximately 2 % in the hadronic event sample from tau pair and two-photon events.

6.2 Lepton Selection

Lepton candidates are identified in these hadronic events by the methods outlined in Chapter 5. Each candidate is required to pass the following cuts:

Lepton Selection Cuts

1. The distance of closest approach from the track to the average beam position must be less than 5 cm in the direction along the beam line , and less than 5 mm in the direction transverse to the beam.
2. The track must not be from an identified e^+e^- pair.
3. The track momentum must be greater than 2 GeV/c and less than 16 GeV/c.
4. The track must have at least 2 hits in the VC and at least 11 total hits in the VC and DC.
5. The track fit must have a χ^2 per DOF value less than 10.

The cut on the distance of closest approach eliminates those tracks unlikely to have been produced near the interaction point. Since the average impact parameter for leptons from B decay is $\sim$ 145 μm , this cut has negligible effect on the impact parameter distribution. The second and fourth cuts are designed to remove non-prompt electrons from photon conversions. Note that the track cuts introduced here serve a different purpose than those given in Section 4.6. The cuts here are designed to ensure reasonable lepton tracks, while the latter cuts will be used in Chapter 7 to define quality tracks for the lifetime measurement.

There are two major sources of non-hadronic background in the event sample. These backgrounds are discussed in detail in Appendix A. One source comes from τ pair production and the other one comes from the two-photon process $e^+e^- \rightarrow e^+e^-+$ Hadrons. Events from the latter source enter the event sample when the two-photon system hadronizes and one of the beam electrons scatters into the detector. These events satisfy hadronic cuts because the scattered electron is usually quite energetic and there are often five or more charged tracks in the hadronic shower. Although

the overall two-photon cross section is very large, the process in which a beam electron is scattered by a large angle into the central detector is greatly suppressed. Even so, the background from this process is sufficiently large to warrant a complete study. Special cuts are introduced to remove most of the two-photon background; these cuts rely on the fact that electrons in these events are typically quite isolated and very energetic. As detailed in Appendix A, after all cuts, the sources of non-hadronic background provide less than 2 % contamination in the electron and muon signals.

6.3 Prompt Lepton Signal

6.3.1 Raw signal

After the cuts discussed in the previous section, there are 2621 electron and 1230 muon candidates. For each candidate the transverse momentum relative to the thrust axis is calculated. The raw lepton signal, divided into (p, p_t) bins, is shown in Table 6.1 and Table 6.2. The distribution of all the candidate leptons in (p, p_t) is shown in Figure 6.1.

Table 6.1: Raw electron signal.

$p \backslash p_t$	0.00	0.25	0.50	0.75	1.00	1.25	1.50
2.0	152.	246.	134.	86.	37.	24.	20.
2.5	73.	178.	105.	52.	36.	31.	24.
3.0	61.	123.	89.	46.	44.	16.	30.
3.5	33.	72.	45.	44.	20.	14.	16.
4.0	34.	48.	51.	26.	29.	10.	24.
4.5	11.	34.	38.	24.	12.	18.	16.
5.0	9.	19.	24.	17.	8.	11.	10.
5.5	12.	22.	24.	14.	9.	10.	10.
6.0	15.	46.	30.	22.	29.	23.	33.

6.3.2 Expected background to the electron signal

The dominant background to the prompt electron signal comes from mis-identified hadrons. A smaller contribution comes from electrons from photon

Table 6.2: Raw muon signal.

$p\backslash p_t$	0.00	0.25	0.50	0.75	1.00	1.25	1.50
2.0	40.	82.	69.	32.	19.	18.	12.
2.5	29.	64.	53.	25.	19.	11.	16.
3.0	26.	51.	40.	28.	17.	12.	16.
3.5	15.	39.	26.	18.	15.	12.	14.
4.0	11.	26.	12.	17.	9.	13.	11.
4.5	9.	20.	22.	7.	9.	5.	15.
5.0	6.	11.	11.	10.	5.	2.	4.
5.5	8.	8.	18.	9.	3.	5.	4.
6.0	5.	21.	25.	28.	14.	15.	14.

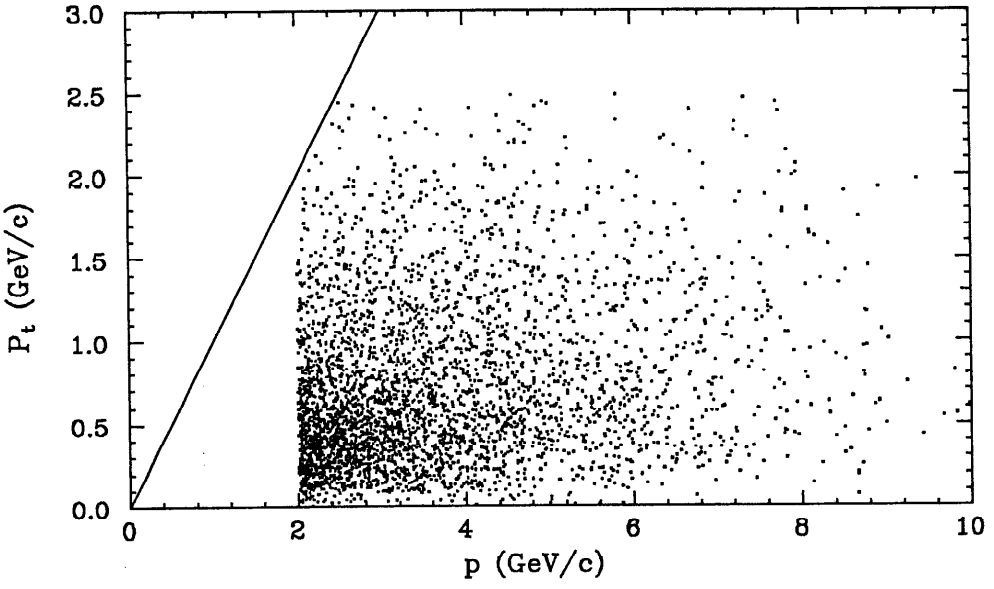

Figure 6.1: Lepton (p,p_t) distribution. This scatterplot shows the lepton candidates distributed in p and p_t. The solid line indicates the kinematic limit.

conversions and Dalitz decays that are not removed by the pair-finder or by the requirement of two VC hits. The expected background to the electron signal from this source is given in Table 5.4. The expected background from mis-identified hadrons is calculated by multiplying the number of hadronic (non-electron) tracks found in the data by the mis-identification probabilities given in Table 5.3. The

hadronic tracks are required to pass all the electron selection cuts, except that they must have $E_{min}/p < 1.1$.* The resulting background expected in the electron signal from mis-identified hadrons is shown in Table 6.3.

Table 6.3: Expected electron background from mis-identified hadrons.

$p \backslash p_t$	0.00	0.25	0.50	0.75	1.00	1.25	1.50
2.0	72.3	138.2	48.1	23.9	11.1	6.2	7.8
2.5	37.8	73.3	33.9	18.5	8.2	4.6	6.1
3.0	22.3	40.6	17.8	10.1	4.4	2.5	3.7
3.5	11.6	23.9	12.6	7.5	3.4	1.9	2.7
4.0	6.9	14.2	7.8	4.9	2.3	1.2	1.8
4.5	4.4	8.8	5.8	4.1	1.6	0.9	1.4
5.0	2.9	6.5	4.3	2.9	1.2	0.7	1.2
5.5	2.1	4.6	3.2	2.3	1.0	0.6	0.9
6.0	4.4	9.7	6.8	5.0	2.4	1.5	2.1

6.3.3 Expected background to the muon signal

The background to the prompt muon signal arises approximately equally from two sources: hadronic tracks that punchthrough and muons from the decays in flight of pions and kaons.

The expected contribution from hadronic punchthrough is shown in Table 6.4. It is calculated by multiplying the number of hadronic tracks in the muon fiducial volume by the punchthrough probabilities given in Table 5.6. In this calculation it is assumed that all hadrons punchthrough with the same probability (including protons).

The background to the muon signal from pion and kaon decays is shown in Table 6.5. This background is computed in the same fashion as that from punchthrough, using the probabilities for a pion or kaon to decay to a reconstructed muon (given in Table 5.7). In addition, it is assumed that 70 % of the hadronic tracks are pions, 20 % are kaons, and 10 % are protons. These percentages are consistent with recent measurements [100].

* A slight correction is needed since some hadrons have $E_{min}/p > 1.1$ and are not included in the hadron track sample. Conversely, there are some electrons with $E_{min}/p < 1.1$ that are included. These effects are negligible, given the errors in the mis-identification probabilities.

Table 6.4: Expected muon background from punchthrough.

$p \backslash p_t$	0.00	0.25	0.50	0.75	1.00	1.25	1.50
2.0	7.8	15.2	10.9	5.5	2.3	1.2	1.5
2.5	5.1	10.2	7.9	4.3	1.9	1.1	1.3
3.0	3.6	7.0	5.9	3.2	1.4	0.8	1.2
3.5	2.4	5.2	4.3	2.5	1.2	0.6	0.9
4.0	1.7	3.7	3.2	2.0	1.1	0.6	0.8
4.5	1.4	2.7	2.5	1.7	0.8	0.5	0.7
5.0	0.9	2.0	2.0	1.3	0.7	0.4	0.6
5.5	0.8	1.5	1.6	1.1	0.6	0.4	0.5
6.0	2.0	4.5	4.8	3.5	2.2	1.3	1.9

Table 6.5: Expected muon background from decays.

$p \backslash p_t$	0.00	0.25	0.50	0.75	1.00	1.25	1.50
2.0	9.0	17.6	12.7	6.3	3.3	1.7	2.3
2.5	6.5	13.2	10.1	5.5	2.8	1.6	2.0
3.0	4.6	8.8	7.5	4.1	2.1	1.1	1.7
3.5	2.8	5.9	4.8	2.9	1.6	0.8	1.2
4.0	1.8	3.8	3.3	2.1	1.3	0.7	0.9
4.5	1.3	2.6	2.4	1.6	0.9	0.5	0.8
5.0	0.7	1.7	1.7	1.1	0.6	0.4	0.6
5.5	0.5	1.1	1.2	0.8	0.4	0.3	0.4
6.0	1.0	2.2	2.3	1.7	1.1	0.6	1.0

Since the probabilities for pion or kaon decay to a reconstructed muon are not very different, the assumption made on the relative percentage of pions and kaons in the data does not introduce a significant systematic error.

6.4 Description of the Lepton (p, p_t) Fit

6.4.1 Parameterization for the number of predicted leptons

Making the assumption that the hadronic event sample contains only events from single-photon quark pair production ($e^+e^- \to q\bar{q}$), the possible sources of lepton candidates are:

1. Background from mis-identified hadrons (electrons: hadron mis-identification in the calorimeter; muons: hadron punchthrough).
2. Background from non-prompt leptons (electrons: remaining photon conversions and Dalitz decays; muons: pion and kaon decays in flight).
3. Prompt leptons from charm decay in $c\bar{c}$ events: **C primary.**
4. Prompt leptons from bottom decay in $b\bar{b}$ events: **B primary.**
5. Prompt leptons from charm decay in $b\bar{b}$ events: **B secondary.**

Using the assumptions made above, the predicted number of events in a particular (p, p_t) bin can be written:

$$\begin{aligned} N_{pre}(p,p_t) \;=\; & f_m \cdot N_{misid}(p,p_t) \;+\; f_d \cdot N_{decay}(p,p_t) \;+ \\ & \epsilon_{tq} \cdot \epsilon_{fd} \cdot \epsilon_{id} \cdot \Big[\, 2\, N_{c\bar{c}}\, \mathrm{BR}(c \to l) \cdot P_{cpri}(<z_c>, p, p_t) \;+ \\ & \qquad 2\, N_{b\bar{b}}\, \mathrm{BR}(b \to l) \cdot P_{bpri}(<z_b>, p, p_t) \;+ \\ & \qquad 2\, N_{b\bar{b}}\, \mathrm{BR}(c \to l) \cdot P_{bsec}(<z_b>, p, p_t) \;\Big] \end{aligned} \tag{6.1}$$

The above expression is written for electrons and muons separately, with the following definitions of the various terms:

The following items are inputs to the fit:

$N_{misid}(p, p_t)$ = The expected number of mis-identified hadrons in each (p, p_t) bin.

$N_{decay}(p, p_t)$ = The expected number of non-prompt leptons from decays in each (p, p_t) bin.

ϵ_{tq} = The track efficiency to pass the lepton selection cuts.

ϵ_{fd} = The fiducial acceptance for lepton tracks.

ϵ_{id} = The efficiency for lepton identification.

$N_{c\bar{c}}, N_{b\bar{b}}$ = The numbers of $c\bar{c}$, $b\bar{b}$ events.

$P_{cpri}(<z_c>, p, p_t)$ = The probability that a C hadron with a given $<z_c>$ will produce a lepton in a given (p, p_t) bin. Similarly for P_{bpri} and P_{bsec}.

The following items are outputs of the fit:

f_m, f_d = Scale factors for the mis-identification and decay backgrounds. These factors allow the background normalization to float.

BR($c \rightarrow l$) = Average charm semi-leptonic branching ratio.

BR($b \rightarrow l$) = Average bottom semi-leptonic branching ratio.

6.4.2 *The variables used in the parameterization*

The expected background contributions N_{misid} and N_{decay} are tabulated in the previous section. The track quality efficiency ϵ_{tq} is found to be 0.78 in the data and 0.81 in the Monte Carlo. The fiducial acceptance for lepton tracks is calculated with the Monte Carlo. This acceptance varies slightly with momentum and is given for electrons and muons in Table 6.6. The acceptance values given in this table are slightly larger than the simple geometric acceptance due to the effects of the hadronic event selection. The lepton identification efficiencies are given in Table 5.2 and Table 5.5.

The numbers of $c\bar{c}$ and $b\bar{b}$ events are determined as follows. Assuming that quark pairs are produced in the process $e^+e^- \rightarrow q\bar{q}$ in proportion to the quark charge squared, then 4/11 of the hadronic events are charm and 1/11 are bottom quark events. In practice, the efficiency for events to pass hadronic event cuts depends slightly on the quark type produced. The Monte Carlo is used to determine these slight variations. Of the events that pass hadronic and jet analysis cuts, it is found that 37.3 % are charm and 9.9 % are bottom. In the total of 65,459 events, these percentages lead to $N_{c\bar{c}} = 23{,}928$ and $N_{b\bar{b}} = 6{,}351$, where we have accounted for a background from non-hadronic events of 2 %.

There are five parameters that are determined by the fit. The first two parameters are the background scale factors f_m and f_d. These factors allow the overall background level to float. There is significant information in the lepton (p, p_t) distributions that can help determine this level.

Table 6.6: Electron and muon fiducial acceptance.

	Acceptance	
P (GeV/c)	Electron	Muon
2.0	0.72	0.43
2.5	0.73	0.44
3.0	0.74	0.44
3.5	0.75	0.45
4.0	0.76	0.45
4.5	0.77	0.46
5.0	0.78	0.47
5.5	0.79	0.48
6.0	0.80	0.49

The next two parameters that are determined by the fit are the branching ratios $\mathrm{BR}(c \to l)$ and $\mathrm{BR}(b \to l)$. These numbers are the average of the semi-leptonic branching ratios for the various charm hadrons (D^0, D^+, D_s^+, etc.) and bottom hadrons (B^0, B^+, B_s^0, etc.), weighted by their relative production cross sections.

The final parameter determined is $< z >$ of the fragmentation function. This parameter is determined by generating Monte Carlo (p, p_t) probability distributions at different values of $< z >$ via the Peterson formula, and then interpolating to determine which value best fits the data.

6.4.3 The Monte Carlo (p, p_t) probability distributions

The probability distributions P_{cpri}, P_{bpri}, and P_{bsec} vary as a function of (p, p_t) and also as a function of the fragmentation parameter $< z >$. These distributions are calculated by means of the Monte Carlo in the following manner. A large number of Monte Carlo events is used for the three different prompt sources: primary charm, primary bottom and secondary bottom. For events which pass hadronic and jet analysis cuts, leptons are identified and their origin $(c_{pri}, b_{pri}, b_{sec})$ determined from the Monte Carlo produced quantities. The number of prompt leptons in each (p, p_t) bin is tabulated along with the total number of charm and bottom semi-leptonic decays. Following Eqn. 6.1, and using primary bottom decays

as an example, the number of detected leptons can be written as:

$$N_{det}(p, p_t) = \epsilon_{tq} \cdot \epsilon_{fd} \cdot \epsilon_{id} \cdot \left[2\, N_{b\bar{b}}\, \mathrm{BR}(b \rightarrow l) \cdot P_{bpri}(< z_b >, p, p_t) \right] . \quad (6.2)$$

In Eqn. 6.2, the Monte Carlo values of $\epsilon_{tq}, \epsilon_{fd}$ and ϵ_{id} are used. The quantity $2\, N_{b\bar{b}}\, \mathrm{BR}(b \rightarrow l)$ is simply the number of primary bottom lepton decays. It is easy to invert Eqn. 6.2, solving for the quantity $P_{bpri}(< z_b >, p, p_t)$. This quantity is the probability that a lepton from the decay of a charm hadron with a given $< z_b >$ will end up in a given (p, p_t) bin. The probability (p, p_t) distributions for various values of $< z >$ are computed in this manner for the three separate sources of prompt leptons. The distributions are slightly different for electrons and muons due to the additional two-photon cuts placed on the electrons. The (p, p_t) distributions are then used as inputs to the fit in order to determine the value of $< z >$ in the data. For brevity, these distributions are not given here.

Events are generated in the primary bottom sample with a range of $< z_b >$ values, as given in Table 6.7. The range used is motivated largely by previous experimental results, as discussed in Chapter 1. The number of Monte Carlo events used at each of the values of $< z_b >$ corresponds to ten times the statistics of the data. The secondary bottom events are generated at a single value of $\epsilon_b = 0.011$.

Table 6.7: Bottom fragmentation function parameter values.

ϵ_b	$< z_b >$
0.150	0.59
0.040	0.70
0.011	0.79
0.004	0.85
0.001	0.90
0.0001	0.96

The $< z_c >$ of charm fragmentation is well determined from exclusive D^* measurements. Therefore, in this analysis, the events in the primary charm sample are generated at a fixed value $< z_c > = 0.68$, corresponding to a value $\epsilon_c = 0.050$.

The number of Monte Carlo $c\bar{c}$ events generated corresponds to six times the statistics of the data.

6.4.4 *The full fit*

The full fit to the inclusive lepton spectra is done using a binned maximum likelihood fit. Representing the number of predicted leptons in the (p, p_t) bin i by the variable x_i, and the number of observed leptons in that bin by n_i, the probability density function can be written for each lepton type separately as:

$$F_i = \frac{x_i{}^{n_i}\, e^{-x_i}}{n_i!} \cdot \frac{e^{-(fm-1.0)^2/2\sigma_m^2}}{\sqrt{2\pi}\,\sigma_m} \cdot \frac{e^{-(f_d-1.0)^2/2\sigma_d^2}}{\sqrt{2\pi}\,\sigma_d} \quad . \tag{6.3}$$

The first term on the right hand side corresponds to the Poisson probability of observing n_i events when x_i events were predicted. The second term represents the probability that the observed mis-identification background scale factor (f_m) agrees with the scale factor expected (1.0), assuming a Gaussian distribution of width given by σ_m. The third term represents the similar probability for the decay background scale, with a width given by σ_d. In this analysis, the values $\sigma_m = 0.40$ and $\sigma_d = 0.20$ were used, in agreement with the expected systematic errors made in the background estimation.

The probability density function, F_i depends on the five parameters used in the fit implicitly through the number of predicted leptons and, in the case of f_m and f_d, explicitly as well. The likelihood function, $\mathcal{L}$, is written as:

$$\mathcal{L}\,(\alpha_j) = \prod_i F_i(\alpha_j) \quad . \tag{6.4}$$

The variable i indicates the product over the 63 (p, p_t) bins and j indicates the five parameters used ($\alpha_j \equiv \mathrm{BR}(c \to l)$, $\mathrm{BR}(b \to l)$, $< z_b >$, f_m, and f_d).

For computational ease, $\log\,(\mathcal{L})$ is maximized with respect to the parameters rather than the likelihood itself. The constraint equation is:

$$\frac{\partial}{\partial \alpha_j}\Big(\log(\mathcal{L})\Big) = \frac{\partial}{\partial \alpha_j}\Big(\sum_i F_i(\alpha_j)\Big) = 0 \quad . \tag{6.5}$$

The computer program MINUIT is used to solve Eqn. 6.5 [101].

6.5 Inclusive Lepton Results and Discussion

The results of the maximum likelihood fits to the electron and muon (p, p_t) distributions are presented in Table 6.8. The first error for each value is statistical and the second is systematic. A discussion of the sources of systematic error follows.

Table 6.8: Results from the inclusive lepton fits.

Quantity	Electron	Muon
BR($c \to l$)	$9.6 \pm 0.7 \pm 1.5$ (%)	$7.8 \pm 0.9 \pm 1.2$ (%)
BR($b \to l$)	$11.2 \pm 0.9 \pm 1.1$ (%)	$11.8 \pm 1.2 \pm 1.0$ (%)
$< z_b >$	$0.85 \pm 0.03 \pm 0.05$	$0.82 \pm 0.04 \pm 0.05$
ϵ_b	$0.0038\ ^{+0.0031\ +0.0059}_{-0.0019\ -0.0027}$	$0.0069\ ^{+0.0067\ +0.0089}_{-0.0038\ -0.0045}$
f_m	$0.87 \pm 0.15 \pm 0.14$	$1.01 \pm 0.19 \pm 0.15$
f_d	$0.83 \pm 0.32 \pm 0.18$	$1.04 \pm 0.18 \pm 0.14$

The values for f_m and f_d determined from the fit lie within one standard deviation of 1.0 for both electrons and muons. This fact indicates that the estimated background level to the prompt lepton signal is approximately correct. The muon background seems to be very well described by the assumed punchthrough and decay probabilities. The amount of electron background is slightly overestimated; the fit prefers more charm in the electron sample than in the muon sample. The correlation coefficients for the electron and muon fits are presented in Table 6.9 and Table 6.10, respectively.

6.5.1 *Systematic errors*

There are a number of things that contribute to the systematic errors on the results presented above. Here we itemize the most important contributions.

Table 6.9: Electron fit correlation coefficients.

	BR($c \to l$)	BR($b \to l$)	$< z_b >$	f_m	f_d
BR($c \to l$)	1.0				
BR($b \to l$)	-0.372	1.0			
$< z_b >$	-0.001	-0.466	1.0		
f_m	-0.773	0.138	0.085	1.0	
f_d	-0.077	0.025	-0.060	-0.388	1.0

Table 6.10: Muon fit correlation coefficients.

	BR($c \to l$)	BR($b \to l$)	$< z_b >$	f_m	f_d
BR($c \to l$)	1.0				
BR($b \to l$)	-0.149	1.0			
$< z_b >$	0.024	-0.398	1.0		
f_m	-0.511	-0.088	-0.111	1.0	
f_d	-0.590	-0.128	0.109	-0.068	1.0

1. **Background:**

   The fitted values of f_m and f_d provide confidence in the estimation of the amount of background. The errors on the fitted values of f_m and f_d are in general lower than the errors assumed, indicating that the fit provides information in setting this scale.* Still, the quantities of physics interest in this analysis (BR($c \to l$) , BR($b \to l$) and $< z_b >$) depend on the estimated amount of background. For that reason, the fits are redone allowing the background levels to vary in scale and in shape within the measured statistical and systematic errors on f_m and f_d. From these fits, the systematic errors on BR($c \to l$) , BR($b \to l$) and $< z_b >$ due to uncertainty in the background

* The estimated background could have an error in the (p, p_t) dependence not reflected in the overall scale. The systematic errors on f_m and f_d represent an estimate of the uncertainty in the shape of the background.

are determined.

2. **Charm Fragmentation:**

   The $< z_c >$ of the charm fragmentation function is chosen from the world average and allowed to vary within the range of 0.68 ± 0.06. This range accounts for the finite precision of the D^* measurements, the possible inclusion of charm hadrons with different fragmentation than the D^* and the use of a different parameterization for the charm fragmentation function than the Peterson form.

3. **Secondary Bottom Decay:**

   The (p, p_t) probability distributions are calculated at only one value of $< z_b >$. The systematic effect of this assumption is estimated by using different $< z_b >$ values for the secondary bottom decay.

4. **Non-Charm Decays of Bottom:**

   The lepton fit is performed assuming that B hadrons decay 100 % of the time to charm species (actually slightly more than this because the B occasionally produces more than one charm quark). The systematic effect of this assumption is estimated by assuming only 0.90 charm quarks from each B decay.*

5. **Efficiencies:**

   The lepton identification efficiency, the fiducial acceptance and the fraction of leptons passing track quality cuts are quantities that have been measured in the data and found to agree with the Monte Carlo within 2-3 %. The systematic effect of incorrectly estimating these efficiencies is calculated assuming an overall error of 5 % in the product of the three quantities.

6. **Number of $c\bar{c}$ and $b\bar{b}$ events:**

   The numbers of $c\bar{c}$ and $b\bar{b}$ events are allowed to vary by ± 5 %. This variation accounts for uncertainty in the amount of non-hadronic events in the data. It also allows for possible differences in acceptance for $c\bar{c}$ and $b\bar{b}$ events from the values assumed, due to uncertainties in the multiplicity and momentum dependence of heavy quark decay.

---

* This correction ends up being small because the momentum spectrum for $(b \rightarrow u)$ transitions is similar to that for $(b \rightarrow c)$ transitions. To first order, the addition of non-charm decays has little effect on the (p, p_t) distributions; it only affects the relative contribution from secondary charm decays.

7. **Monte Carlo Assumptions:**
   A systematic error of 2 % is assigned to account for uncertainties in the rest-frame momentum and p_t distributions of leptons from heavy quarks. In addition, we do not include a term in the fit to account for leptons from $B \rightarrow \tau \rightarrow l$ decays. It is estimated that 3 % of the leptons could come from this source. A systematic uncertainty of this magnitude is included.

6.5.2 Checks on the fit

In order to check the analysis procedure, the same code and fit are applied to a sample of 100,000 hadronic Monte Carlo events. The values of $\mathrm{BR}(c \rightarrow l)$, $\mathrm{BR}(b \rightarrow l)$, $< z >$, f_m, and f_d found by the fit are in good agreement with the values used in the Monte Carlo generation.

To check the quality of the fits, the binned χ^2 is calculated using:

$$\chi^2 = \sum_i \frac{(\text{ Observed} - \text{Predicted })^2}{\text{Predicted}} \quad , \tag{6.6}$$

where the sum runs over the 63 (p, p_t) bins. The electron fit has a χ^2 value of 85.8 for 58 DOF, while the muon fit has a χ^2 value of 51.7 for 58 DOF. The bin by bin χ^2 values are given in Ref. 95. There are no significant concentrations of large χ^2 values in the (p, p_t) plane for either the electron or muon fits. This fact indicates that the fits are not systematically incorrect in an obvious manner.

6.5.3 Composition of the predicted signal

In the beginning of Section 6.4, the assumed contributions to the lepton signal are given. Using the results of the fit obtained, it is straightforward to compute the composition of the predicted signal in terms of these assumed contributions. The bin by bin compositions to the predicted signal are given in Ref. 95. In Figure 6.2, the momentum spectrum of the electron signal is shown for values of low ($p_t < 1.0$ GeV/c) and high ($p_t > 1.0$ GeV/c) transverse momentum.

Figure 6.3 illustrates the transverse momentum spectrum of the electron signal. In these figures, the observed lepton signal is represented by the points while the predicted signal is represented by the bar graphs. The muon momentum and transverse momentum spectra are shown in Figure 6.4 and Figure 6.5, respectively.

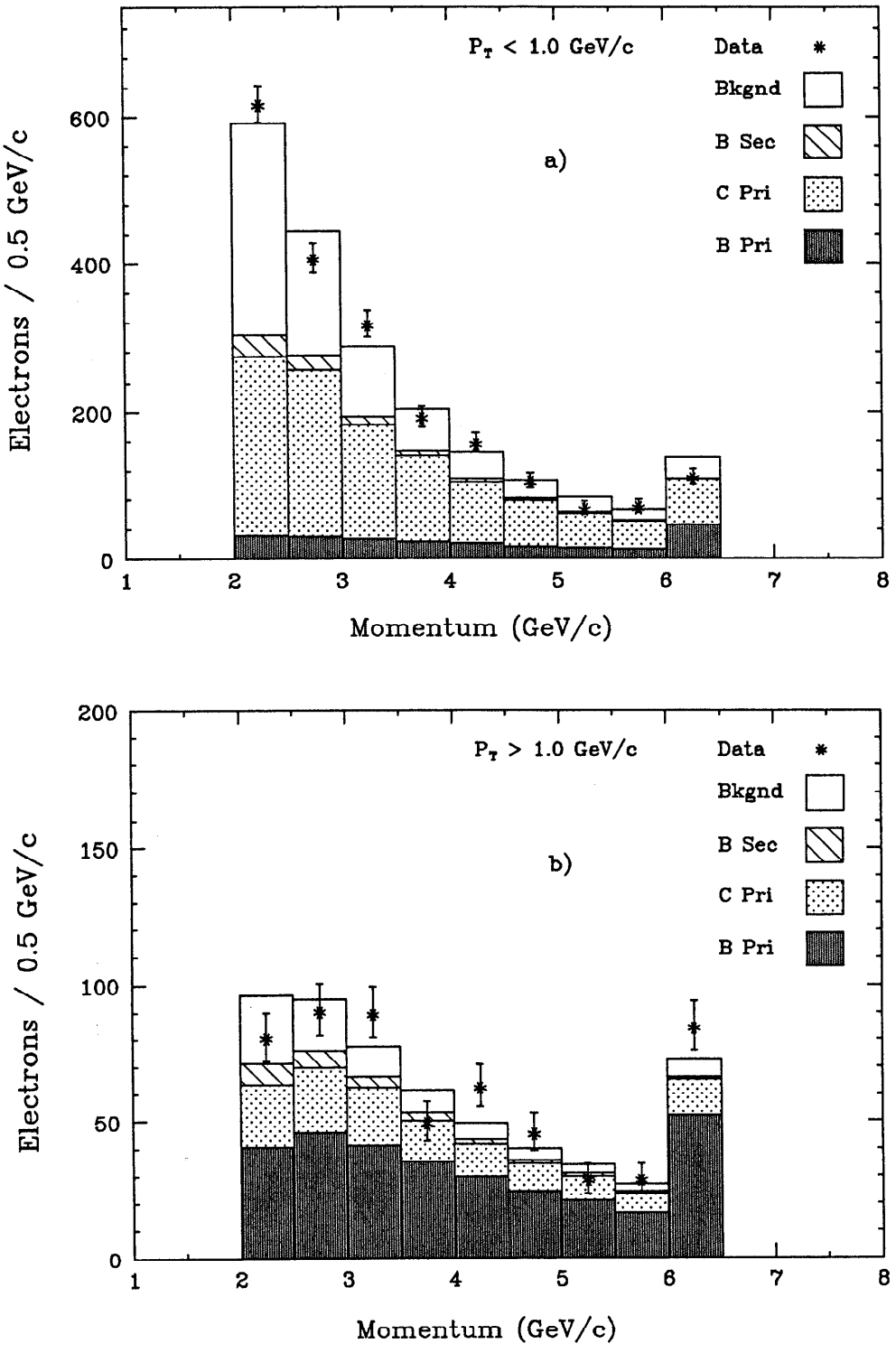

Figure 6.2: Electron momentum distributions. The momentum distribution for electrons is shown for a) low and b) high values of transverse momentum. The results of the fit are shown by the bargraphs, as discussed in the text.

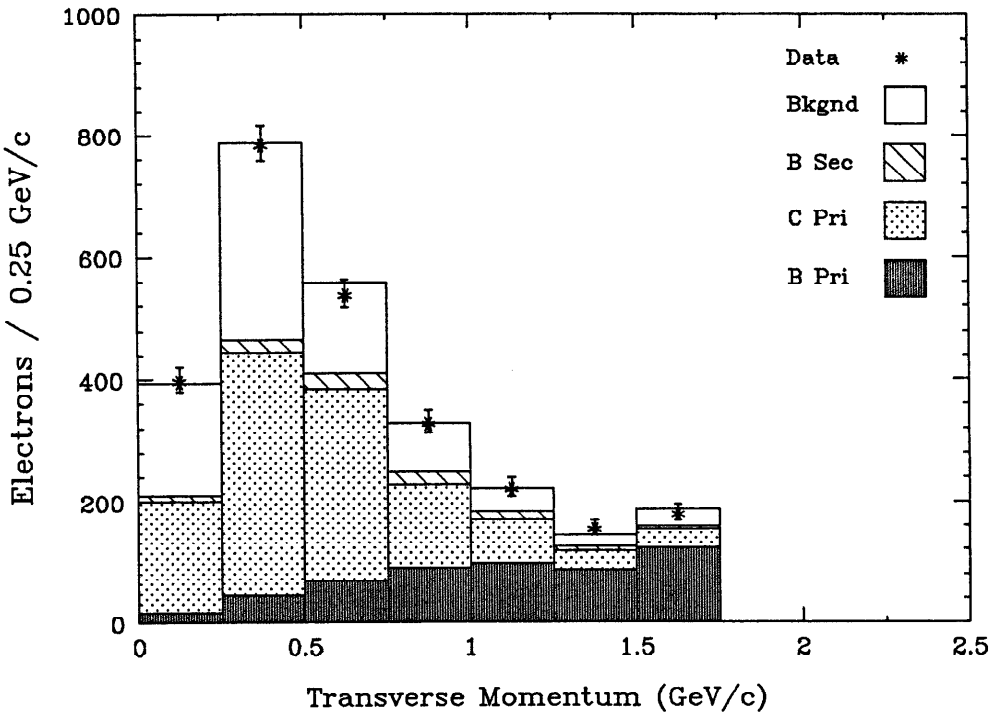

Figure 6.3: Electron transverse momentum distribution.

6.5.4 Selecting B and C enhanced regions

From the results of the fit, it is easy to see that background sources make up the largest contribution to the signal at low values of momentum and transverse momentum. In the region of momentum greater than 3 GeV/c and transverse momentum less than 1 GeV/c, the dominant species is primary charm. Primary bottom is the most important constituent of the signal for transverse momentum greater than 1 GeV/c.

Using these observations, it is straightforward to calculate the composition of the predicted lepton signal in two different kinematic regions, one enhanced by charm production and the other by bottom production. The decomposition of the lepton signal into C enhanced and B enhanced regions is given in Table 6.11. From the table, we see that approximately 60 % of the leptons in the B enhanced region come from primary or secondary B hadron decay and approximately 55 % of the leptons in the C enhanced region come from C hadron decay. The C enhanced region has a sizable background contamination; the B contamination is reduced in this region by requiring transverse momentum to be less than 0.75 GeV/c.

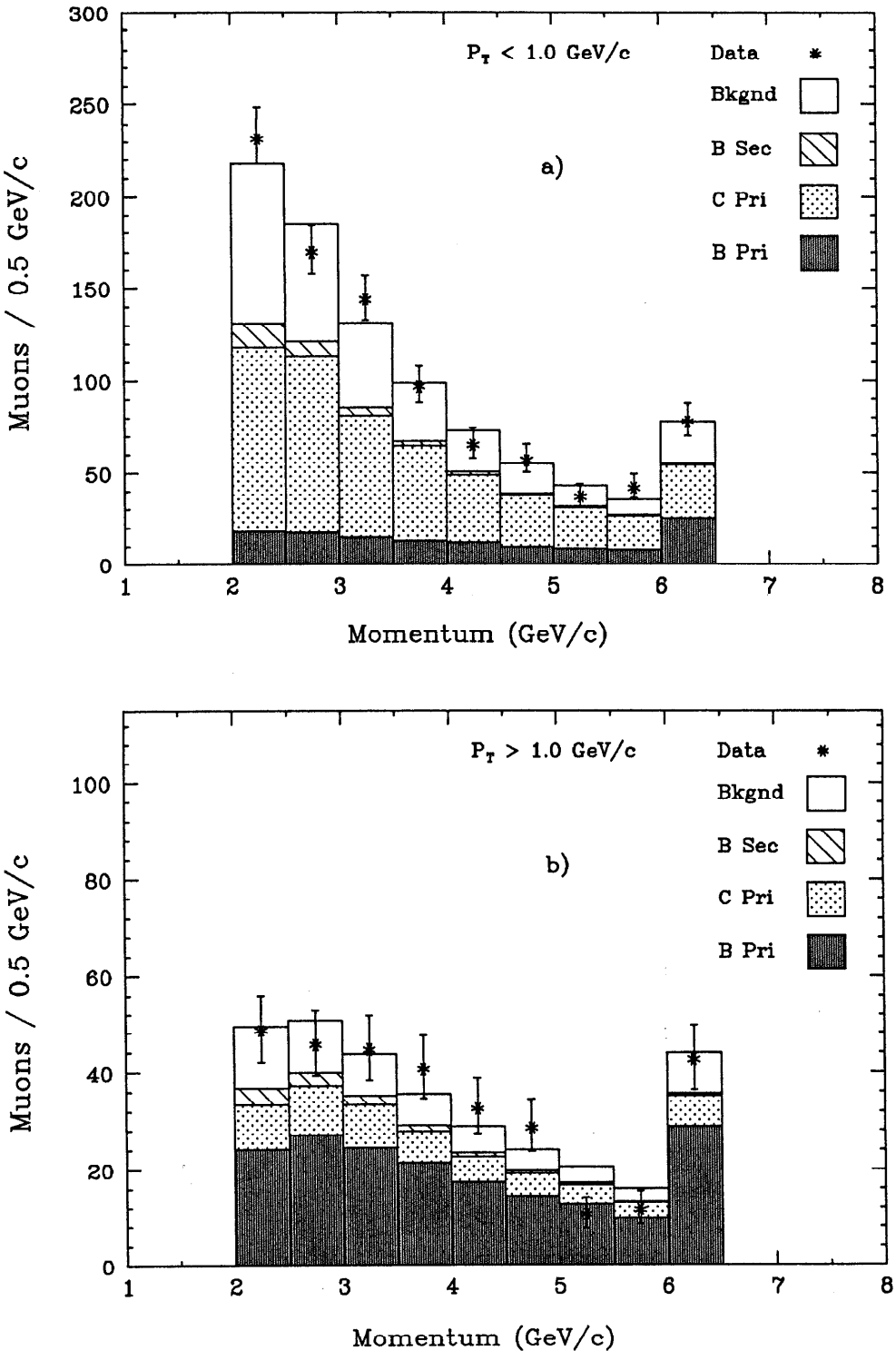

Figure 6.4: Muon momentum distributions. The muon momentum distribution is shown for a) low and b) high values of transverse momentum.

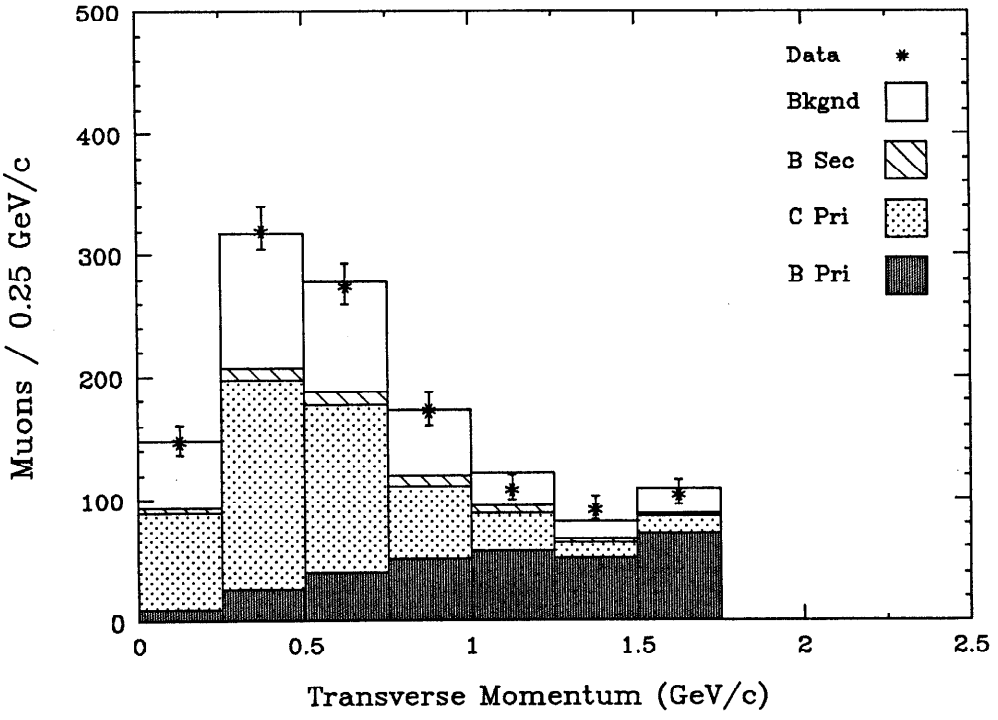

Figure 6.5: Muon transverse momentum distribution.

Table 6.11: C and B enhanced regions.

	C Enhanced Region ($p > 3.0$, $p_t < 0.75$) Fractions (%)		B Enhanced Region ($p > 2.0$, $p_t > 1.0$) Fractions (%)	
Source	Electron	Muon	Electron	Muon
Background	28.4 ± 3.5	31.5 ± 5.2	15.6 ± 3.0	20.0 ± 3.5
Charm	57.7 ± 4.1	52.6 ± 5.8	24.1 ± 4.7	18.6 ± 4.1
B Primary	11.6 ± 2.1	13.7 ± 2.3	55.5 ± 4.5	57.6 ± 4.0
B Secondary	2.3 ± 0.7	2.2 ± 0.6	4.8 ± 1.2	3.8 ± 0.9
# of Leptons	840	410	564	309

The errors on the fractions presented in Table 6.11 reflect the statistical precision of the fit as well as the estimated systematic uncertainty.

6.5.5 Comparison with other experiments

In Table 6.12 the results of this analysis are compared with those of other experiments, weighted by their statistical and systematic errors added in quadrature [102]. Mark II values are excluded from these averages.

Table 6.12: Comparison of inclusive lepton results.

Quantity	Previous Mark II	This Work	World Average
BR($c \rightarrow e$) (%)	6.4 $\pm$ 1.3 $\pm$ 2.8	9.6 $\pm$ 0.7 $\pm$ 1.5	10.2 $\pm$ 0.8
BR($c \rightarrow \mu$) (%)	8.1 $\pm$ 1.6 $\pm$ 1.8	7.8 $\pm$ 0.9 $\pm$ 1.2	8.2 $\pm$ 0.8
BR($b \rightarrow e$) (%)	12.9 $\pm$ 2.5 $\pm$ 2.0	11.3 $\pm$ 0.9 $\pm$ 1.1	12.5 $\pm$ 1.3
BR($b \rightarrow \mu$) (%)	12.2 $\pm$ 5.0 $\pm$ 3.0	11.8 $\pm$ 1.2 $\pm$ 1.0	12.4 $\pm$ 1.0
$< z_b >$: e	0.79 $\pm$ 0.06 $\pm$ 0.06	0.85 $\pm$ 0.03 $\pm$ 0.05	0.80 $\pm$ 0.03
$< z_b >$: μ	0.73 $\pm$ 0.15 $\pm$ 0.10	0.82 $\pm$ 0.04 $\pm$ 0.05	0.80 $\pm$ 0.03

The average branching ratios in Table 6.12 are computed from measurements at PEP and PETRA experiments. These averages are consistent with measurements made at SPEAR for charm hadrons and at CESR and DORIS for bottom hadrons. The average $< z_b >$ values are computed from both electron and muon measurements. The results of this present analysis agree well with those from other experiments and in most categories have a statistical precision comparable to the world average.

Table 6.12 also gives the results of the previous Mark II analysis of inclusive leptons [94]. There are two noticeable differences between the results presented in this analysis and the previous Mark II results. One difference is that the measured branching ratio for charm into electrons is significantly larger than previously measured. This difference is probably due to a statistical fluctuation in the early data, as well as a previous overestimate of the background in the electron signal. The other difference is that the measured value for $< z_b >$ is perhaps larger in the present analysis. This fact is probably because of a number of things that are different about this analysis: the use of a more accurate charm fragmentation

function, the use of a more sophisticated Monte Carlo program (one that better represents the data), and the understanding gained in the choice of the appropriate fragmentation variable.

The Impact Parameter Method

The B hadron lifetime presented in this thesis is inferred from the impact parameter distribution of lepton tracks from B decay. In this chapter, we define the impact parameter and the method by which its sign is determined. The impact parameter distribution for leptons in the B enhanced region is then presented. The effects of resolution on this distribution are reduced by making event and track cuts, and by introducing a method to determine the B production point on an event by event basis. The distribution obtained after these improvements is used in the following chapter to determine the average B lifetime.

7.1 Impact Parameter Definition

As shown in Figure 7.1, the impact parameter is defined as the distance of closest approach from a track to the assumed primary production point. In the Mark II detector, this measurement is done only in the xy plane because the extrapolated track resolution is considerably worse in the z direction. The relationship between the projected lepton impact parameter δ and the B decay length l is given by:

$$\delta = l \cdot \sin\theta \sin\psi \quad , \tag{7.1}$$

where θ is the polar angle of the B momentum vector and ψ is the decay angle between the B direction and the lepton trajectory projected in the xy plane. The decay length is defined as:

$$l \equiv \gamma \beta c \tau_b \quad . \tag{7.2}$$

The average decay length of B hadrons produced at PEP is $\sim 570\,\mu$m for a B lifetime of 1 ps ($\gamma\beta \sim 1.9$). The average $\sin\theta$ for B decays giving leptons in the Mark II fiducial volume is 0.85. For leptons in the B enhanced region ($p > 2$ GeV/c, $p_t > 1$ GeV/c), the average angle ψ is $\sim 17.6°$, resulting in a mean impact parameter of approximately $145\,\mu$m.

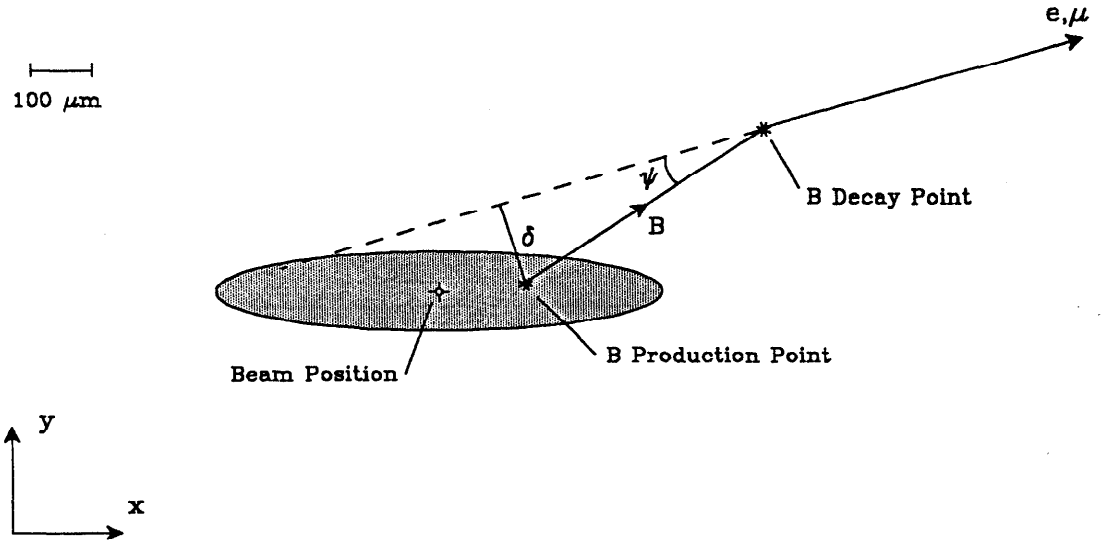

Figure 7.1: Impact parameter definition. The B decay length in the xy plane is the line segment between the "*" symbols. The impact parameter of the extrapolated lepton track is measured relative to the production point.

There is, of course, a correlation between the decay angle and the mean B hadron momentum ($p = \gamma\beta m$). As the momentum increases the decay angle decreases. As a result, the mean impact parameter saturates for high enough values of $\gamma\beta$. This effect is shown in Figure 7.2. At PEP energies, the impact parameter distribution is not fully saturated; there is still a dependence of the distribution on the mean $\gamma\beta$.* This dependence is considerably weaker than the corresponding one between the decay length and the mean $\gamma\beta$. As a result, the determination of the B lifetime from the impact parameter distribution is less sensitive to uncertainties in the B momentum spectrum than is the lifetime determination from the distribution of decay lengths.

* The dependence of the impact parameter distribution on the average B momentum can be translated into a dependence on $<z>$ of the B fragmentation function. The systematic effect of this dependence is investigated in Chapter 9.

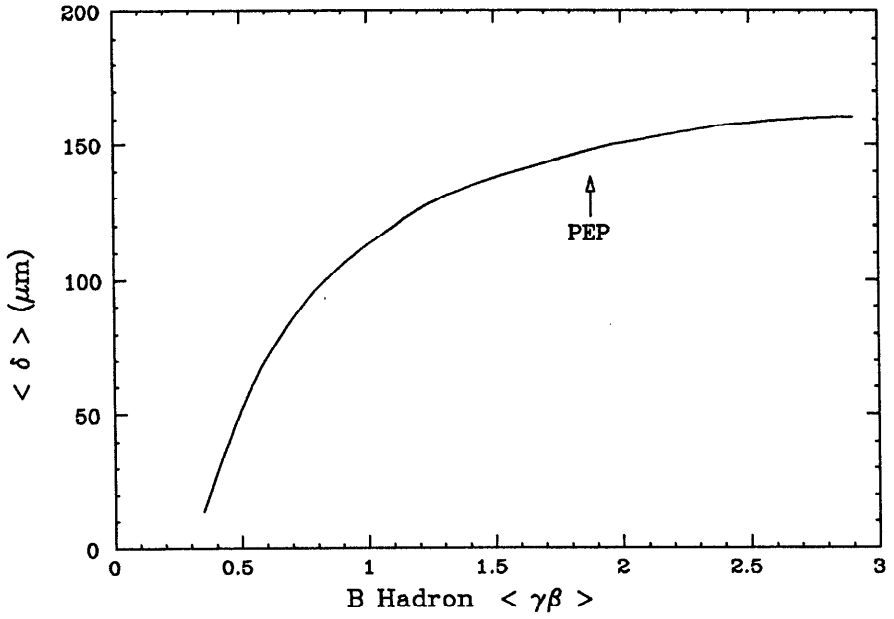

Figure 7.2: Average lepton impact parameter versus mean B hadron $\gamma\beta$. This plot is the result of a Monte Carlo calculation that includes the effects of acceptance and thrust uncertainties. The arrow indicates the mean $\gamma\beta$ for B hadrons produced at PEP.

In Figure 7.3, the average lepton impact parameter is shown as a function of (p, p_t) . This figure illustrates the effects of detector acceptance. In order to maximize purity, the B enhanced region is defined as $p_t > 1.0$ GeV/c. Conveniently, the average impact parameter is sizable in this region.

7.2 Resolution Effects on the Impact Parameter Distribution

With perfect resolution, the position where the lepton track crosses the B hadron trajectory corresponds to the B decay point. This observation provides an appropriate convention for signing the impact parameter. If the crossing point is in the same (opposite) hemisphere as the lepton track the impact parameter receives a positive (negative) sign. As shown in Figure 7.4 a, with perfect resolution the impact parameters for leptons from B decay are overwhelmingly positive. A tiny fraction of the leptons have negative impact parameters, resulting from backward going decays.

Unfortunately, since the B hadron is not fully reconstructed, its direction is not directly known. Instead, the thrust axis is used to approximate the B direction. This approximation is not exact because of tracking losses, ignored neutral particles,

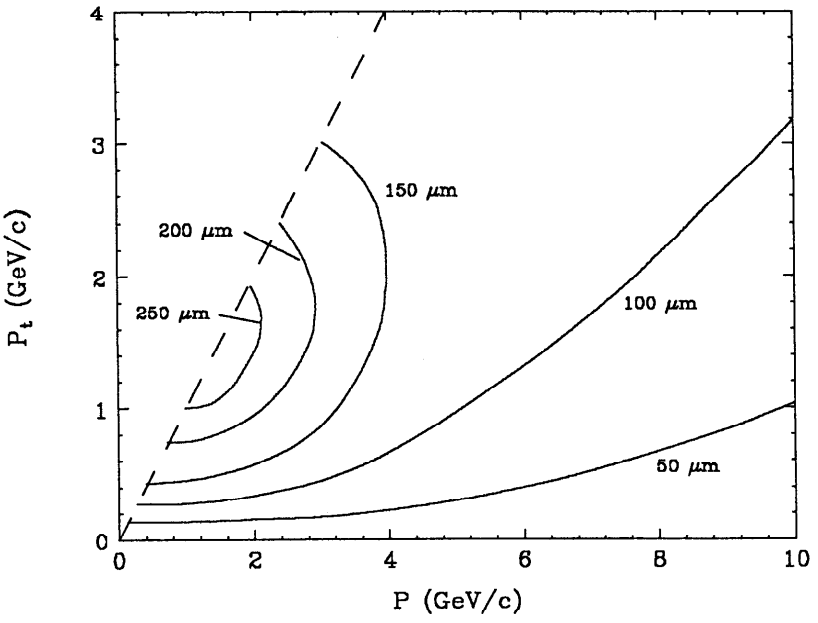

Figure 7.3: Average lepton impact parameter from B decay versus (p,p_t). This contour plot is determined from the Monte Carlo assuming τ_b=1 ps. The effects of thrust uncertainties are included. The dashed line corresponds to the kinematic limit.

events that are not two jet-like in nature, etc. The Monte Carlo indicates that the thrust axis reproduces the B hadron direction in the xy plane to within $\sim$ 0.15 radians (Figure 3.3).

The effect of thrust uncertainties on the lepton impact parameter distribution is shown in Figure 7.4 b. The average impact parameter is lowered slightly due to events with negative impact parameters. This figure illustrates the importance of reducing the effect of thrust uncertainty as much as possible; a mistake made in the estimate of the B direction can flip the impact parameter sign.

There are two contributions to the resolution from measurement errors. As outlined in Chapter 4, tracks are not extrapolated to the origin with perfect resolution. The typical impact parameter error due to chamber resolution is $\sim 90\,\mu$m. An even more significant error is caused by not knowing where the primary interaction point (B production point) is located. To first order, the average beam position (determined over a large number of events) can serve as an unbiased estimate of the primary interaction point. With this estimate, the overall impact

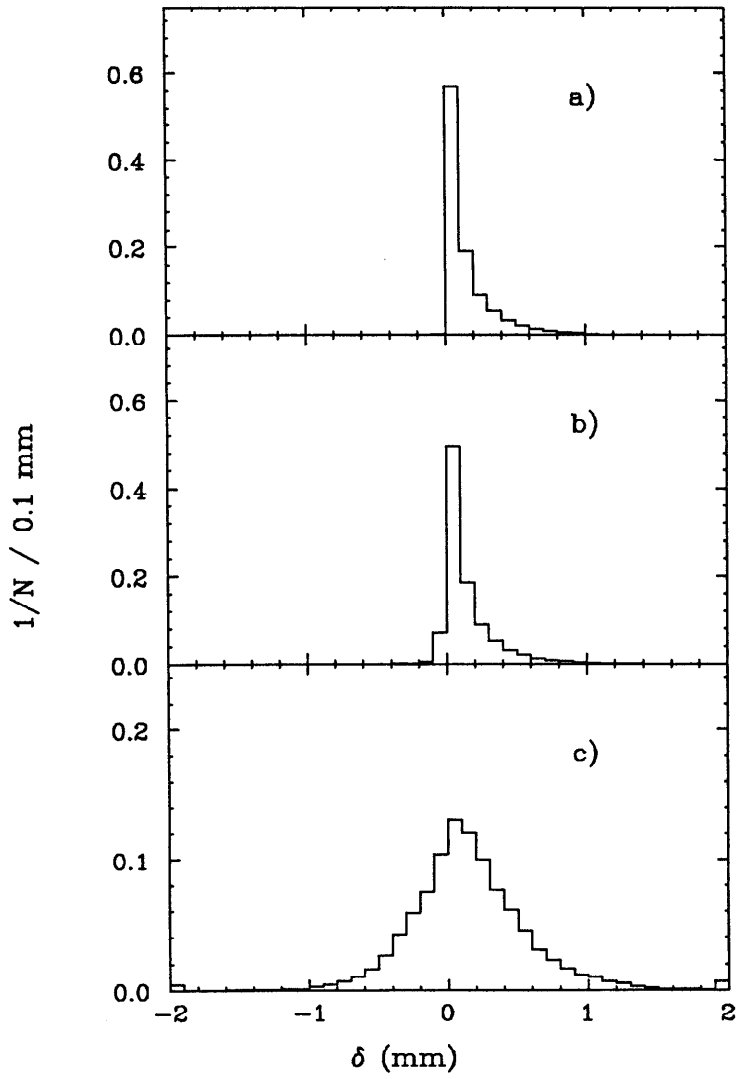

Figure 7.4: Impact parameter distribution for leptons from B decay. These three plots are derived using the Monte Carlo with τ_b=1 ps. a) shows the impact parameter distribution with perfect resolution. In b) the effects of thrust uncertainties are included. In c) the resolution effects due to the beam size and the extrapolation of tracks have been added. Leptons in the B enhanced region are used and δ is measured relative to the average beam position.

parameter error for a track with azimuthal angle ϕ is:

$$\sigma_\delta^2 \;=\; \sigma_{\rm VC}^2 \;+\; \sigma_x^2 \sin^2\phi \;+\; \sigma_y^2 \cos^2\phi \;\; . \tag{7.3}$$

In the first term, $\sigma_{\rm VC}$ is the impact parameter resolution due to the extrapolation of the track from the Vertex Chamber (see Eqn. 4.4). The remaining terms are the contributions to impact parameter error from the projection of the beam sizes

(σ_x and σ_y) on the track trajectory. (Values of σ_x and σ_y are given in Table 4.1). The resolution effects caused by the chamber and the beam size are illustrated in Figure 7.4 c; clearly these effects have an important influence on the shape and statistical significance of the impact parameter distribution.

The contribution to the resolution from the track extrapolation is minimized by the excellent spatial resolution of the Vertex Chamber. A technique to reduce the contribution to the resolution from the beam sizes is discussed later.

7.3 Lepton Impact Parameter Distributions

As itemized in 6.11, there are 564 electron and 309 muon tracks in the B enhanced region. Since we are interested in having accurate estimates of the beam position, leptons found in runs with significant beam motion are removed (see Section 2.3). This cut reduces the sample to 534 electrons and 296 muons.

In order to ensure that the lepton tracks are well measured, we require them to pass the track quality cuts listed in Section 4.6. As indicated in Table 4.2, the cuts on the quality of the track fit in the VC and DC and on the number of VC hits have the largest effect of any of the cuts on reducing the data sample. In addition to the cuts listed in Section 4.6, if a lepton track contains only two hits in the inner VC layers, we require it to be greater than one-fifth of a wire spacing away from the nearest charged track. This cut, designed to remove tracks that are completely overlapped, eliminates $\sim$3 % of the tracks.

In addition to cuts on lepton track quality, we make the following cut on the event thrust:

$$\boxed{\text{Thrust} > 0.75} \tag{7.4}$$

This cut is designed to remove those events in which the thrust direction provides a poor estimate of the B hadron direction, as indicated in Figure 3.3.

After applying the track quality cuts and the cut on thrust, we are left with 416 electrons and 252 muons in the B enhanced region. The impact parameter distributions of the leptons before and after these cuts are shown in Figure 7.5.

The mean impact parameter of both distributions in Figure 7.5 is significantly positive, however there are fewer tracks in the tails of the distribution after the thrust and track quality cuts have been made.

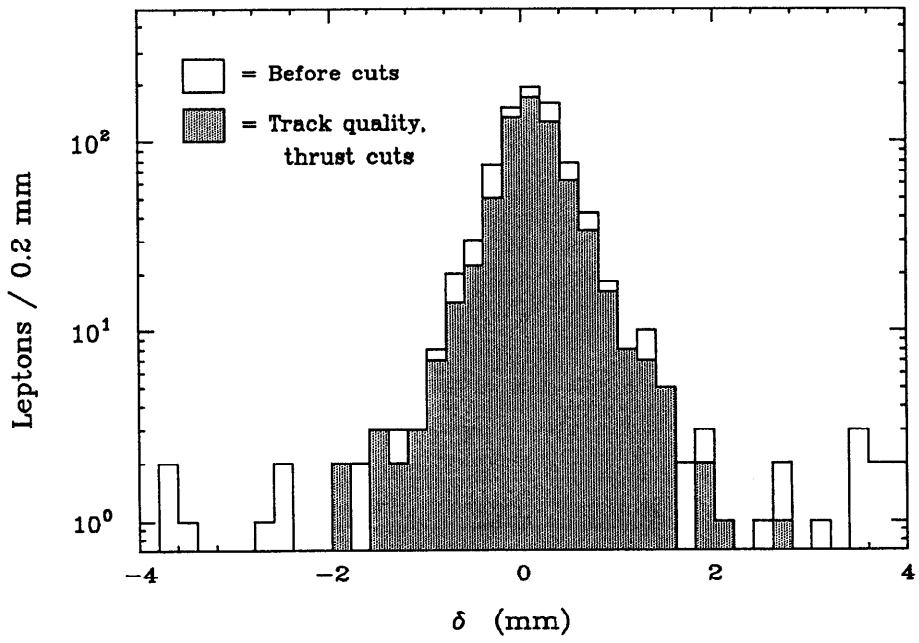

Figure 7.5: Lepton impact parameters, B enhanced region. In this figure δ is measured with respect to the beam position. The unshaded histogram corresponds to the data before any cuts are made on thrust and track quality. The shaded histogram represents the data after these cuts are made.

In Figure 7.6, the impact parameter distribution after cuts are made is duplicated, except the bin width is half as large and a linear scale is used. (In this figure, and in all subsequent impact parameter distributions, the mean value is calculated for $|\delta| < 2.0$ mm, to reduce the effect of tails. The extreme bins contain all underflows and overflows.)

The width of the distribution in Figure 7.6 ($\sim 460\,\mu$m) is dominated by the horizontal beam size. Figure 7.7, shows the distribution of impact parameter errors, as defined in Eqn. 7.3. The peak in the error distribution at large values is due to the horizontal beam size.

7.4 Determining the B Production Point

Up to now, we have measured impact parameters with respect to the average beam position (determined over a number of runs). In a given event, it would be advantageous to determine the B production point with better precision, using the tracking information present in that event. A technique to do such a determination is introduced in this section.

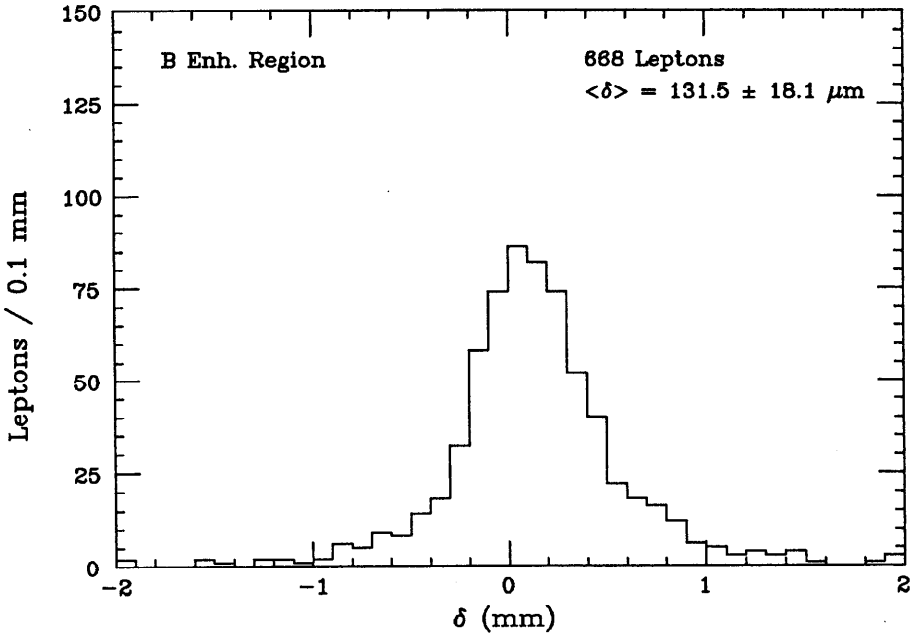

Figure 7.6: Lepton impact parameters, B enhanced region. This figure contains the same data as in Figure 7.5 after the cuts on thrust and track quality.

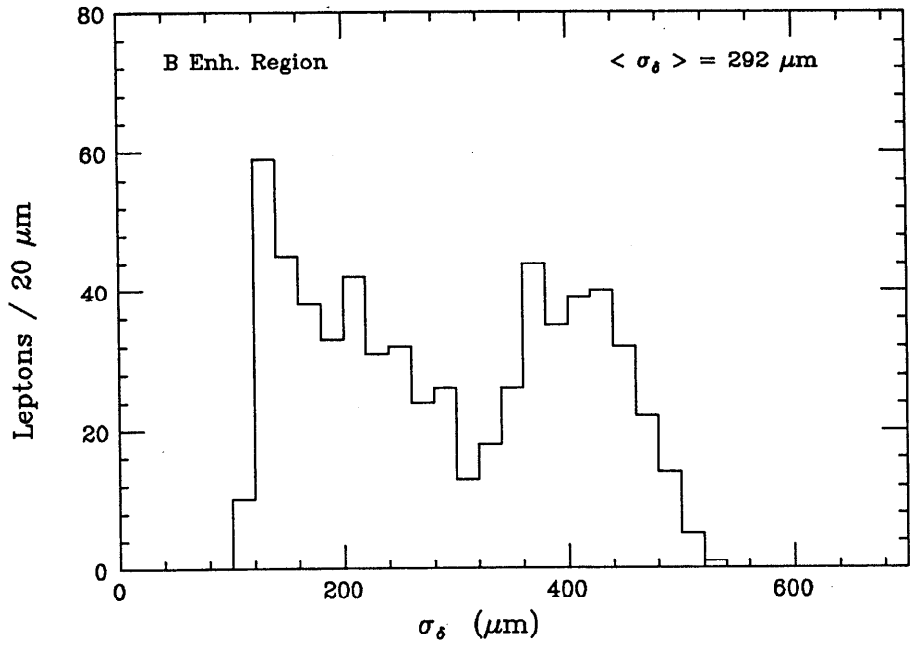

Figure 7.7: Lepton impact parameter errors, B enhanced region. In this figure, δ is measured with respect to the beam position.

7.4.1 Introduction on the use of the decay length method

The decay length method has been extensively used to measure the lifetimes of short-lived particles, such as the τ, D^0, and D_s^+ [103]. This method is fully discussed in Appendix B; it makes the following assumptions. A short-lived particle is produced at the e^+e^- collision point. The particle travels a finite distance and decays into a number of tracks. The putative decay point is estimated by constructing the vertex of the detected tracks. Using the momentum sum of the tracks as an estimate for the particle direction, the primary production point is determined by extrapolating from the decay vertex into the beam ellipse. The decay length is the distance from this estimated production point to the decay point. From the distribution of decay lengths the particle's lifetime can be determined. The statistical precision of the lifetime determination is improved by reconstructing a primary production point because one makes use of the directional information contained in the event.

The decays of the D^0 and D_s^+ mesons are fully reconstructed (i.e. all the decay products are detected). In the τ lepton decay $\tau \rightarrow \pi\pi\pi\nu$ there is a undetected neutrino; however the three detected pions come from the τ decay point and their momentum sum provides a good estimate of the τ direction [55]. In this analysis, we make no attempt to reconstruct B hadron decays. In a given jet there are tracks coming from the primary production point, the B decay point, and the charm hadron decay point. This situation is illustrated in Figure 7.8.

In $b\bar{b}$ events, the only track known with reliability to have come from the B decay point is the high p_t lepton. Therefore, a secondary vertex of all the tracks in a jet does not necessarily correspond to the B decay point. However, it can be shown that on the average this "jet vertex" point lies on a vector connecting the B production and decay points. Therefore the decay formalism can be applied to the case of B decays, and one can deduce the correct primary production point.

As shown in Figure 7.8, by letting the thrust axis approximate the B direction, the production point can be estimated by extrapolating from the jet vertex into the beam ellipse. The lepton impact parameter is then measured relative to the estimated production point. In using this approach, the assumption is made that a $b\bar{b}$ event can be divided into two independent jets.* The decay length method is

* Although this assumption is not strictly true, the cut on thrust (Eqn. 7.4) helps to eliminate

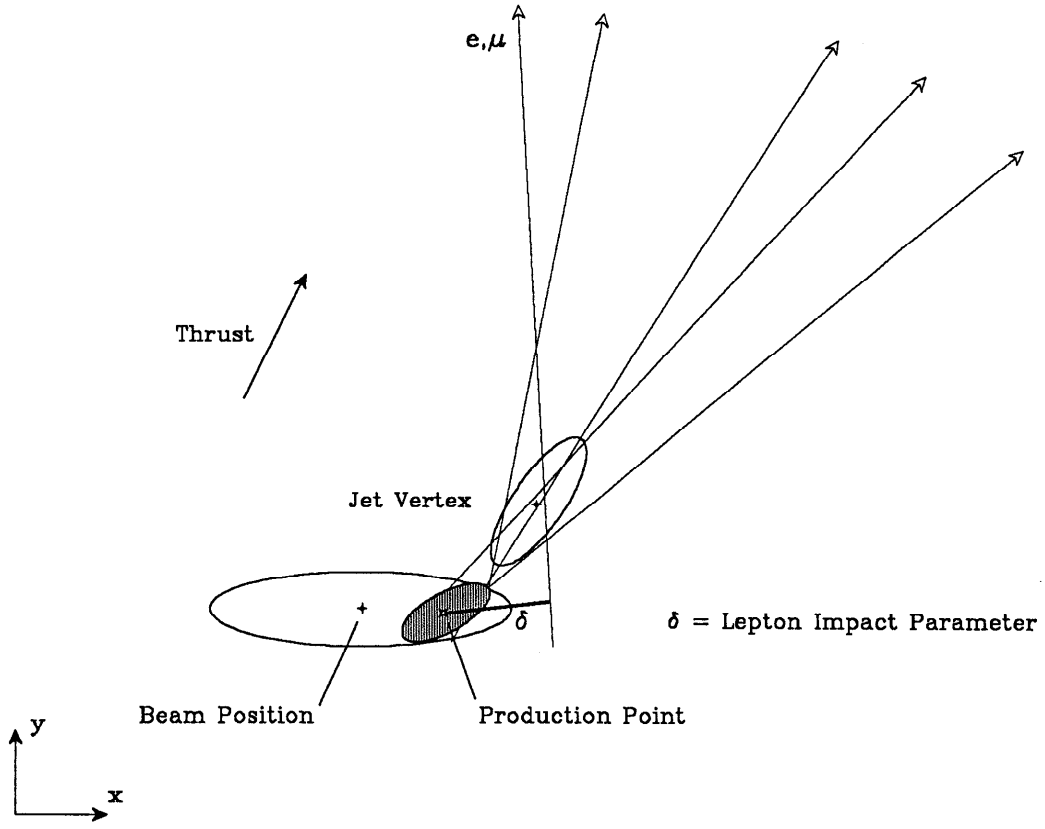

Figure 7.8: The jet-vertex method of finding the B production point. This figure schematically represents one hemisphere of a $b\bar{b}$ event. See the text for an explanation of the terms.

used on each jet separately to determine the production point.

7.4.2 The algorithm to find the B production point

Each event is divided into two hemispheres (or jets) based on the plane perpendicular to the thrust direction. The following algorithm is applied to each hemisphere separately:

- Each track in the hemisphere is subjected to the track quality cuts listed in Section 4.6. We require at least two tracks in the jet to pass these cuts.
- The jet vertex is determined from the quality tracks (including any leptons). The vertex reconstruction procedure finds the position in three dimensions that minimizes the distance of closest approach to each track given its fit parameters and errors, as discussed in Ref. 58.

---

most non two jet-like events.

We wish to ensure that vertices found in this manner are reasonable. It is important to remove jets having poor vertex fits because one or more of the tracks are mismeasured. However, we need to remain efficient for long-lived B decays. As discussed earlier, the tracks in the vertex do not necessarily originate from the same point; therefore jets containing long-lived hadrons will typically have somewhat poorer fits than those with shorter lived species. A cut on the quality of the vertex fit applied indiscriminately could remove these long lifetime events. To address this somewhat delicate problem, the following procedure is used:

- For vertices initially containing three or more tracks, the χ^2 of the vertex fit is calculated. Using the number of degrees of freedom for the fit,† the probability of the fit is calculated for the given χ^2 value. This probability distribution is shown in Figure 7.9 a.‡ We require the probability to be greater than 0.005; if a jet fails this cut, its vertex is refitted with all possible combinations of one fewer track. The combination with the best probability is selected. If the jet still has a vertex probability less than 0.005, or its vertex contains only two tracks, it is rejected entirely.
- For vertices initially containing two tracks, both tracks are required to have a value of impact parameter/error less than four.* With two tracks, there is only one degree of freedom (in the z direction). The distribution of the χ^2 values in the z direction is shown in Figure 7.9 b. Jets having χ^2_z greater than five are rejected.

The previous algorithm removes most of the poorly measured vertices from further consideration. In addition, by having an iterative fitting procedure (allowing tracks to be dropped from the fit), and by allowing certain two track combinations, the algorithm retains maximal efficiency. In Chapter 9, we consider the systematic effects of the cuts used in the algorithm on the lifetime determination. The distribution of the number of tracks used in determining the jet vertex is shown

† The number of degrees of freedom is equal to $(2 \times N) - 3$, where N is the number of tracks.

‡ In all distributions in this section, we use events containing a lepton with momentum greater than 2.0 GeV/c. This sample is chosen to provide a statistically large sample of events enhanced in heavy quark decay. The distributions for events in the B enhanced region alone are essentially the same as those presented in this section.

* The impact parameter is measured relative to the average beam position. This cut removes most of the large impact parameter tracks from K^0 decay; it is highly efficient for all other tracks.

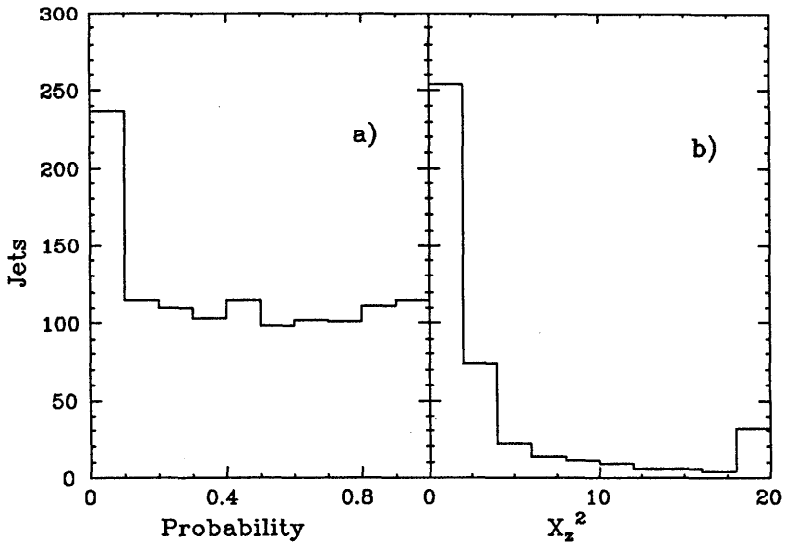

Figure 7.9: Vertex fit parameters. In a) the probability of the fit is shown for vertices with three or more tracks. In b) the values of χ_z^2 are shown for two track vertices. Events are required to have a lepton with momentum greater than 2 GeV/c.

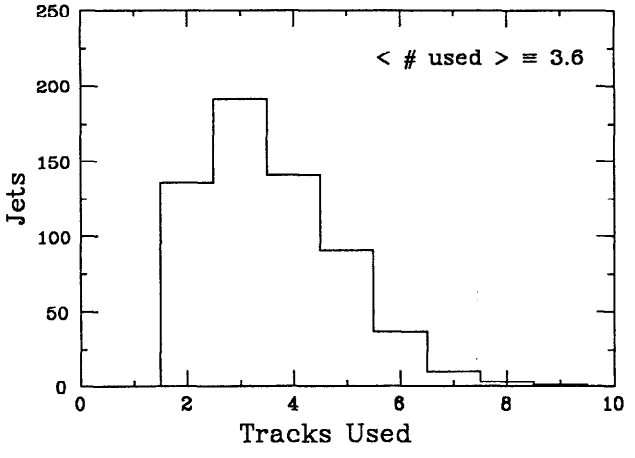

Figure 7.10: Number of tracks used in jet vertex Events in this plot are required to have a lepton with momentum greater than 2.0 GeV/c.

in Figure 7.10.

Having determined the jet vertex, the decay length method (see Appendix B) is used to estimate the primary production point. The effects of uncertainties in the thrust direction are taken into account. The efficiencies for jets to pass the algorithm cuts are given in Table 7.1. The overall efficiency for finding an estimate of the production point is 73 % per jet. Approximately 92 % of *events* have an

estimate of the production point from at least one jet, and 53 % of *events* have estimates from both jets. For the latter class of events, the jet with the smaller errors on the position of the production point is used.

Table 7.1: Production point method efficiencies. ϵ_1 is the jet efficiency to have two or more tracks passing quality cuts. ϵ_2 is the jet efficiency to pass the vertex fit cuts.

Category	Efficiency (per jet)
ϵ_1	84.1 %
ϵ_2	86.3 %
Overall	72.6 %

Figure 7.11, illustrates the algorithm for a particular event.

7.4.3 Checks on the production point algorithm

There are two important checks that must be made to ensure that the production point algorithm is reasonable. It is first necessary to ensure that the algorithm efficiency is constant as a function of secondary decay length (or particle lifetime). Secondly, the algorithm should be bias-free in offset and error; it should produce an estimate of the primary production point consistent with the real point given the errors, even in the presence of tracks with large impact parameters.

The efficiency of the algorithm is shown in Figure 7.12, plotted as a function of the generated B decay length. The average B decay length is 570 μm for a B lifetime of 1 ps. Although there is a slight drop in efficiency for very long decay lengths, the vertexing algorithm is seen to have constant efficiency for B lifetimes several times longer than the currently measured lifetime.

To check for bias, one can compare the estimated production point to the position generated in the Monte Carlo. This comparison shows that the estimated position agrees with the generated one within errors. Another check for bias (one that is more relevant for the B lifetime analysis) is to compare the measured lepton impact parameter with the generated one. In particular, the quantity $(\delta_{\rm meas} - \delta_{\rm mc})/\sigma$ should be a unit width Gaussian centered on zero.

Figure 7.13 shows the mean and width of $(\delta_{\rm meas} - \delta_{\rm mc})/\sigma$ in $b\bar{b}$ events plotted as a function of the B hadron decay length. In Figure 7.13, we see that even for

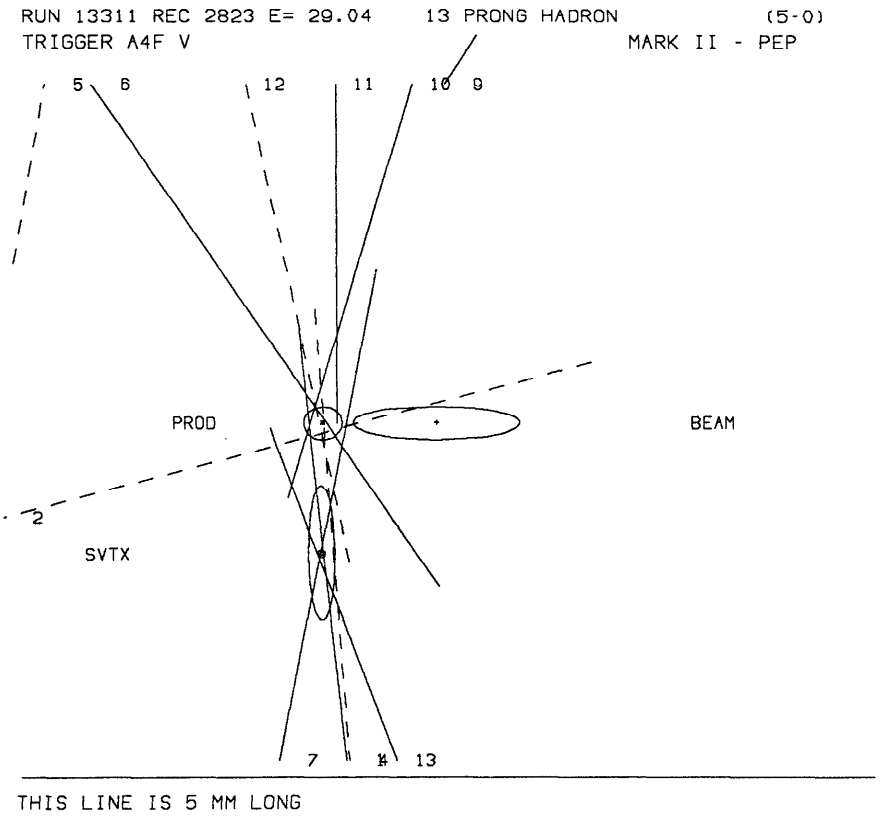

Figure 7.11: Determining the B production point for a given event. This figure shows an event magnified in the region near the beam position. The tracks drawn solid (dashed) are those that pass (fail) quality cuts. The center track in the lower hemisphere is an 8 GeV/c muon. The error ellipses for the beam, the secondary vertex, and the production point are identified by the labels "BEAM", "SVTX", and "PROD", respectively.

very long B decay lengths the estimated primary production point agrees on the average with the Monte Carlo generated point.

The Monte Carlo checks show that the method of determining the B production point is reasonable. Since more than half of the events have an estimate of the production point from both jets, the data can be used to further check the method. A schematic representation of a two jet $b\bar{b}$ event is shown in Figure 7.14; the jet containing the lepton tag is lablled the "leptonic side", whereas the other jet is labelled the "hadronic side", although there could be a lepton on this side as well.

As a check for bias, the differences $(\Delta x, \Delta y)$ between the estimated production point determined from the leptonic side and that from the hadronic side are calculated. The distributions of these differences are centered on zero and have widths that agree with expectations [104].

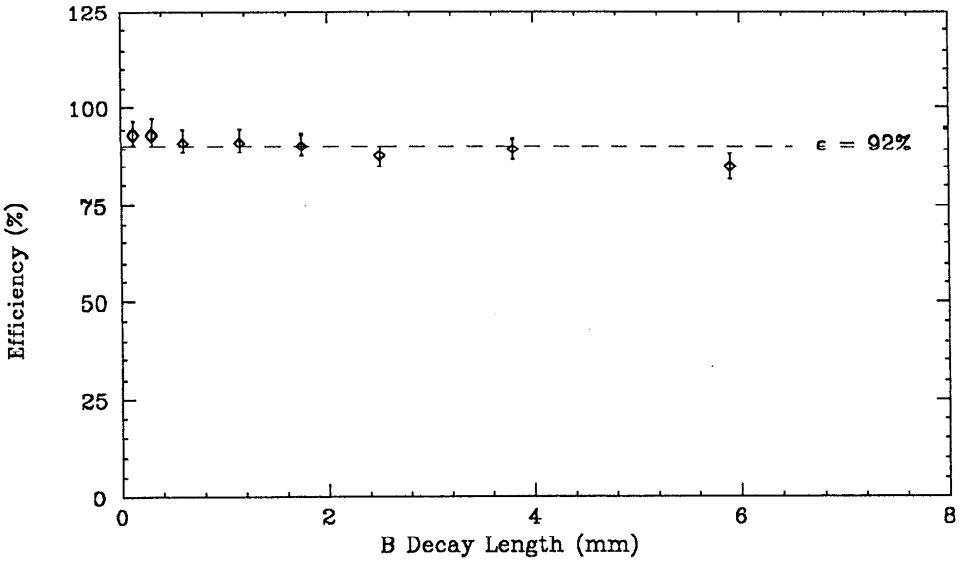

Figure 7.12: Algorithm efficiency versus B decay length. The decay length of the B hadron that is parent to the lepton track is used. Efficiency is defined here as the percentage of events having an estimate of the production point from at least one jet.

As a complete check on the overall consistency of the algorithm, one can construct a χ^2 describing how well the two estimates of the production point agree. This χ^2 is given by the formula:

$$\chi^2 = \frac{\sigma_{yy}\Delta x^2 + \sigma_{xx}\Delta y^2 - 2\sigma_{xy}\Delta x\Delta y}{\sigma_{xx}\sigma_{yy} - \sigma_{xy}^2} , \tag{7.5}$$

where $(\Delta x, \Delta y)$ are defined previously; the matrix σ is the sum of the production point error matrices from the two estimates.* This χ^2 is plotted in Figure 7.15, along with the expected χ^2 distribution for two degrees of freedom. The good agreement between the observed χ^2 distribution and the expected one indicates that the production points estimated from each side agree with one another.

7.5 Application of the Production Point Algorithm

The method of determining the B production point on an event by event basis has been shown to be robust. We now wish to examine the gain in resolution

* There is a slight caveat in calculating the χ^2 from Eqn. 7.5. Since each side estimates the production point with some common information (the beam position and thrust axis), there exists a correlation between the two estimates. This problem is treated by removing the correlated term from the σ matrices. A more general form of Eqn. 7.5 is discussed in Ref. 105.

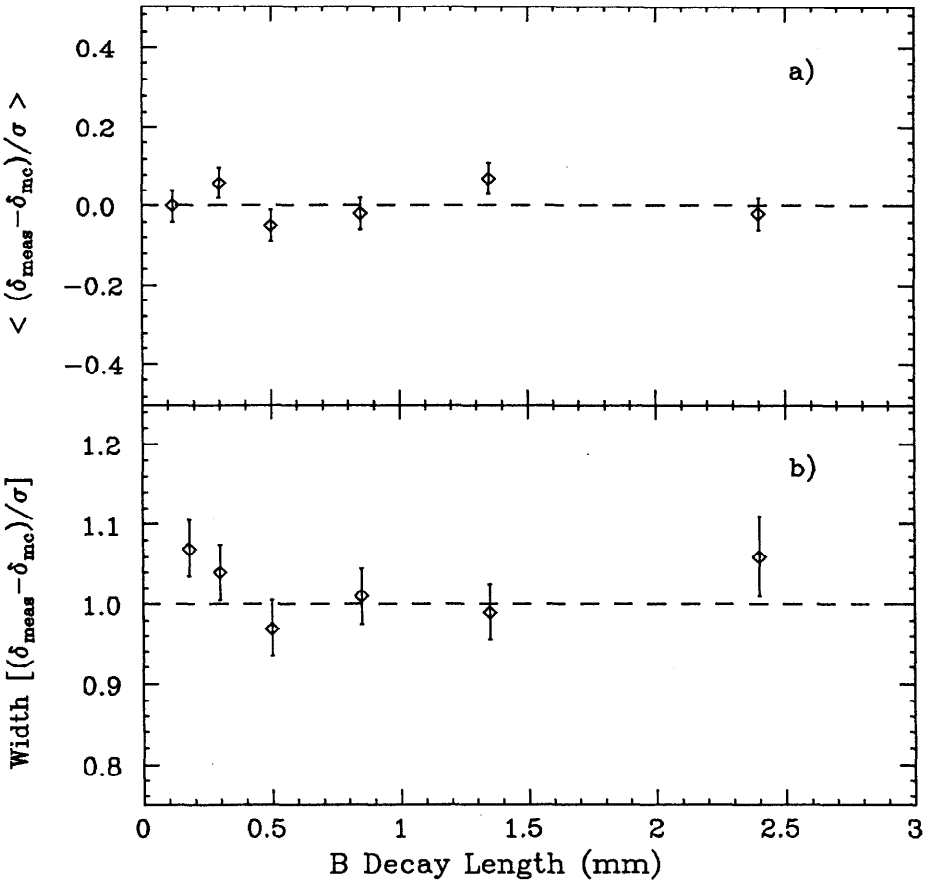

Figure 7.13: Mean and width of $(\delta_{\rm meas} - \delta_{\rm mc})/\sigma$ vs. B decay length. In this figure, the decay length of the B hadron that is parent to the lepton track is used.

as a result of using this method. In Figure 7.16, the lepton impact parameters are shown, now measured with respect to the estimated B production point. This figure shows a striking improvement in resolution over Figure 7.6. The exponential decay distribution is now more clearly visible. The cuts applied in the production point algorithm have reduced the event sample in the B enhanced region to 386 electrons and 231 muons (617 total).

The gain in precision is also illustrated in Figure 7.17, which shows the lepton impact parameter errors. As compared to Figure 7.7, we see that the contribution to the impact parameter error from the horizontal beam size is significantly reduced.

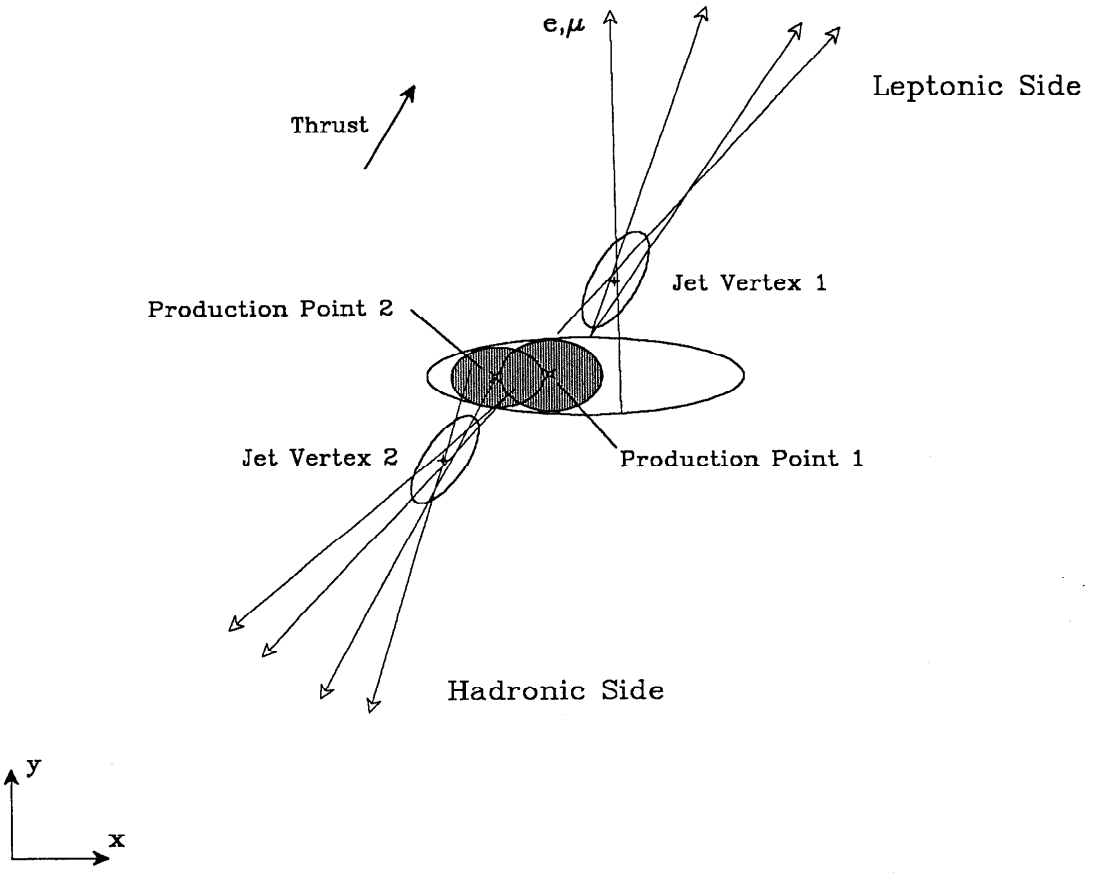

Figure 7.14: Checking the production point algorithm in the data. Comparing the production point determined from one jet with that determined from the other.

7.6 Summary of Cuts Applied to the Lepton Sample

In this chapter a number of cuts are applied to the lepton events in order to improve the reliability and precision of the impact parameter measurement. The effects of these cuts on the lepton sample in the B and C enhanced regions are shown in Table 7.2. This table lists the number of electrons and muons in the two regions before and after the cuts. In addition, it lists the average impact parameter for the various samples.

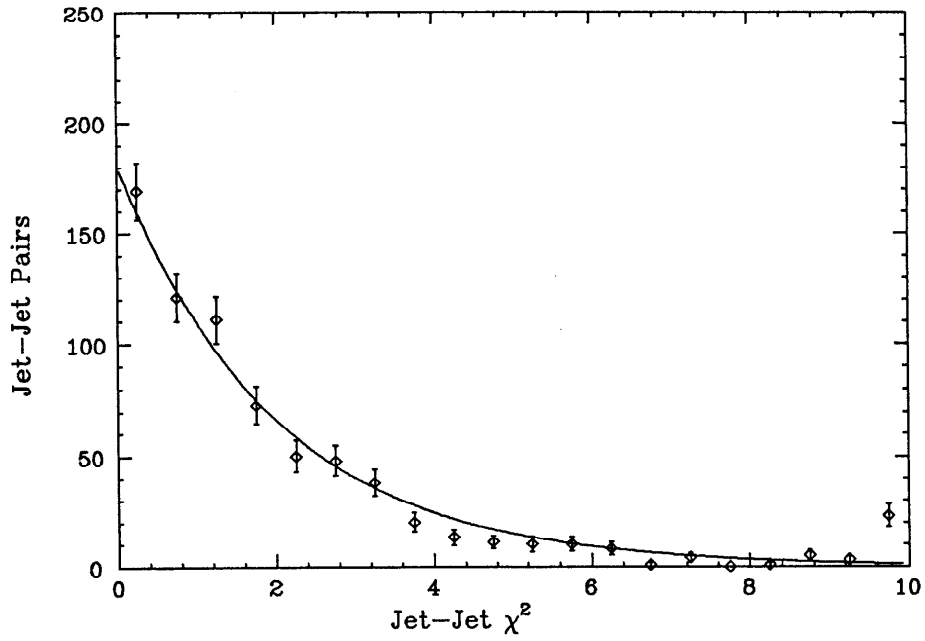

Figure 7.15: Jet-jet χ^2 using the production point algorithm. Events in this plot are required to have a lepton with momentum greater than 2 GeV/c. The curve drawn is the expected χ^2 distribution for two degrees of freedom.

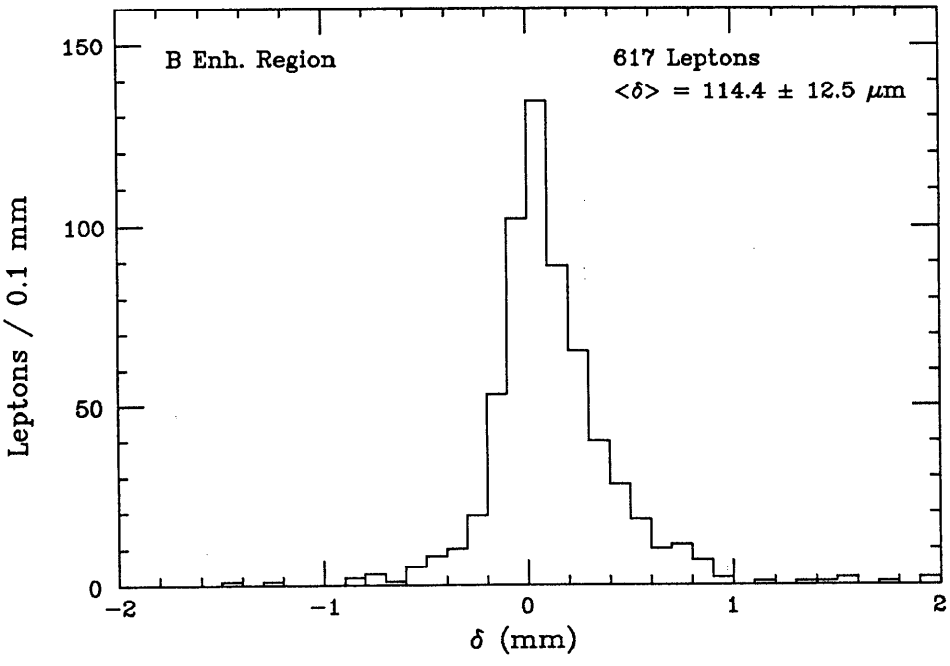

Figure 7.16: Lepton impact parameters, B enhanced region. In this figure, δ is measured with respect to the estimated production point.

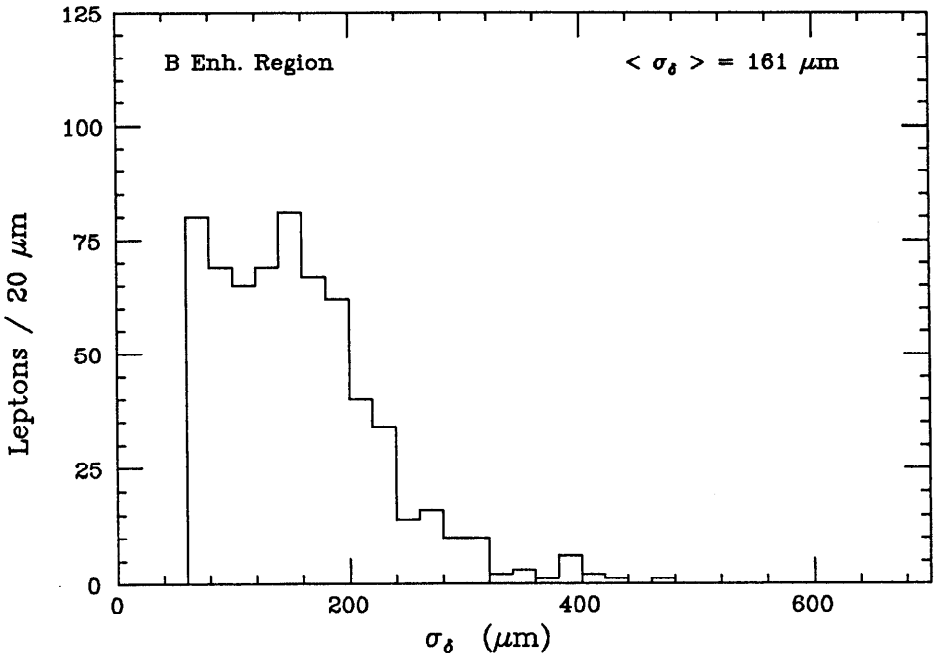

Figure 7.17: Lepton impact parameter errors, B enhanced region. In this figure, δ is measured with respect to the estimated production point.

Table 7.2: Cuts applied to the lepton sample. The definitions of the B and C enhanced regions are given in Table 6.11. The average impact parameter values in this table are calculated for $|\delta| < 2.0$ mm. The various cuts are described in the text.

B Enhanced Region

Category	Electrons	Muons	Total	$< \delta >$ (μm)
No cuts	564	309	873	121.8 ± 16.0
Remove beam motion	534	296	830	115.9 ± 16.2
Thrust, track quality cuts	416	252	668	131.4 ± 18.2
Prod. point algorithm	386	231	617	114.4 ± 12.5

C Enhanced Region

Category	Electrons	Muons	Total	$< \delta >$ (μm)
No cuts	840	410	1250	41.4 ± 12.8
Remove beam motion	796	397	1193	40.7 ± 12.9
Thrust, track quality cuts	677	327	995	32.3 ± 12.2
Prod. point algorithm	620	295	915	35.3 ± 8.2

The Lifetime Fits

In the previous chapter, we measured the impact parameter and its error for each of our lepton tracks. After all cuts, a sample of 617 leptons remain in the B enhanced region and 915 leptons in the C enhanced region. In conjunction with the Monte Carlo simulation, we now use a maximum likelihood fit to extract the average B and C hadron lifetimes from the data.

8.1 The Fitting Function

We assume that each lepton comes from one of four possible sources: background, C hadron decay, primary B hadron decay, or secondary B hadron decay. There are two types of background contributions: mis-identification and decay.* Therefore, we use a fitting function that represents the sum of each of these contributions, weighted by their appropriate fractions. For each track i, this fitting function can be written:

$$\begin{aligned} P(\delta^i, \sigma_\delta^i) \;=\; & f_{mis}\, P_{mis}(\delta^i) \;+\; f_{dk}\, P_{dk}(\delta^i) \;+ \\ & f_c\, P_c(\delta^i, \sigma_\delta^i) \;+\; f_b\, P_b(\delta^i, \sigma_\delta^i) \;+\; f_{bc}\, P_{bc}(\delta^i, \sigma_\delta^i) \quad . \end{aligned} \tag{8.1}$$

The functions P_{mis}, P_{dk}, P_c, P_b, and P_{bc} are the probability density functions for the contributions from mis-identification, decay, charm, primary bottom, and

* The mis-identification category includes hadron mis-identification in the calorimeter (e) and punchthrough (μ). The decay category includes conversions and Dalitz decays (e) and hadron decays in flight (μ).

secondary bottom sources, respectively. These functions are normalized (their integral is equal to one) and are weighted by the lepton fractions f_{mis}, f_{dk}, f_c, f_b, and f_{bc}. The overall fitting function in Eqn. 8.1 is the probability density function corresponding to the observation of a lepton with a given value of δ and σ_δ.† This fitting function is written separately for leptons in the B and C enhanced regions and for electrons and muons.

8.2 Inputs to the Fitting Function

We now describe in more detail the elements of the fitting function.

8.2.1 The lepton fractions

The results of the inclusive lepton analysis are used to give us the fractions f_{mis}, f_{dk}, f_c, f_b, and f_{bc}. We can not use the values given in Table 6.11 directly, however, because a number of cuts are placed on the lepton tracks in the lifetime analysis that are not present in the inclusive lepton analysis. In particular, we require the leptons to pass the track quality cuts (Section 4.5), we make event cuts to determine the primary production point (Section 7.3), and we make an overall thrust cut (Eqn. 7.4).

To address this problem, the inclusive lepton fit is redone with exactly the same cuts that are made in the lifetime analysis. In the new fit, fragmentation $< z >$ and the semi-leptonic branching ratios are fixed to the values determined from the lepton analysis (Table 6.8). We allow the background scale factors (f_m, f_d) to vary, and use new values for the quantities N_{misid}, N_{dk}, ϵ_{tq}, and the (p, p_t) probability distributions (see Eqn. 6.1). These quantities are determined in exactly the same manner as in Chapter 6, except that the additional cuts used in the lifetime analysis are imposed.

The expected background contribution N_{misid} and N_{dk} are affected by these cuts in two ways. The probabilities for hadron mis-identification and non-prompt decays are slightly changed* and the number of normalizing hadronic tracks in

† The impact parameter error σ_δ is included in the fit to make use of the resolution knowledge for each event. In principle, there are additional variables (e.g. p, p_t ...) that could be used in the fit [91]. In the present analysis, it was determined that these additional variables gave only slight statistical improvement.

* The largest change comes from the reduced muon background from pion and kaon decays due to the stiffer track quality cuts.

the lepton fiducial volume decreases. The track quality efficiency ϵ_{tq} is lowered to account for the tighter tracking cuts. In addition, ϵ_{tq} is now calculated as a function of (p, p_t). The (p, p_t) probability distributions are slightly altered by the event cuts (thrust and production point algorithm).

After these modifications, the lepton sample used in the lifetime analysis is fit in the same manner as in Chapter 6. The scale factors f_m and f_d are found to agree well with the expected value of 1.0. The lepton fractions determined from this fit are given in Table 8.1.

Table 8.1: Lepton fractions. The values in this table are determined after accounting for the cuts placed in the lifetime analysis. The errors on the fractions represent the combined statistical and systematic uncertainty.

	C Enhanced Region Fractions (%)		B Enhanced Region Fractions (%)	
Source	Electron	Muon	Electron	Muon
f_{mis}	24.4 ± 4.5	16.7 ± 5.1	14.0 ± 3.6	9.9 ± 3.1
f_{dk}	4.3 ± 0.8	14.8 ± 4.5	1.5 ± 0.3	9.7 ± 2.8
f_c	56.2 ± 5.3	51.1 ± 7.4	20.8 ± 5.6	16.0 ± 4.8
f_b	12.6 ± 2.7	15.1 ± 3.1	58.3 ± 5.3	60.1 ± 5.1
f_{bc}	2.5 ± 0.8	2.3 ± 0.8	5.4 ± 1.4	4.3 ± 1.0
Leptons	620	295	386	231

From Table 8.1, we see that the C enhanced region has approximately the same fractions as those before the cuts are imposed (Table 6.11). In the B enhanced region, the b fraction is slightly larger because of the suppression of background (due to track quality cuts) and the suppression of three jet $c\bar{c}g$ events (due to the thrust cut).

8.2.2 *The background contribution*

The probability density functions describing the background contribution are given by P_{mis} and P_{dk} of Eqn. 8.1. These functions are determined from the distribution of impact parameters for non-leptonic ("hadronic") tracks in the data.

A sample of hadronic tracks is first isolated. These tracks are chosen with the same momentum and acceptance cuts as the leptons, but are required to fail the lepton identification criteria (5.2 and 5.5). The selection of the hadronic tracks is weighted as a function of (p, p_t) by the probabilities for mis-identification and decay. Therefore, hadronic events are sampled with a weight given by the number of tracks in the B and C enhanced regions, and these individual tracks are accepted with the same (p, p_t) distribution that we believe the background tracks in the lepton sample to have.

The hadronic tracks are subjected to the same event and track cuts that are placed on the leptons. Their impact parameters relative to the production point are determined. The impact parameter distribution for hadronic tracks in the B enhanced region is shown in Figure 8.1. This distribution has a mean of $29.6 \pm 4.8\,\mu$m .* The fact that the mean of the distribution is not zero reflects the contributions from the decays of long lived particles (i.e. charm hadrons, bottom hadrons, K_s^0's, and Λ^0's). The mean of the hadronic impact parameter distribution for tracks in the C enhanced region is $15.9 \pm 3.1\,\mu$m .

We now normalize the hadronic impact parameter distributions in the B and C enhanced regions to the total number of events. These normalized distributions should represent the shape of the background probability density function P_{mis}. (We expect the function P_{dk} to be somewhat different than P_{mis} because of additional impact parameter generated from the secondary decay. We will discuss this effect shortly.)

For calculational reasons the exact impact parameter distributions are not used. Instead, they are fit by a piecewise continuous function in the central region ($|\delta| < 1$ mm), and by an exponential function in the wings ($|\delta| > 1$ mm). The choice of this particular form of the fit is arbitrary.† The fit describes the data well and has the same mean impact parameter as the data. The normalized background impact parameter distribution is shown in Figure 8.2, on a logarithmic scale, along with the fit used.

The fit curve in Figure 8.2 is used as the probability density function for

---

* As in the previous chapter, the means of distributions are quoted for tracks having $|\delta| < 2.0$ mm. The extreme bins contain all underflows and overflows.

† Other fits were tried as well (e.g. an offset Gaussian with exponential tails or a sum of two Gaussians). The effects of these differing fits on the lifetime results were negligible.

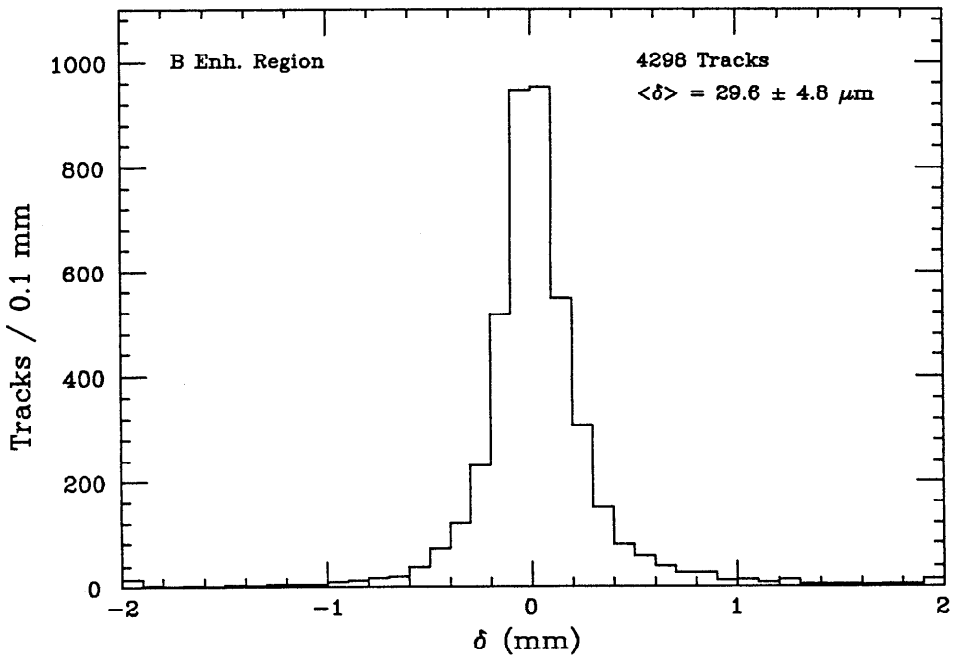

Figure 8.1: Impact parameter distribution for hadronic tracks. Tracks are required to be in the B enhanced region.

the mis-identification background P_{mis}. The background function P_{dk} is broader than P_{mis}. This broadening comes about because decays in flight can generate additional impact parameter (from the kink in the reconstructed track). Monte Carlo studies indicate that this effect leaves the mean of the background impact parameter distribution unchanged, but increases its width by about 20 %.

The probability density function for the background from decays can then be written as:

$$P_{dk}(\delta) = \frac{1}{\sqrt{2\pi}\sigma_{dk}} \int_{-\infty}^{\infty} P_{mis}(\epsilon)\, e^{-(\epsilon-\delta)^2/2\sigma_{dk}^2}\, d\epsilon \qquad (8.2)$$

for $\sigma_{dk} = 1.2 \pm 0.2$.

8.2.3 *The prompt lepton contribution*

We now turn our attention to the probability density functions describing the prompt lepton contributions (c, b, and bc). These distributions are functions of δ and σ_δ, and of course they also depend on the B and C hadron lifetimes. Therefore,

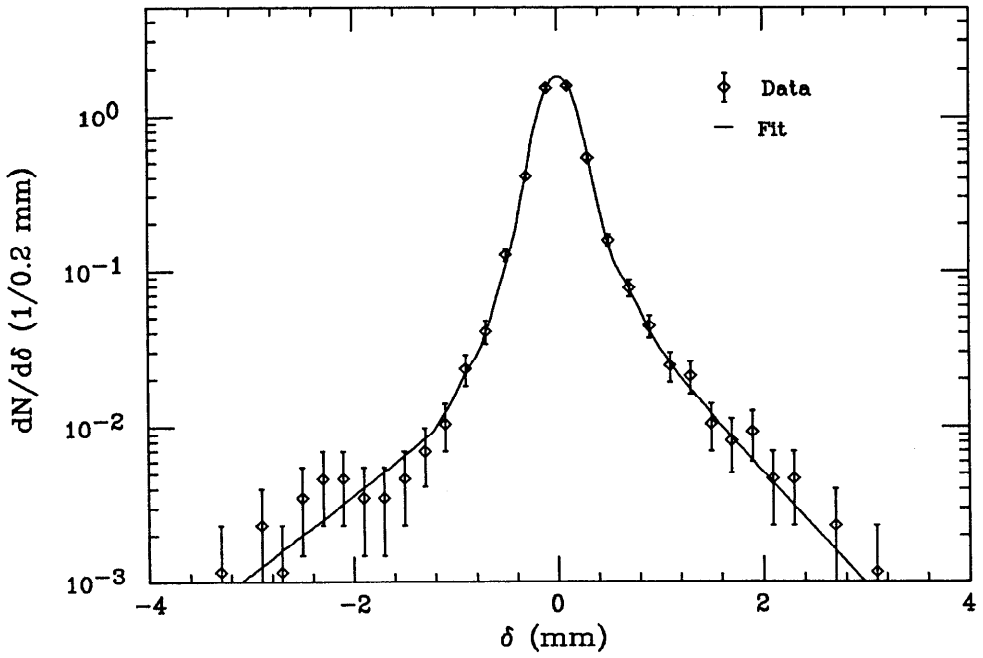

Figure 8.2: Normalized hadronic track impact parameter distribution. Tracks are required to be in the B enhanced region. The distribution is normalized to the total number of tracks. The fit curve represents the function used as the background probability density distribution.

the functions describing the prompt lepton contributions in Eqn. 8.1 can more accurately be expressed as:

$$P_l\,(\delta,\sigma_\delta) \;\rightarrow\; P_l\,(\delta,\sigma_\delta,\tau_b/\tau_c\,...) \quad , \tag{8.3}$$

for $l = c, b, bc$. The (...) indicates that the lepton probability density functions depend in a lesser way on other parameters (e.g. $< z >$ of fragmentation). For the moment, we assume such parameters are fixed; their variation will be studied in the context of systematic errors.

The term τ_b/τ_c indicates that P_l depends on either τ_b or τ_c depending on the lepton source. P_l depends on τ_b for the primary bottom contribution ($l = b$) and on τ_c for the charm contribution ($l = c$). For the secondary bottom contribution ($l = bc$), it turns out that P_l depends essentially entirely on τ_b . In other words, the impact parameters for leptons from charm hadron decay in a $b\bar{b}$ event are largely determined by the B lifetime.*

* In the B enhanced region, this fact comes about because the impact parameters from B decay

We now turn our attention to the expected shape of the prompt lepton distributions. Consider an experiment that reconstructed a decaying particle's direction with complete accuracy, and achieved perfect impact parameter resolution on the tracks from the decay vertex. Such an experiment would measure an exact projected impact parameter distribution given by:

$$F^{\text{exact}} = \int_0^\infty \frac{2\,y\,z^2}{(z^2+y^2)^2}\,e^{-z}\,dz \quad , \tag{8.4}$$

where y is the scaled impact parameter:

$$y \equiv \frac{\delta}{c\tau} \quad , \tag{8.5}$$

for the particle lifetime τ [106]. The function F^{exact} is shown in Figure 8.3; it is valid in the extreme relativistic limit $\gamma \to \infty$, and approximately so otherwise.

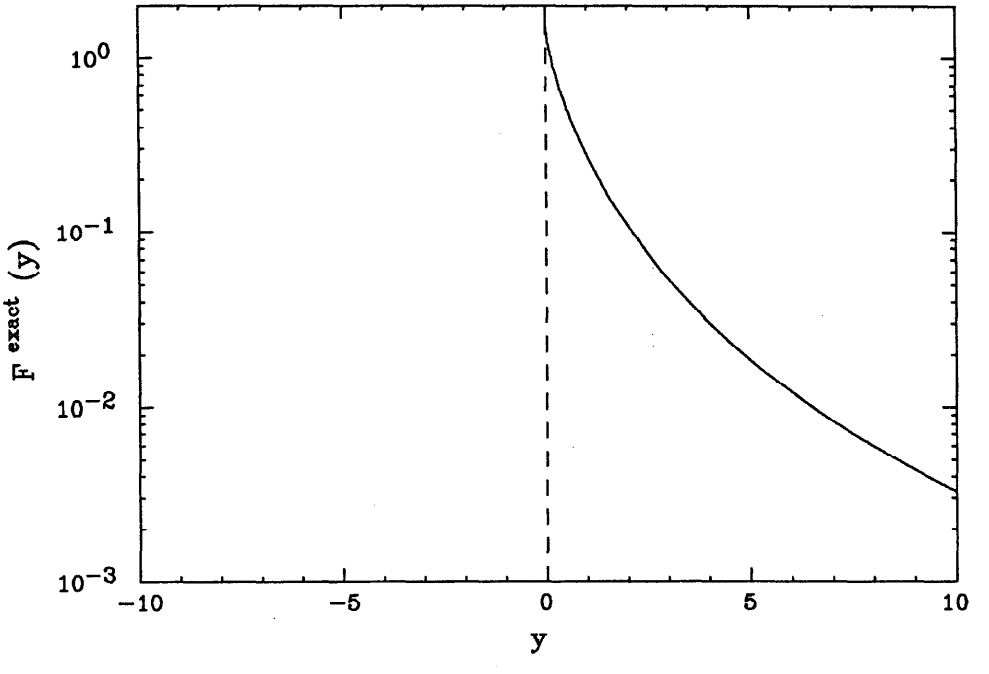

Figure 8.3: Exact impact parameter distribution. This figure illustrates the hypothetical impact parameter distribution for a perfect detector. The variable y is the scaled impact parameter $y \equiv \delta/c\tau$.

---

are much larger than those from C decay. In the C enhanced region, the statement is not quite true, but the effect of the secondary bottom decays there is small.

Resolution effects degrade the impact parameter distribution shown in Figure 8.3. In this analysis, there are two such effects. The first one comes from the uncertainty in the hadron direction, as discussed in Chapters 3 and 7. The B direction is approximated by the thrust axis, and is used to determine the sign of the impact parameter. The thrust axis uncertainty causes a small fraction ($\sim 10\,\%$) of impact parameters to have negative sign.

The second effect on the exact impact parameter distribution comes from having limited experimental resolution. For this measurement, the experimental resolution is limited by the error on the position of the production point and by the extrapolated track resolution of the Vertex Chamber.

Monte Carlo simulations rarely (if ever) fully account for all actual experimental resolution effects. Therefore, in this analysis, we divide the function P_l into two parts. One part accounts for the exact impact parameter distribution and uncertainty in the thrust direction (presumed to be well modelled in the Monte Carlo). The other part accounts for the experimental resolution.* The function P_l is the convolution of these two parts:

$$P_l\left(\delta, \sigma_\delta, \tau_b/\tau_c\right) \;=\; R\left(\sigma_\delta\right) \otimes F_l\left(\delta, \tau_b/\tau_c\right) \quad . \tag{8.6}$$

The function F_l, is termed the "Physics Function" (the MC impact parameter distribution incorporating thrust uncertainty). The function R is termed the "Resolution Function", it only depends on σ_δ and not on δ, the lifetimes, or the lepton type. We separately discuss the determination of each of these two functions.

8.2.4 The physics functions

There are actually six physics functions to be determined from the Monte Carlo. There are three sources of prompt leptons (c, b, and bc), in both the B and C enhanced regions.

Using a large sample of $b\bar{b}$ and $c\bar{c}$ Monte Carlo with full detector simulation, prompt leptons are identified and categorized as coming from charm, primary

* It may be argued that thrust uncertainty is part of the experimental resolution. Technically speaking this argument is true. Because the thrust uncertainty cannot be directly measured in the data, however, we use the Monte Carlo to estimate its effects. In the resolution function that we will determine in the following section, thrust uncertainties are present, but they are completely washed out by the impact parameter resolution.

bottom, or secondary bottom decays. Each event must meet the same requirements as placed on the data used in the lifetime analysis.† The leptons are required to meet the same identification and track quality criteria as leptons in the data. For each surviving lepton track, an impact parameter is calculated using the exact trajectory of the lepton (as generated in the Monte Carlo). This impact parameter is measured with respect to the generated (true) B production point, but the *measured* thrust axis is used to determine the sign of δ. The resulting impact parameter distribution is the physics function F_l.

In Figure 8.4, the physics function for leptons from B decay in the B enhanced region is shown. The mean of this distribution is $\sim 143\,\mu$m for a B lifetime of 1 ps. Table 8.2 gives the means of the six physics functions. The Monte Carlo samples contain at least twenty times the statistics of the data for each category.

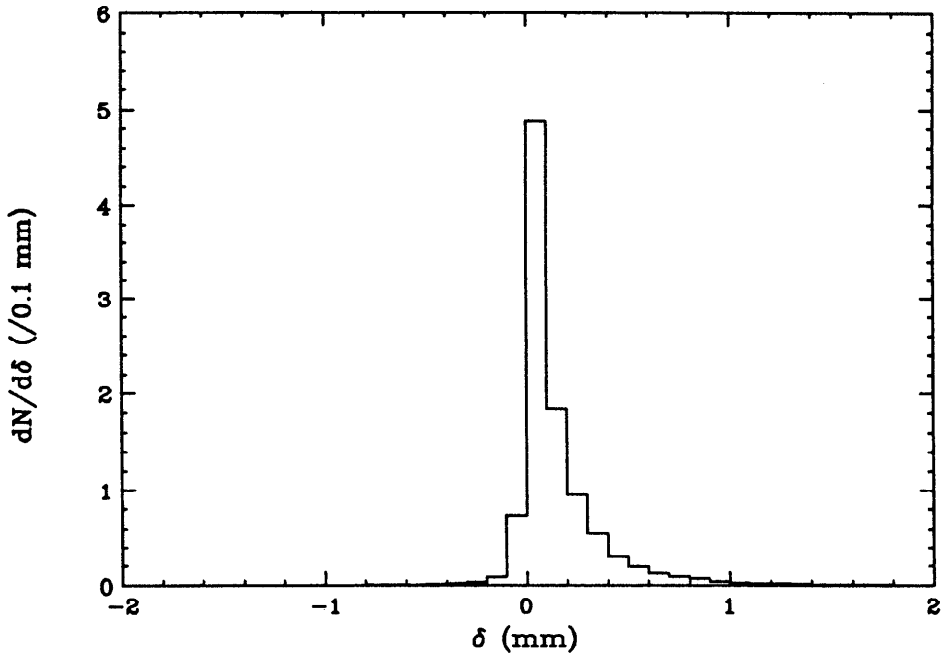

Figure 8.4: Physics function for leptons from B decay. The MC impact parameter distribution, or physics function, is shown for leptons from B decay in the B enhanced region.

The impact parameter distribution shown in Figure 8.4 is determined at a single value of τ_b. It would be inconvenient to generate many such samples at different

† To reiterate, these requirements are: hadronic event selection, thrust cut, and primary production point cuts.

Table 8.2: Mean impact parameters for leptons in the Monte Carlo. In this table, the mean values of the physics functions for the various lepton sources are shown. These values are determined using $\tau_b = 1$ ps and $\tau_c = 0.68$ ps.

Source	C Enhanced Region $< \delta > (\mu m)$	B Enhanced Region $< \delta > (\mu m)$
C	38.4 ± 0.6	39.7 ± 1.3
B Pri	44.7 ± 2.7	142.8 ± 2.1
B Sec	53.1 ± 4.2	167.3 ± 3.5

lifetimes. Instead, we take advantage of the scaling property of the variable y (defined in Eqn. 8.5). For tracks from charm decay, we use τ_c in the expression for y. For tracks from bottom decay (both primary and secondary), τ_b is used. The physics function F_l is then expressed in terms of y and need only be generated at one lifetime value.

In Figure 8.5, the physics function for leptons from B decay in the B enhanced region is shown. This plot is the same as Figure 8.4, except that the function is expressed in terms of y and not δ, and the scale is logarithmic.

Also shown in Figure 8.5 is a fit to the distribution by the following parameterization:

$$\begin{aligned} F_l(\delta, \tau_b/\tau_c) \;=\; & A_+ e^{-B+y} + C_+ e^{-D+y} \quad (y > 0) + \\ & A_- e^{B-y} + C_- e^{D-y} \quad (y < 0) \quad . \end{aligned} \tag{8.7}$$

The coefficients $(A, B, C, D)_+$ describe the positive y behavior of the fit and the coefficients $(A, B, C, D)_-$ describe the negative y behavior. The values for these coefficients for the various lepton sources are given in Table 8.3. As in the case of the background function, this particular parameterization is arbitrary; it is chosen for calculational convenience. The fits provide good representation of the underlying impact parameter distributions.

8.2.5 The resolution function

The final ingredient needed for the lifetime fit is the resolution function $R(\sigma_\delta)$. We would like to determine this function from the impact parameter distribution for

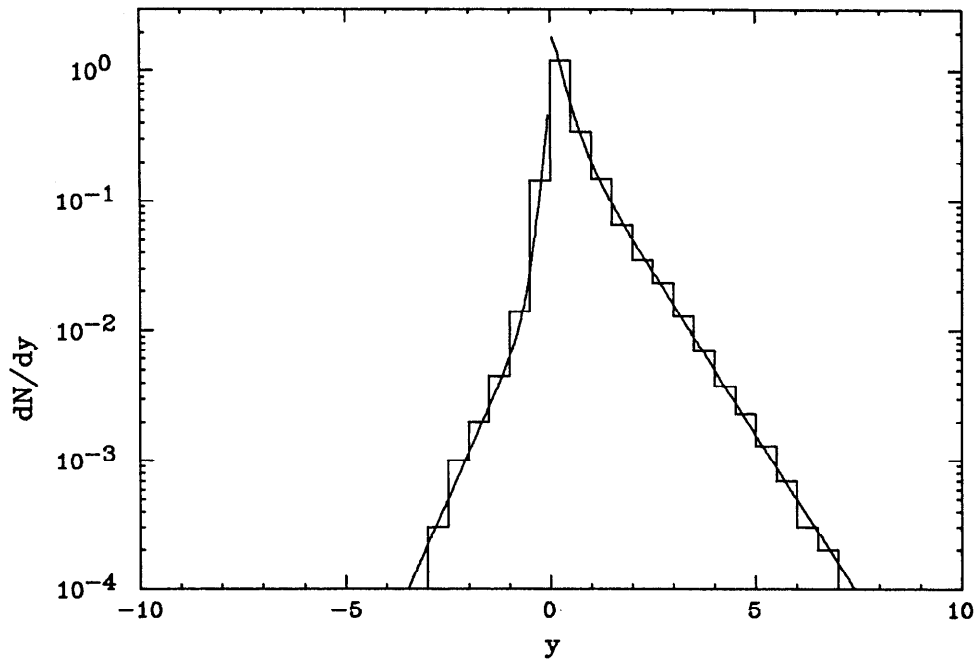

Figure 8.5: Physics function for leptons from B decay. The MC impact parameter distribution is shown for leptons from B decay in the B enhanced region. The variable y is the scaled impact parameter defined in Eqn. 8.5.

Table 8.3: Coefficients for the physics function parameterization. This table gives the values of the coefficients for the parameters of the various physics functions. Eqn. 8.7 defines the form of the parameterization.

	C Enhanced Region			B Enhanced Region		
Coefficient	C	B pri	B sec	C	B pri	B sec
A_+	0.370	0.619	0.026	0.145	0.498	0.301
B_+	1.324	1.942	0.835	0.932	1.151	1.242
C_+	2.884	3.368	2.309	2.822	1.879	1.076
D_+	5.801	7.457	3.279	4.723	3.710	1.648
A_-	0.056	0.068	0.313	0.099	0.030	0.063
B_-	1.054	1.566	2.694	1.211	1.637	1.991
C_-	1.539	1.719	2.912	2.055	0.618	0.510
D_-	7.006	6.695	12.85	9.244	7.521	5.995

hadronic tracks. As shown previously, however, such a distribution has a non-zero

mean (i.e. there are tracks with lifetime information). It is possible to extract the resolution function from this distribution by a de-convolution procedure, accounting for lifetime effects (see Ref. 91). Instead, we make use of the fact that the impact parameter is measured projected into the xy plane. This fact allows us to select a sample of hadronic tracks with small lifetime effects.

The set of tracks with a given momentum and transverse momentum is shown in Figure 8.6. The locus of this set of tracks is a cone of constant (p, p_t) around the thrust axis. Because of the correlation between impact parameter and p_t , tracks on this cone with their p_t vector in the xy plane have maximal lifetime information in that plane. Conversely, those tracks whose p_t vector is parallel to the z direction have no lifetime information in the xy plane. The only impact parameter that such tracks have must be due to resolution effects.

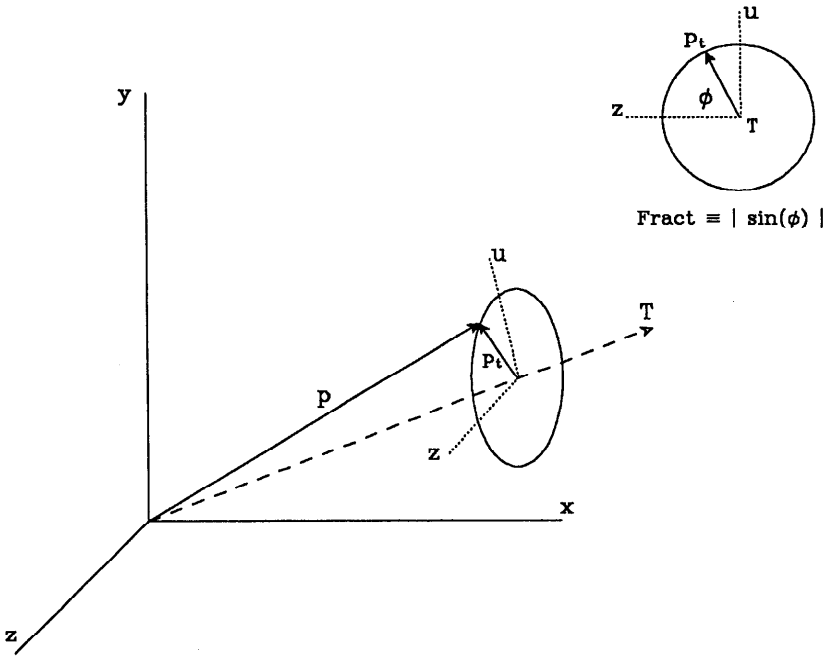

Figure 8.6: Definition of the fract variable. This figure shows the set of tracks with a given p and p_t. The vector T is the thrust axis; ϕ is the angle between the p_t vector and the z axis. Fract is defined as the sine of the angle between the p_t vector and the z direction.

We define a variable "fract" to provide a measure of the track p_t in the xy plane. The definition of fract is given in Figure 8.6.* Tracks with high values of

* Other possible definitions of such a quantity exist. This particular one is used because the lepton fractions are not changed if a cut on fract is made.

fract have maximal lifetime information in the xy plane and vice-versa.

The distribution of fract values for hadronic tracks in the data is shown in Figure 8.7. In practice, there are very few tracks with vanishing fract values. However, the lifetime bias can be reduced to a negligible amount by selecting tracks with low values of fract:

$$\text{Fract} < 0.5 \quad . \tag{8.8}$$

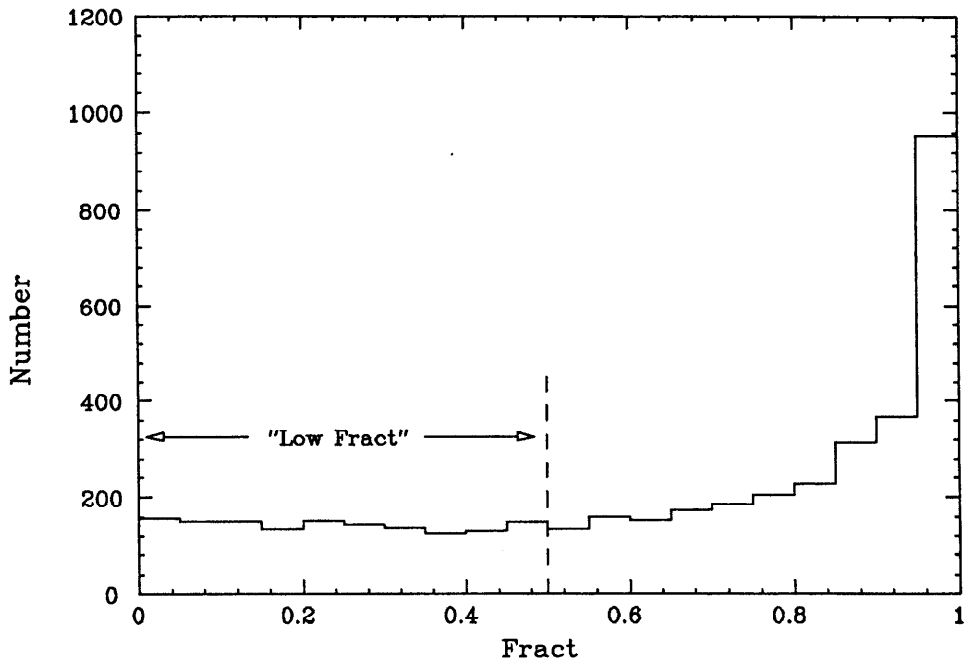

Figure 8.7: Fract distribution for hadronic tracks. Tracks are required to lie in the same kinematic regions as the leptons.

To determine the resolution function, we use a sample of hadronic tracks that have the same (p, p_t) distribution as the lepton tracks, but satisfy Eqn. 8.8. The resolution function for these tracks is expected to be the same for the leptons.*

The impact parameter and its expected error is determined for each low fract track. The expected error includes the extrapolated track resolution and the error on the estimated production point (see Eqn. 7.3). The distribution of δ/σ_δ for the low fract hadron sample is shown in Figure 8.8.

* In order to check this assumption, a study was made of the characteristics of the hadronic tracks in comparison with those in the lepton sample. It was found that the two samples are very similar in the important characteristics that determine resolution (e.g. track isolation, number of hits on the track, χ^2 values, etc.).

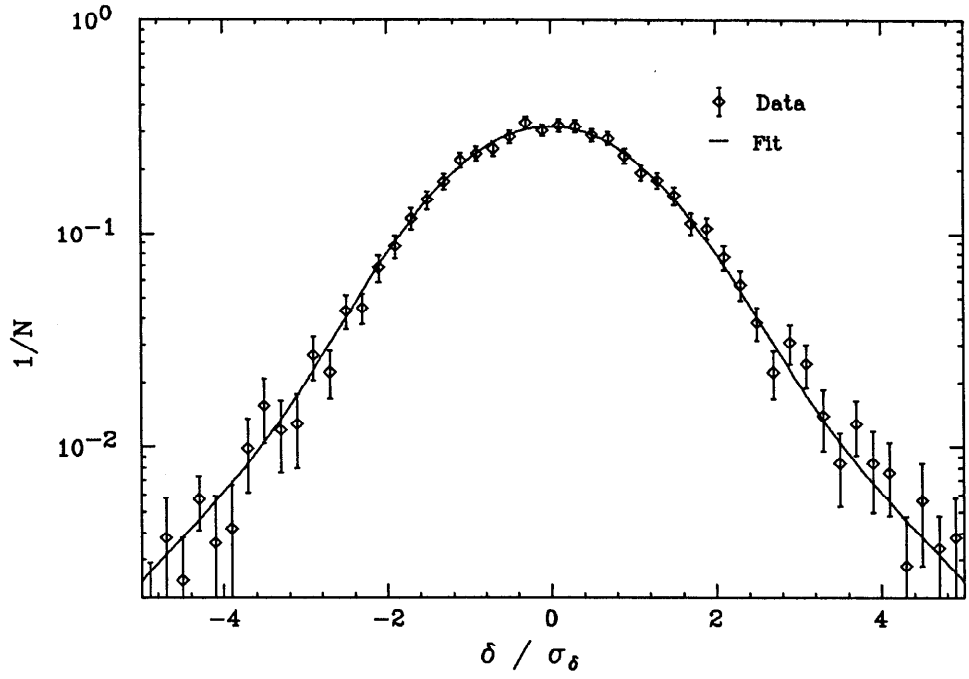

Figure 8.8: Impact parameter/error for low fract hadronic tracks. Tracks are required to be in the same (p,p_t) regions as the lepton tracks. The fit curve represents the resolution function determined from the low fract distribution for $\delta/\sigma<0$.

The mean of the δ/σ_δ distribution is 0.04, indicating that there is very little lifetime information in this distribution. (By contrast, the similar distribution for all hadronic tracks has a mean of 0.18.) The central region is well described by a Gaussian of width 1.14. This observation implies that after all of the improvements to the resolution in Chapter 4, and all of the production point methodology in Chapter 7, the expected error in the core of the distribution is understood to within 14 %.

There are significant tails to the distribution shown in Figure 8.8. To account for these tails the distribution is fit to a sum of two Gaussian functions:

$$R(\delta,\sigma_\delta) = \frac{1-x_t}{\sqrt{2\pi}(r_c\sigma_\delta)} e^{-\delta^2/2(r_c\sigma_\delta)^2} + \frac{x_t}{\sqrt{2\pi}(r_t\sigma_\delta)} e^{-\delta^2/2(r_t\sigma_\delta)^2} \quad , \qquad (8.9)$$

where r_c and r_t are parameters determined from the fit that describe the widths of the central and tail regions of the distribution, respectively. The parameter x_t is the fractional amplitude of the tail distribution.

The fit to the low fract distribution with the form given by Eqn. 8.9 is shown

in Figure 8.8, with the values $r_c = 1.09$, $r_t = 2.30$, and $x_t = 0.08$. The fit is performed only over the negative side of the distribution. It can be seen that there is only a small amount of excess on the positive side due to lifetime effects. Since thrust uncertainties flip the sign of only a fraction of the tracks, the effect of any lifetime bias in the negative half on the width of the fitted curve is negligible.

8.3 Fitting the Impact Parameter Distributions

The complete fitting function is now reviewed. This function is defined for the B and C enhanced regions separately. The probability density function describing the background contribution to the impact parameter distribution is written as:

$$f_{mis}\, P_{mis}\,(\delta^i) \;+\; f_{dk}\, P_{dk}\,(\delta^i) \quad , \tag{8.10}$$

where f_{mis} and f_{dk} are given in Table 8.1; P_{mis} is the distribution resulting from the fit to the hadronic track impact parameter distribution (Figure 8.2) and P_{dk} is given in Eqn. 8.2.

The probability density function for the prompt lepton contribution to the impact parameter distribution is written as:

$$\sum_l f_l\, P_l\,(\delta, \sigma_\delta, \tau_b/\tau_c) \;=\; \sum_l f_l \int_{-\infty}^{\infty} R\,(\epsilon - \delta, \sigma_\delta)\, F_l\,(\delta, \tau_b/\tau_c)\, d\epsilon \quad , \tag{8.11}$$

for $l = c$, b, or bc. The fractions f_l are given in Table 8.1. The physics function F_l is given in Eqn. 8.7 and the resolution function R in Eqn. 8.9. Since the convolution in Eqn. 8.11 is the integral of Gaussian and exponential functions, it can be done analytically.

The entire fitting function for a given track is the sum of the background and prompt lepton terms:

$$P\,(\delta^i, \sigma^i_\delta, \tau_b, \tau_c) \;=\; f_{mis}\, P_{mis}\,(\delta^i) + f_{dk}\, P_{dk}\,(\delta^i) + \sum_l f_l\, P_l(\delta^i, \sigma^i_\delta, \tau_b/\tau_c) \quad . \tag{8.12}$$

We now use the maximum likelihood method to find the most probable τ_b and τ_c in the data. The likelihood is defined as the product of the probability density

functions for the individual events:

$$\mathcal{L}\,(\tau_b, \tau_c) \;=\; \prod_i P\,(\delta^i, \sigma_\delta^i, \tau_b, \tau_c) \quad , \tag{8.13}$$

where i runs over electrons and muons in the B and C enhanced regions. For computational ease, $\log\,(\mathcal{L})$ is maximized with respect to τ_b and τ_c rather than the likelihood itself. The constraint equation is:

$$\frac{\partial}{\partial \tau_b}\Big(\log(\mathcal{L})\Big) \;=\; \frac{\partial}{\partial \tau_b}\Big(\sum_i P(\delta^i, \sigma_\delta^i, \tau_b, \tau_c)\Big) \;=\; 0 \quad , \tag{8.14}$$

and similarly for τ_c .

8.4 Results of the Fits

The fit to the lepton samples in both the B and C enhanced regions gives $\tau_c = 0.74^{+0.14}_{-0.12}$ ps and $\tau_b = 0.98 \pm 0.12$ ps. The two dimensional log likelihood contour for this fit is shown in Figure 8.9. This plot indicates that both τ_b and τ_c are comfortably excluded from having values of zero.

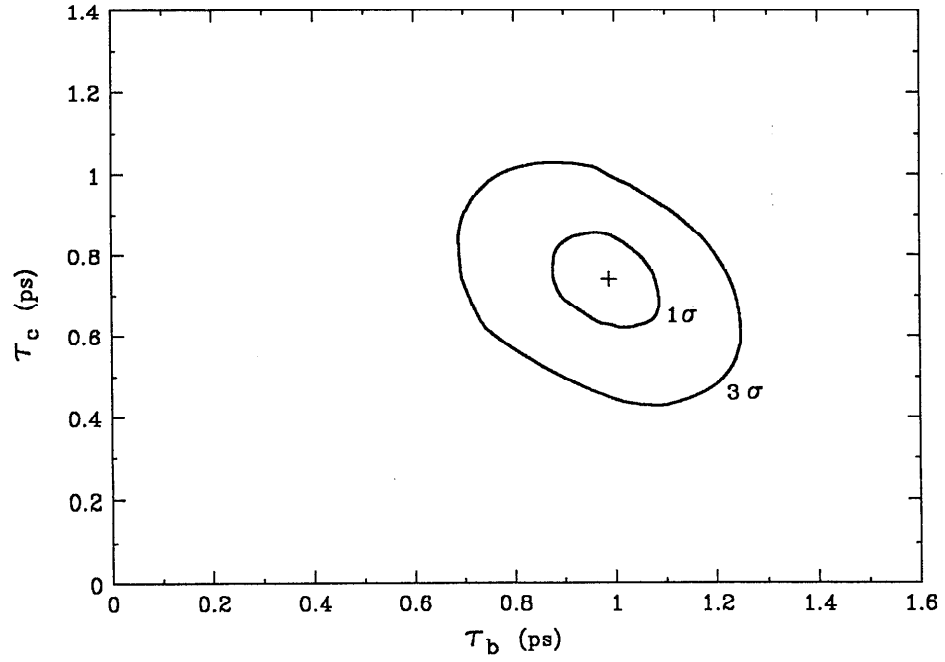

Figure 8.9: Two dimensional log likelihood contours. The 1σ and 3σ contours come from the fit to all leptons in both B and C enhanced regions.

A number of various other fits are also performed, as shown in Table 8.4. Fits are made to the B and C enhanced regions separately, and then to each region with fixed values of τ_b and τ_c . These fits in general agree well with the combined fit allowing both τ_b and τ_c to vary.*

Table 8.4: Lifetime fit results.

Fit made	τ_b (ps)	τ_c (ps)
Both B and C regions	0.98 ± 0.12	0.74 ± 0.13
B region only	1.06 ± 0.13	0.62 ± 0.17
B region only; fix $\tau_c = 0.74$	1.03 ± 0.12	-
C region only	0.83 ± 0.18	0.94 ± 0.16
C region only; fix $\tau_b = 0.98$	-	0.67 ± 0.13

We therefore have confidence that the data is self-consistent in the two regions. For the final lifetime answers, we use the combined fit to both regions:

$\tau_b = 0.98 \pm 0.12$ ps

$\tau_c = 0.74 \pm 0.13$ ps

(Statistical errors only)

The B hadron lifetime is determined with a statistical precision of 12 %; the charm hadron lifetime determination has a statistical precision of 18 %. In principle, we could get a slightly better statistical precision on τ_b by fixing the value of τ_c and fitting in both regions.

The log likelihood contour in the combined region fit is shown in Figure 8.10, as a function of the B lifetime. The statistical errors on the lifetimes correspond to

* The fit that produces lifetime values most different from $\tau_b = 0.98$ ps and $\tau_c = 0.74$ ps is that in the C enhanced region allowing both lifetimes to vary. This difference is not significant because the B fraction is small in this region and its mean impact parameter is not much different from than of charm.

a log likelihood change of 0.5. In the following chapter, we check to make sure that these statistical errors are reasonable given the sample size.

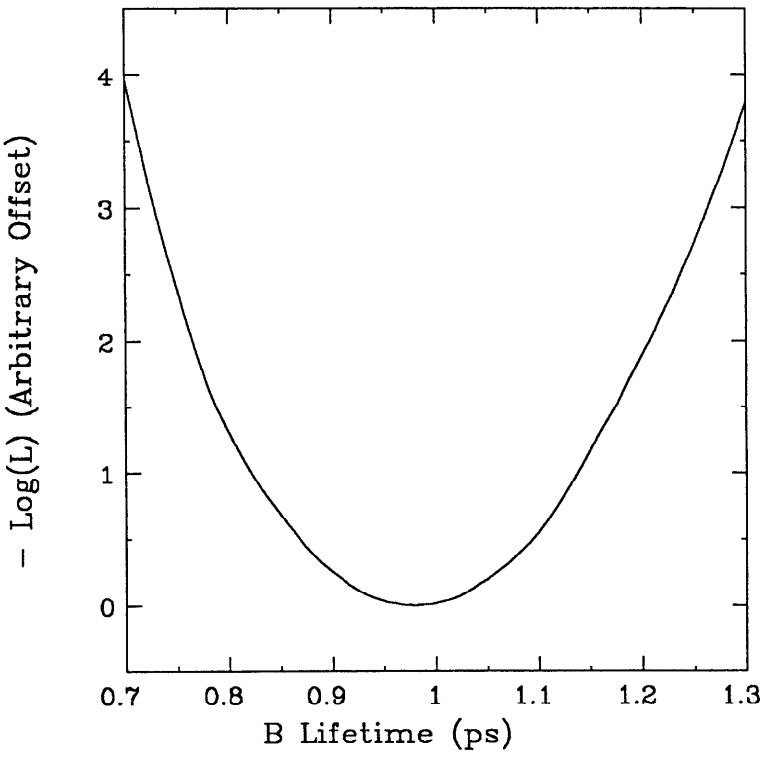

Figure 8.10: Log likelihood contour as a function of τ_b . The 1σ statistical errors on the B lifetime are determined from this contour.

The final fit to the lepton impact parameter distribution in the B enhanced region in shown in Figure 8.11. The similar fit in the C enhanced region in shown in Figure 8.12. These figures indicate that the fitting function provides a good description of the data.

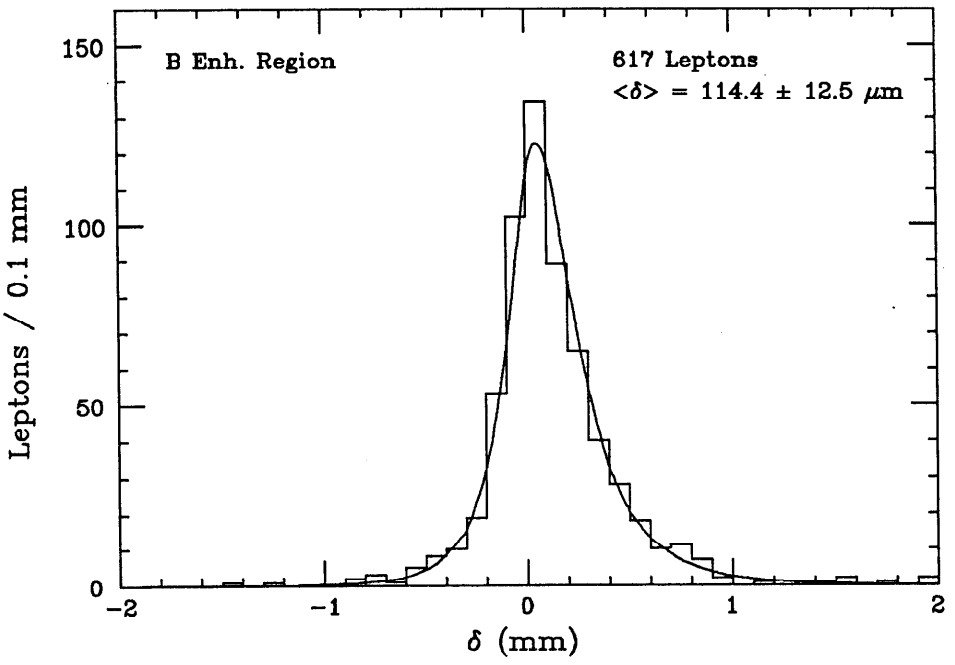

Figure 8.11: Fit to lepton impact parameter distribution, B enhanced region. The curve drawn comes from the fit to both regions simultaneously.

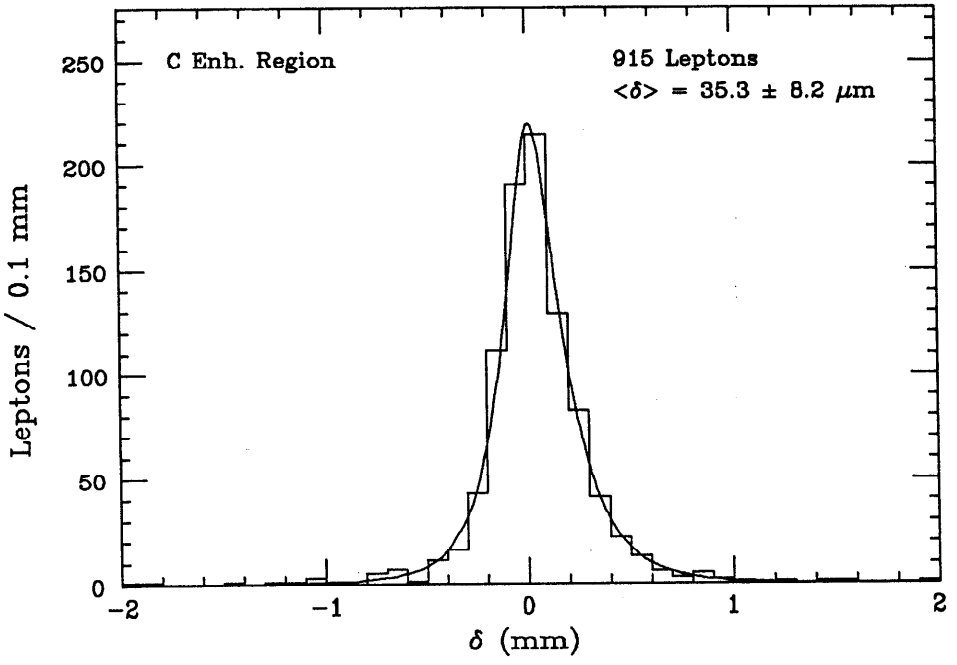

Figure 8.12: Fit to lepton impact parameter distribution, C enhanced region. The curve drawn comes from the fit to both regions simultaneously.

Checks and Systematic Errors

Now that the B and C hadron lifetimes have been determined from the fit, we make a number of checks to verify that the analysis and fitting procedures are robust. We concentrate in this chapter on checks of the B lifetime determination and make an estimate of the systematic uncertainty in the lifetime determination.

9.1 Checks on the Analysis and Fitting Procedures

9.1.1 Average charm lifetime

The average charm lifetime is measured to be $\tau_c = 0.74 \pm 0.13$ ps. This value is quite consistent with the expected value of 0.68 ps (see Eqn. 3.5), providing checks on the lepton (p, p_t) analysis, the impact parameter techniques, and on the assumed value of $< z >$ of the charm fragmentation function.

9.1.2 Two-photon cuts

In the lepton analysis, a set of cuts is imposed to remove two-photon background events. These cuts are described in detail in Appendix B. The impact parameter distribution for electrons in the events removed by these cuts is shown in Figure 9.1. Since 70 % of these events are in the B enhanced region, we expect an average impact parameter of $\sim 85\ \mu$m , if the events were all hadronic in nature. An

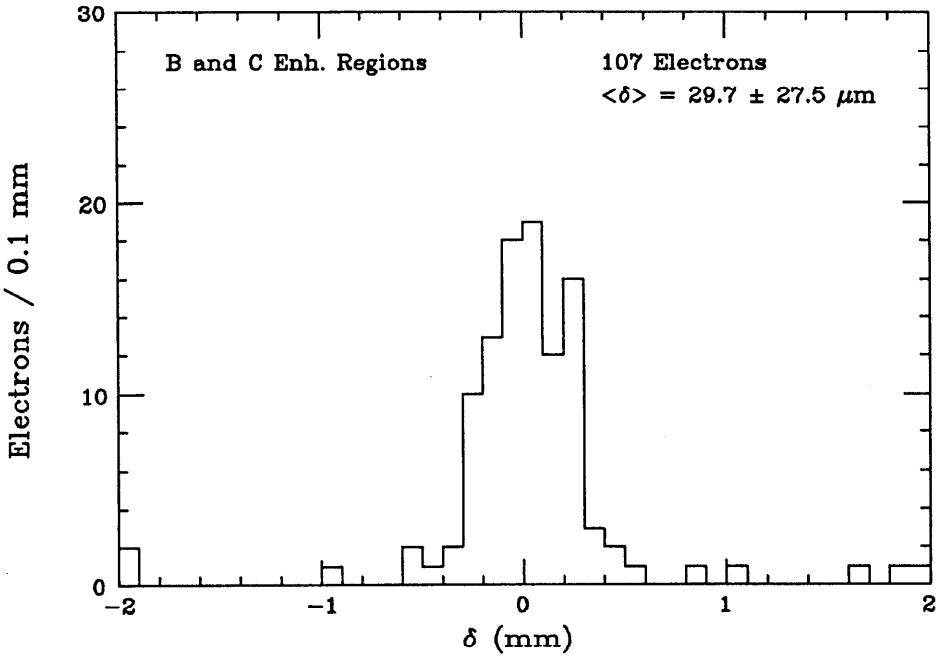

Figure 9.1: Electron impact parameters, events removed by two-photon cuts.

average impact parameter of $29.7 \pm 27.5\,\mu$m is observed, indicating that the events have a sizable two-photon contribution.*

9.1.3 *Tau lifetime determination*

As a check on the impact parameter techniques used in this analysis, we measure the lifetime of the τ lepton. Because the τ commonly decays to one or three charged particles, it is relative easy to isolate a sample of τ pair events with low background. In this analysis, we select 1-3 and 3-3 τ events using previously described selection criteria [55]. In each event the production point is found using the formalism introduced in Chapter 7. The thrust axis is used to estimate the τ direction. The impact parameter for each track in these events with momentum greater than 500 MeV/c is measured relative to the production point. The tracks are required to pass the same quality cuts that are placed on the leptons. After all cuts, a total of 2906 tracks remain in 1248 events. The impact parameter distribution for these tracks is shown in Figure 9.2. The mean of the distribution is $61.2 \pm 4.4\,\mu$m.

* Although the two photon-cuts are not applied to the muon sample, it is instructive to examine the impact parameter distribution of muons that *would* fail the cuts. This distribution is found to have a mean of $82.3 \pm 43.1\,\mu$m, consistent with the expected value.

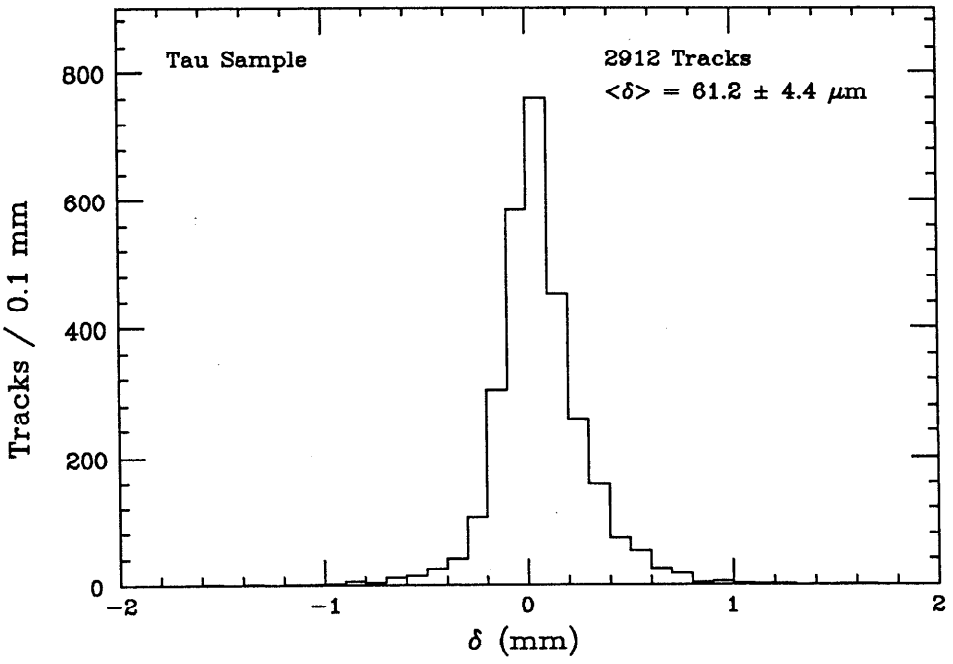

Figure 9.2: Impact parameters for tracks in tau events. The impact parameter is measured relative to the estimated production point. Tracks in this figure are required to have momentum greater than 1 GeV/c.

The τ lifetime is determined by calibrating the impact parameter distribution with samples of Monte Carlo produced events. We use events produced at three different lifetime values: 0.0, 1 τ_o, and 2 τ_o, for τ_o = 0.286 ps. The lifetime is determined by comparing the mean impact parameter measured in the data with the values measured in the three Monte Carlo samples, as illustrated in Figure 9.3. We place a cut of 2.0 mm on the absolute impact parameter. The average impact parameter measured in the data corresponds to a τ lifetime of 0.282 ± 0.020 ps. However, we must account for a background contamination in the data sample from two-photon and low multiplicity hadronic events. This background is estimated to be $3.8 \pm 1.4\,\%$ of the number of events. The background events can be expected to have a short lifetime, therefore their presence raises the measured lifetime value slightly to 0.293 ± 0.021 ps.*

The systematic error in the lifetime determination comes from a number of sources. One contribution comes from possible measurement bias. The mean of the impact parameter distribution for events in the zero lifetime Monte Carlo is

* In determining the statistical error, we properly account for the correlated information obtained from measuring impact parameters for several tracks from a single decay.

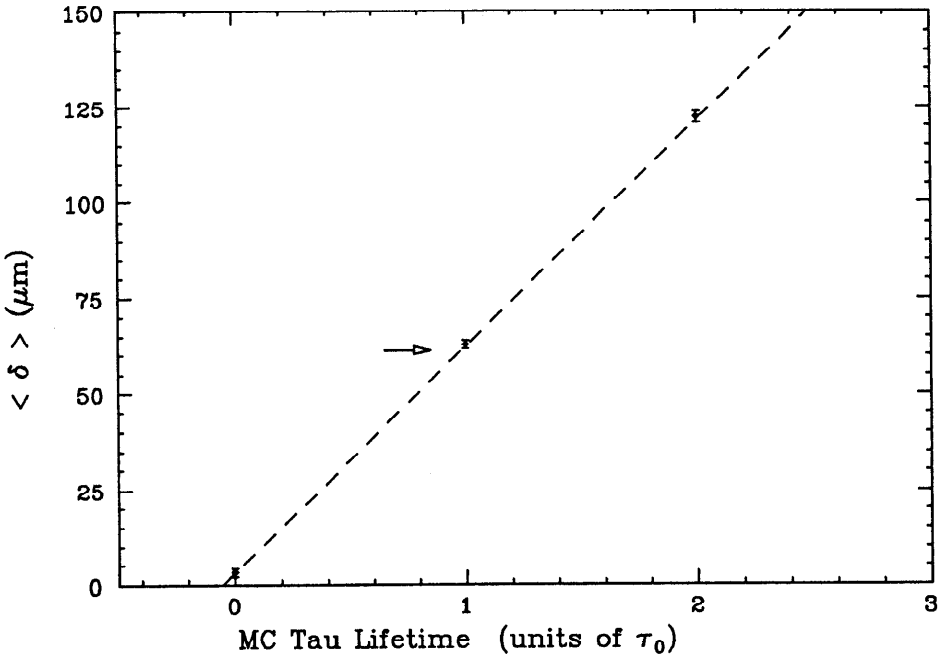

Figure 9.3: Determination of the tau lifetime. In this figure the mean impact parameter is shown for three different input lifetimes in the MC (τ_0=0.286 ps). The arrow indicates the average impact parameter measured in the data.

$3.1 \pm 1.1\,\mu$m, indicating that a small bias exists. We assume an error of 100 % in the estimation of this bias (i.e. $\pm 3.1\,\mu$m), leading to a 5 % systematic error on the lifetime determination.

Another source of systematic error comes from possible resolution effects. Since we do not use the resolution for each event in a likelihood fit, these effects are expected to be manageable, and an estimate of 4 % for such effects is deemed adequate.

The systematic uncertainty from the effect of the 2 mm impact parameter cut is estimated to be 3 %. This number is found by measuring the lifetime with a range of impact parameter cuts imposed. The uncertainty due to imperfect knowledge of the non-tau background is estimated to be 1.5 %. This number includes the possibility of the background having a non-zero lifetime contribution. The systematic uncertainty from the different effects of track quality cuts on the data and Monte Carlo track samples is estimated to be 2 %.

The systematic error for the τ lifetime measurement is found by adding the errors listed in quadrature, giving a total error of 8 %. Therefore, using the same

machinery as in the B lifetime measurement, the τ lifetime is determined to be:

$$\tau_\tau = (0.293 \pm 0.021 \pm 0.023)\ \text{ps} \quad , \tag{9.1}$$

where the first error is statistical and the second is systematic. This measured value agrees well with the current world average [80].

9.1.4 Consistency checks

A number of other checks are useful to make, purely as a matter of consistency. For example, it is valuable to compare the background impact parameter distribution in the data and Monte Carlo. Even though the data is used to estimate the background distribution, a large disagreement between it and the Monte Carlo might indicate a possible problem in the background determination. The mean impact parameters for hadronic tracks in the data and Monte Carlo are compared in Table 9.1. Although the means in the data are slightly higher, they agree within statistical error with those in the Monte Carlo.

Table 9.1: Hadronic impact parameters. In this table, the mean impact parameters for hadronic tracks in the data and MC are compared.

Region	$< \delta >$ Data (μm)	$< \delta >$ MC (μm)
B Enhanced	29.6 $\pm$ 4.8	24.6 $\pm$ 2.5
C Enhanced	15.9 $\pm$ 3.1	13.4 $\pm$ 1.8

In the previous chapter, the variable "fract" was introduced. A cut on fract was used to select a sample of hadronic tracks with minimum lifetime information. Therefore, a cut placed on the lepton tracks to *remove* the low fract contribution should enhance the lifetime effect. In Figure 9.4, the impact parameter distribution is shown for leptons with fract greater than 0.70. The mean of this distribution is $145.4 \pm 18.4\,\mu$m , a value significantly higher than that of Figure 8.11. Using the high fract sample, a value of $\tau_b = 0.95 \pm 0.14$ ps is obtained (statistical error only), agreeing with the value determined from the entire distribution ($\tau_b = 0.98 \pm 0.12$ ps).

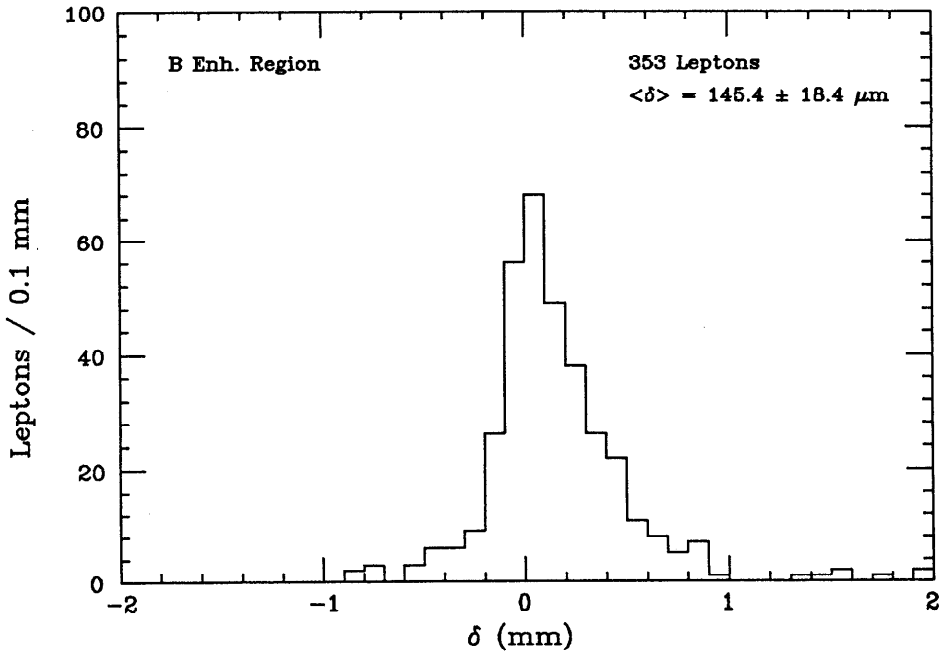

Figure 9.4: Lepton impact parameters, high fract. The leptons in this plot are required to have values of fract greater than 0.70.

To check the production point algorithm, one can compare those events in which the lepton side is used in the algorithm to those in which the non-lepton side is used. The B lifetime values determined from these two cases are consistent with one another, as shown in Table 9.2.

Finally, the impact parameter distributions for electrons and muons can be compared. These distributions are shown in Figure 9.5, normalized to the number of events. The distributions agree well with one another. The mean impact parameter of the electron distribution is $112.3 \pm 16.0\,\mu$m and that of the muon distribution is $117.9 \pm 21.1\,\mu$m . The lifetime values determined from the electron and muon samples separately are given in Table 9.2.

The only significant difference between the impact parameter distributions of the electron and muon subsets is the presence of one event in the muon sample with two tracks at large impact parameter (2.0 mm and 2.7 mm). This event is somewhat unusual and is discussed in Appendix C.

9.1.5 *Simple mean determination of the lifetimes*

In the previous chapter, a somewhat complex fit was introduced and used to

Table 9.2: Consistency checks. This table compares the B lifetime determined from various subsets of the data sample. The high fract sample consists of those leptons with fract greater than 0.7. The classification by lepton/non-lepton sides refers to the particular side used in the production point algorithm. The B lifetime from the entire data sample is measured to be 0.98 ± 0.12 ps.

Data Subset	τ_b (ps)
High fract sample	0.95 ± 0.14
Lepton side only	0.95 ± 0.14
Non-lepton side only	1.12 ± 0.17
Electrons only	0.93 ± 0.15
Muons only	1.08 ± 0.21

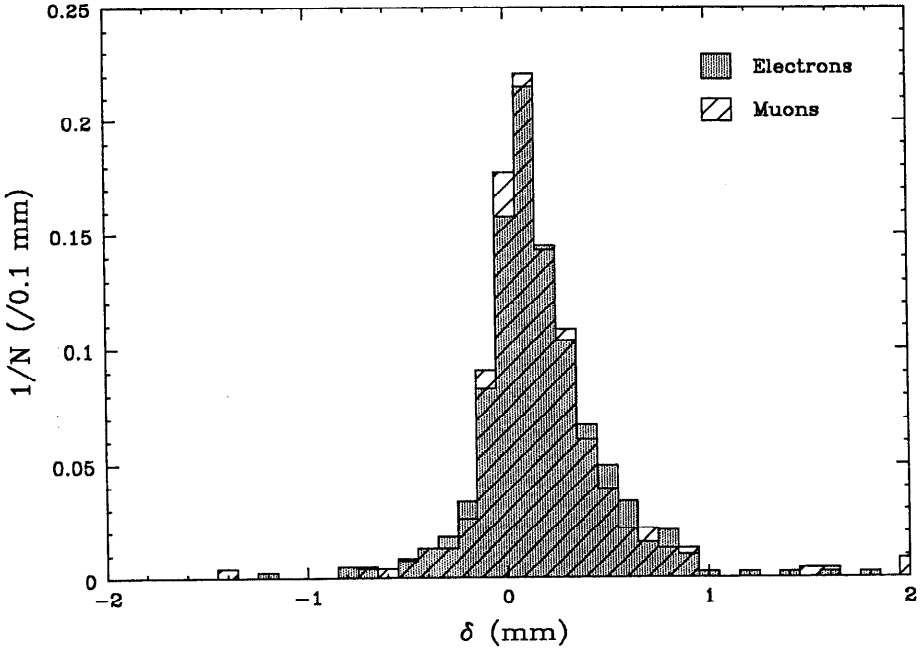

Figure 9.5: Electron and muon impact parameter distributions (normalized to the number of events).

determine the B and C lifetimes. In a simpler approach, one can calculate the lifetimes from the means of the impact parameter distributions. By taking the

mean on both sides of Eqn. 8.1, one can write:

$$\begin{aligned} < \delta >_{meas} = \; & f_{bkg} < \delta >_{bkg} + f_c < \delta >_c + \\ & f_b < \delta >_b \quad + f_{bc} < \delta >_{bc} \quad . \end{aligned} \tag{9.2}$$

The quantity $< \delta >_{meas}$ is the average measured impact parameter in the B and C enhanced regions ($114.4 \pm 12.5\,\mu$m and $35.3 \pm 8.2\,\mu$m , respectively). The fractions come from Table 8.1, with $f_{bkg} = f_{mis} + f_{dk}$. In the determination of the fractions used in Eqn. 9.2, the electron and muons values are combined weighted by their relative number of events. The average impact parameters for the background contributions are taken from Table 9.1. The average impact parameters for the prompt lepton contributions are taken from Table 8.2, and are expressed in terms of the impact parameter per unit ps of lifetime.

Using these inputs, Eqn. 9.2 can be written for the B and C enhanced regions separately, with τ_c and τ_b as independent variables. Two equations and two unknowns result:

$$\begin{aligned} \tau_c + 0.25\,\tau_b &= 0.99 \quad \text{(C Region)} \quad , \\ \tau_c + 8.36\,\tau_b &= 9.88 \quad \text{(B Region)} \quad , \end{aligned} \tag{9.3}$$

with τ_c and τ_b in ps. These two equations are illustrated graphically in Figure 9.6; lines are drawn to represent the solutions to the equations. The slopes of the lines indicate the degree to which τ_c and τ_b are coupled. In the B enhanced region, the value of τ_b is almost completely independent of τ_c . Approximately 90 % of the impact parameter information in the B region is determined by τ_b . In the C enhanced region, the value of τ_c is significantly coupled to that of τ_b. Approximately 63 % of the impact parameter information in the C region is determined by τ_c. (In these percentages, we account for the background contribution.)

The intersection of the two lines in Figure 9.6 gives mean lifetime values of $\tau_b = 1.10 \pm 0.17$ ps and $\tau_c = 0.72 \pm 0.21$ ps. These values are consistent with those given obtained from the maximum likelihood fit.

9.1.6 *Measuring τ_b in the Monte Carlo*

As an check on the entire lifetime determination, it is essential to accurately measure the B lifetime in the Monte Carlo, for a range of input lifetimes. To make

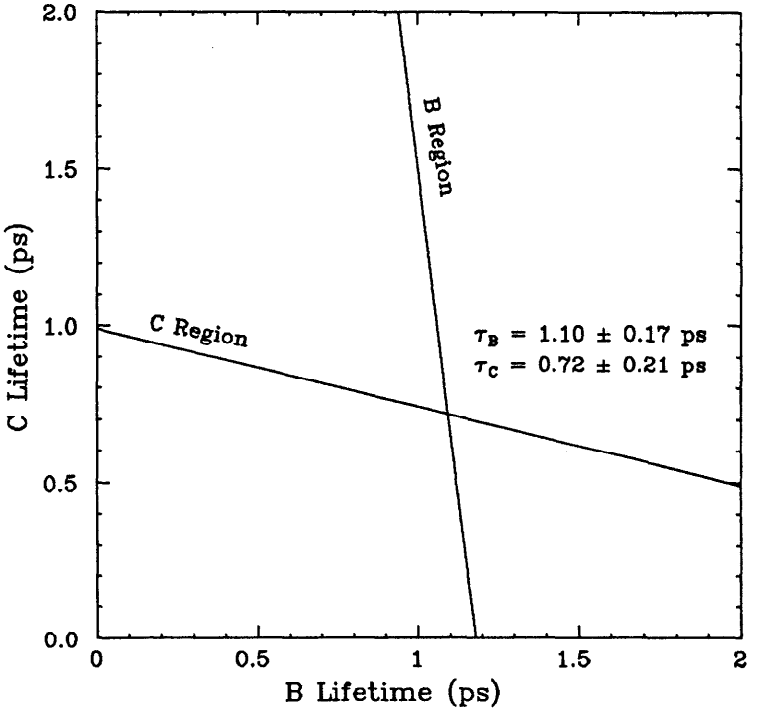

Figure 9.6: Simple mean calculation. This figure shows the determination of τ_b and τ_c from the means of the impact parameter distributions. The lines correspond to the solutions of Eqn. 9.3 in the B and C enhanced regions.

this check, we use samples of Monte Carlo events generated at input lifetimes of $\tau_b = 0$, 1, 2 and 3 ps. Each sample has at least four times the statistics of the data. The events are passed through the same analysis and fitting programs that are used on the data, except that the resolution function in the Monte Carlo is taken to be a unit width Gaussian.* The B lifetime values determined from the MC samples are shown in Figure 9.7. There is good agreement between the input lifetime and the value determined from the entire analysis procedure.

9.1.7 Checking the statistical errors

From the maximum likelihood fit, the B lifetime is determined with a precision of 12 %. Is this precision reasonable given the size of the lepton sample used in this analysis? To answer this question, we use a set of 50 test "experiments", generated with the help of the Monte Carlo. Each experiment contains the equivalent sample

* Based on the comprehensive studies in Chapter 4, it was found that any possible resolution degradation in the Monte Carlo (due to pattern recognition for example) is much less significant than the degradation observed in the data (largely due to cross-talk).

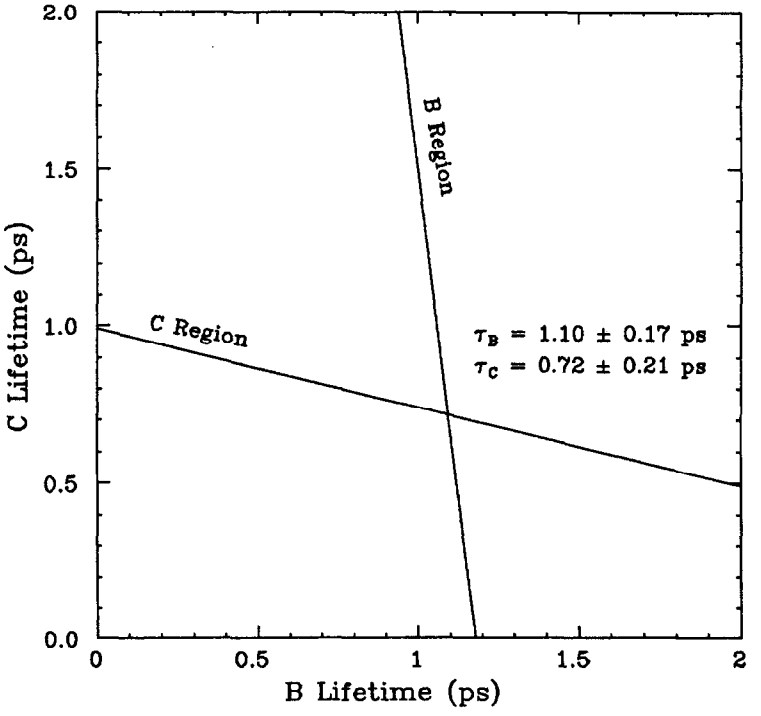

Figure 9.6: Simple mean calculation. This figure shows the determination of τ_b and τ_c from the means of the impact parameter distributions. The lines correspond to the solutions of Eqn. 9.3 in the B and C enhanced regions.

this check, we use samples of Monte Carlo events generated at input lifetimes of $\tau_b = 0$, 1, 2 and 3 ps. Each sample has at least four times the statistics of the data. The events are passed through the same analysis and fitting programs that are used on the data, except that the resolution function in the Monte Carlo is taken to be a unit width Gaussian.* The B lifetime values determined from the MC samples are shown in Figure 9.7. There is good agreement between the input lifetime and the value determined from the entire analysis procedure.

9.1.7 Checking the statistical errors

From the maximum likelihood fit, the B lifetime is determined with a precision of 12 %. Is this precision reasonable given the size of the lepton sample used in this analysis? To answer this question, we use a set of 50 test "experiments", generated with the help of the Monte Carlo. Each experiment contains the equivalent sample

* Based on the comprehensive studies in Chapter 4, it was found that any possible resolution degradation in the Monte Carlo (due to pattern recognition for example) is much less significant than the degradation observed in the data (largely due to cross-talk).

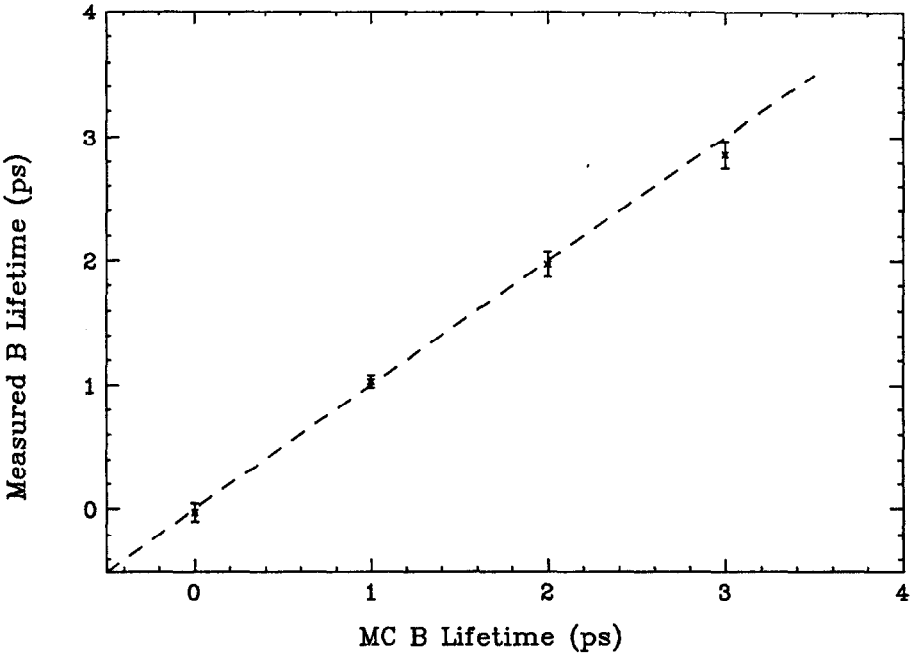

Figure 9.7: Measuring the B lifetime in the Monte Carlo. The measured value of τ_b is shown for various input lifetimes in the Monte Carlo.

of prompt leptons as used in the data. An input lifetime value of $\tau_b = 1$ ps is used for the test experiments.

For each experiment, a value of τ_b is determined, along with a statistical error σ_τ. The distribution of $(\tau_b - \tau_o)/\sigma_\tau$ (where $\tau_o = 1$ ps) is consistent with a unit width gaussian. This fact indicates that the statistical errors are being evaluated correctly. In addition, the average statistical error found from the test experiments is 10.5 %; therefore the error of 12 % found from the fit to the data is reasonable.

9.2 Systematic Errors

As a result of the various checks just described, we have confidence that the B lifetime measurement is sound and largely bias-free. Still, it is not completely free from systematic uncertainty. For example, the lepton fractions are not known with perfect accuracy, nor is the mean B hadron energy. We expect an error in the lifetime determination from systematic effects; in this section we *estimate* that error. The systematic error associated with the C lifetime measurement is summarized at the end of this chapter.

There is no well prescribed method for determining the systematic error due to

a particular parameter (call it x). In this analysis, two different methods are used. In the first method, the B lifetime measured in the data is studied varying the parameter x within its expected one sigma range. In the limit of infinite statistics, this method should work well. However, its accuracy can be influenced by statistical fluctuations and constraints imposed on the data.*

The second method to estimate systematic effects is to use a Monte Carlo sample with high statistics to determine a "correlation coefficient" that describes the coupling of uncertainty in x to uncertainty in the lifetime. This method works well if the Monte Carlo provides a good representation of the data. It also has the advantage that systematic errors can be easily estimated without having to refit the data many times. In this analysis, if possible, we use both methods to calculate systematic errors, and the larger value so determined is taken. It is found in most cases that the second method gave more conservative (i.e. larger) values for the estimated systematic errors.

9.2.1 Uncertainty in the lepton fractions

In Table 8.1, the fractions for the various contributions to the lepton signal are given, along with their estimated errors. These errors reflect the combined statistical and systematic uncertainties in the fractions resulting from the inclusive lepton fit. The errors include contributions from sources that do not affect the B lifetime measurement. For example, contributions to the fraction errors from the overall normalization (efficiencies, luminosity, etc.) cancel out in the determination of the B lifetime. The fraction errors also include uncertainty in the charm fragmentation function to be considered in the following section. Therefore, by using the errors given in Table 8.1, we place a conservative upper limit on the systematics due to uncertainty in the fractions.

The systematic effects due to the fractions are itemized in Table 9.3. This table lists the various fractions in the B and C enhanced regions and their one sigma errors. These errors are used to determine the fractional change in the B lifetime by means of appropriate correlation coefficients. For example, the correlation

* For example, suppose the uncertainty in the background is dominated by a peculiar background shape (as determined from the data) rather than by the calculation of the background fraction. Variation of the background fraction by a substantial amount may then have little effect on the measured B lifetime. With a different background shape the effect could be substantial.

Table 9.3: Systematic errors due to uncertainty in the lepton fractions. In this table, the percentage error on each fraction is given. This percentage error is passed on to the B lifetime measurement by the appropriate correlation coefficient determined from the Monte Carlo. (The mis-identification and decay fractions are combined, as are the primary and secondary bottom fractions. Since the fractions are constrained to add up to one, we need only consider the variation of two fractions in each region.)

Quantity	Nominal value and range	% Change	Correlation Coefficient	$\Delta\tau_b / \tau_b$ (%)
B Region f_b	e: 63.7 ± 5.5 μ: 64.4 ± 5.2	8.4	-0.76	6.4
B Region f_{bkg}	e: 15.5 ± 3.7 μ: 19.6 ± 4.2	23.1	$+0.21$	4.9
C Region f_c	e: 56.2 ± 5.3 μ: 51.1 ± 7.4	11.2	$+0.07$	0.8
C Region f_{bkg}	e: 28.7 ± 4.6 μ: 31.5 ± 6.8	17.9	$+0.04$	0.7
			Total Contribution	8.1

coefficient of -0.76 for f_b means that if the B fraction is increased by 10%, the B lifetime is lowered by 7.6%.

Table 9.3 shows that the largest systematic error is caused by uncertainty in the value of f_b in the B enhanced region. Since 90% of the impact parameter effect in this region is due to B decays, this result is not surprising. The effect of f_b on the measured value of the B lifetime is shown in Figure 9.8.

9.2.2 *Fragmentation uncertainty*

As discussed in Chapter 7, the impact parameter calibration is based on the mean B and C hadron energies, expressed in terms of the parameter $< z >$. Using the data summarized in Ref. 14, we obtain world average values of $< z_b >= 0.80 \pm 0.05$ and $< z_c >= 0.68 \pm 0.03$.* In this thesis, we use the world average value for $< z_c >$, and to be conservative, we assign it an error of ± 0.06. This error

* The errors on these $< z >$ values are somewhat more conservative than those that the authors of Ref. 14 choose to use. This conservatism reflects a reluctance to combine common systematic errors from a number of experiments in quadrature.

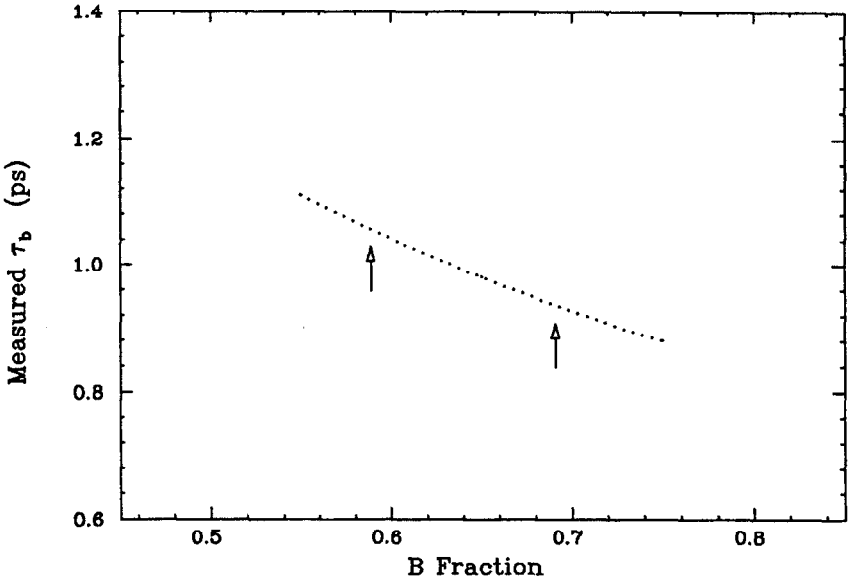

Figure 9.8: Effect of the B fraction on the measured lifetime. The arrows indicate the one sigma limits of variation.

accommodates the discrepancy between the $< z_c >$ values measured from inclusive lepton analyses and those determined from the exclusive D^* measurements.

Instead of taking the world average $< z_b >$, we use the results of the inclusive lepton fit presented in Chapter 6. This fit determined $< z_b >$ values of $0.85 \pm 0.03 \pm 0.05$ for the electron sample and $0.82 \pm 0.04 \pm 0.05$ for the muon sample. In the lifetime analysis, we use $< z_b >= 0.84$ and assign it an error of ± 0.07. This error covers any uncertainty in the exact shape of the fragmentation function (i.e. the particular parameterization used). The effect of fragmentation uncertainty on the determination of the B lifetime is shown in Table 9.4.

Table 9.4: Systematic errors due to uncertainty in fragmentation.

Quantity	Nominal value and range	% Change	Correlation Coefficient	$\Delta\tau_b / \tau_b$ (%)
$< z_b >$	0.84 ± 0.07	8.4	-0.61	5.1
$< z_c >$	0.68 ± 0.06	8.8	-0.06	0.5
			Total Contribution	5.2

The value of the $< z_b >$ has a significant effect on the determination of τ_b, as shown in Figure 9.9. This effect is significantly smaller for the impact parameter technique to determine the B lifetime for a decay length method. Not surprisingly, the value of the charm fragmentation function has little effect on the determination of τ_b.

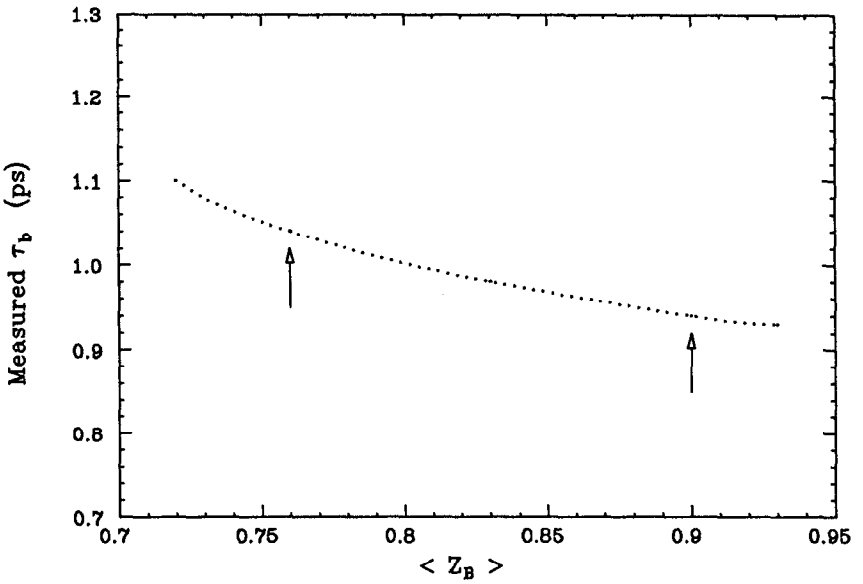

Figure 9.9: Effect of $<z_b>$ on the measured B lifetime. The arrows indicate the one sigma limits of variation.

9.2.3 *Uncertainty in the resolution*

In the previous chapter, we determined the resolution function from a fit to the impact parameter/error distribution for low fract hadrons. Studies indicate that these hadron tracks provide a good representation for the lepton tracks used in the lifetime analysis. However, the exact shape of the resolution function determined in this manner is subject to some uncertainty.

As written in Eqn. 8.9, there are three parameters describing the resolution function: σ_c, σ_t, and x_t. The variation of the measured B lifetime as a function of these parameters is shown in Table 9.5. All three parameters are negatively correlated with τ_b. An increase in the width or the amount of tails in the resolution function causes the measured B lifetime to decrease. This situation is easily understood; while the resolution function is symmetric around zero, the impact

Table 9.5: Variation of the resolution function parameters. This table shows the effect on the B lifetime from varying the parameters describing the resolution function. The statistical error in all cases is approximately 12 %.

σ_c value	τ_b (ps)	σ_t value	τ_b (ps)	x_t value	τ_b (ps)
0.89	1.07	2.00	1.01	0.04	1.02
1.09	0.98	2.30	0.98	0.08	0.98
1.29	0.90	2.60	0.96	0.12	0.95

parameter distribution reflecting lifetime is asymmetric. Therefore, any increase in the width or tails of the resolution function reduces the lifetime contribution.

The range of the three parameters is found by allowing them to vary in the fit to the low fract distribution. In Figure 9.10, for example, the range allowed for the amplitude of the tail contribution (x_t) is shown.

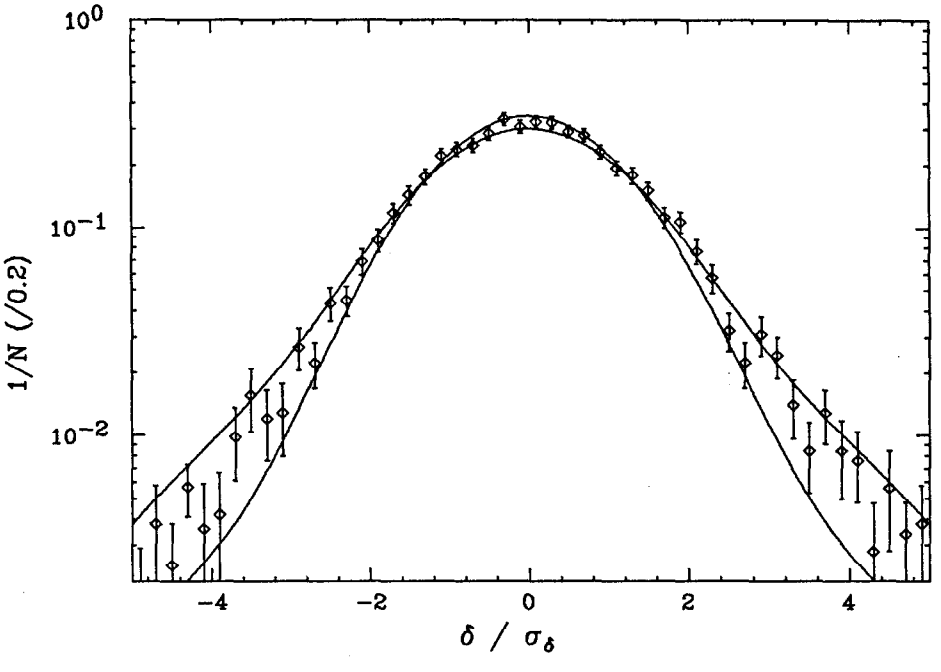

Figure 9.10: Uncertainty in the resolution function. This figure shows the impact parameter/error distribution for low fract hadrons. The lines drawn indicate the range of variation in the parameter describing the amount of tails in the resolution function.

The systematic error on the B lifetime from the variation of the resolution function is shown in Table 9.6. The overall systematic error is found by adding

the contributions from each parameter in quadrature. This combined error is certainly an overestimate of the actual uncertainty because the three parameters are negatively correlated with one another.

Table 9.6: Systematic errors due to uncertainty in the resolution function. The parameters are defined in Eqn. 8.9.

Quantity	Nominal value and range (%)	$\Delta\tau_b / \tau_b$ (%)
σ_c	1.09 ± 0.10	4.3
σ_t	2.30 ± 0.30	2.5
x_t	0.08 ± 0.04	3.5
Total Contribution		6.1

It is interesting to note that by using a unit width Gaussian for the resolution function ($\sigma_c = 1.0$ and $x_t = 0.0$), one obtains a value of $\tau_b = 1.12$ ps. Not surprisingly, we conclude that resolution effects have a significant effect on the lifetime value determined in a measurement of this type; these effects must be properly accounted for.

9.2.4 *Measurement bias and analysis cuts*

It is possible to have a measurement bias such that the lifetime value determined is systematically offset from the true value. For example, there could be a bias in the Vertex Chamber tracking that causes systematic impact parameter shifts. From the studies presented in Chapter 4, we assume that bias of this type is negligible in comparison with other uncertainties.

As another example, if the production point algorithm reduced the average impact parameter slightly, it could result in a shorter measured lifetime. Since the full detector Monte Carlo is used to determine the physics functions, if this type of bias existed, it should accounted for. Indeed, earlier in this chapter it was shown that the lifetime values determined in the Monte Carlo are completely consistent with the generated values. The value of the τ lifetime agrees with that measured

by other experiments. Therefore, we add no contribution to the systematic error from measurement bias.

A number of cuts are placed on the lepton sample, before the lifetime measurement is made. We make cuts associated with the production point algorithm, an overall thrust cut, and track quality cuts. The effect of these cuts on the lifetime measurement is studied by allowing them to vary over a large range. For example, the lifetime found with much looser and tighter track quality cuts agrees well with the value of 0.98 ps.*

From these studies, we conclude that the analysis cuts do not strongly affect the lifetime measurement. We have reason to believe, however, that they probably *reduce* the systematic uncertainties. The quality cuts remove poorly measured tracks; the thrust cut reduces uncertainty in the thrust direction and the contribution in the B region from $c\bar{c}g$ events.

In this analysis, a loose cut at 5 mm is made on the absolute impact parameter. This cut does not actually remove any leptons that would otherwise show up in the final sample. Therefore, the analysis is essentially free from annoying systematic error caused by the need to truncate or trim the impact parameter distribution. As an interesting exercise, the B lifetime is shown in Figure 9.11 as a function of a cut on the absolute impact parameter.

9.2.5 Thrust uncertainties

Uncertainty in the thrust direction affects the lifetime determination largely through the signing of impact parameters. The Monte Carlo is used to evaluate the effects of thrust uncertainties on the generated impact parameter distributions. However, if the thrust direction is systematically different in the data than in the Monte Carlo, it could affect the lifetime determination. Although this type of effect is somewhat hard to quantify, we make a number of checks of it.

In events with enough tracks, the thrust direction can be estimated from each jet separately. The estimates from each jet can be compared with one another in the data and Monte Carlo. From this comparison, it is found that the rms accuracy

* It might be thought that the cuts used in the production point algorithm (e.g. the cut on vertex χ^2 for three track vertices and impact parameter/error for two track vertices) might discriminate against long-lived events. To check this possibility, the cuts are removed entirely. No significant addition of positive impact parameters is observed. If the cuts are tightened substantially, the measured lifetime is only slightly decreased (to 0.95 ps).

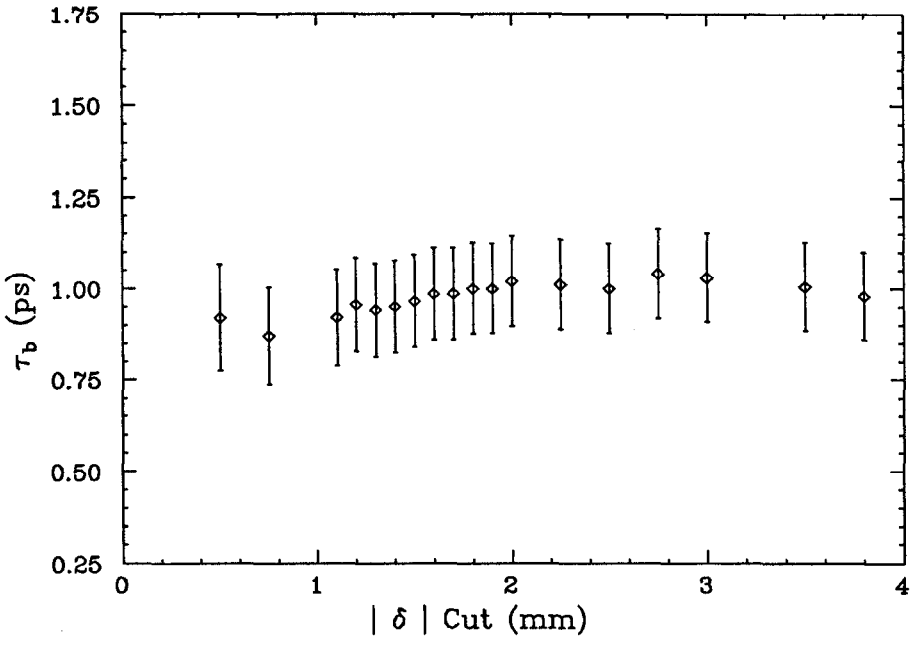

Figure 9.11: The effect of truncating the impact parameter distribution. This figure shows the B lifetime value determined from the data versus the position of a cut on the absolute value of the impact parameter.

with which a single jet determines the thrust direction is approximately the same in the data and Monte Carlo. The comparison has relatively large errors, however, and does not exactly test the right quantity.

One can study the effects of thrust uncertainty on τ_b by systematically changing the measured direction of thrust. The B lifetime is re-determined with the thrust direction moved in each event (by an amount equal to 50 % of its assumed error) in a direction towards or away from the lepton track. The lifetime is also determined assuming a 50 % larger uncertainty in the thrust direction.* The typical shift in τ_b is approximately 3 %, although greater shifts can occur if several large impact parameters change sign. In the observed impact parameter distribution, there are two leptons with $\delta < -1.0$ mm, an amount consistent with expectation. We have reason to believe, therefore, that the thrust axis simulation in the Monte Carlo is approximately correct and we assign a systematic error of 3 % due to thrust uncertainty.

* In the Monte Carlo, we artificially increase the error in the thrust axis determination by 50 % (when calculating the physics functions) and then remeasure the B lifetime from the data.

9.2.6 *Fitting procedure assumptions*

In the previous chapter, a number of assumptions are made in the impact parameter fit. Particular parameterizations are used to represent the prompt lepton physics functions (Eqn. 8.7) and the impact parameter distribution for hadronic background (Figure 8.2). In addition, the Monte Carlo is used to understand the broadening of the background distribution for leptons from decays. The assumptions made in these fits contribute negligible systematic error.

9.2.7 *Two-photon background*

In the inclusive lepton analysis, the background from the two-photon process $e^+e^- \rightarrow e^+e^-q\bar{q}$ was studied. After introducing cuts to remove most of this background, it was estimated that a contamination of approximately 2 % remained in the electron sample. In the B enhanced region alone, however, this contamination is estimated to be ~4 % of the electron sample and 3 % of the total. Since this background is not completely removed, we assign a systematic uncertainty of 3 % to the measurement of τ_b.

9.2.8 *Non-charm decays of bottom*

The physics functions used in the lifetime fit are derived assuming that B hadrons decay 100 % of the time to charm species. There is almost no difference between the impact parameter distribution for leptons from $(b \rightarrow u)$ decays and for $(b \rightarrow c)$ decays. In addition, from Eqn. 1.30, we know that possible $(b \rightarrow u)$ decays constitute less than 5 % of all bottom decays. Therefore, assuming that there are no $(b \rightarrow u)$ decays introduces negligible systematic uncertainty.

9.2.9 *Other systematic errors*

There are a number of other possible origins of systematic error. For example, there are errors caused by limited Monte Carlo statistics and by contributions to the lepton signal from sources not properly accounted for in the Monte Carlo (e.g $B \rightarrow \tau \rightarrow l$). It is assumed that the effect on the measurement of τ_b from all such sources is negligible.

9.2.10 Summary of the systematic errors

Table 9.7 summarizes the systematic errors affecting the B lifetime measurement. The largest errors come from imperfect knowledge of the resolution function and of the values of parameters obtained from the inclusive lepton analysis (the fractions and fragmentation). The errors in Table 9.7 are added in quadrature and rounded up, giving a total systematic uncertainty of $\pm 13\,\%$.

Table 9.7: Summary of systematic errors affecting τ_b .

Source	$\Delta\tau_b / \tau_b$ (%)
Lepton fractions	8.1
B and C fragmentation	5.2
Two-photon background	3.0
Thrust uncertainty	3.0
Resolution uncertainty	6.1
Total	12.2

Is it reasonable to add the systematic errors in quadrature? Of the largest contributors, the uncertainty in the resolution is almost surely independent of that associated with the inclusive lepton analysis. A significant correlation could exist between the lepton fractions and the fragmentation parameters. This correlation was investigated in the inclusive lepton analysis. It was found that the fractions and fragmentation parameters are correlated at the 10 % level or less. Therefore, although the contributions to the systematic error on τ_b are not completely independent, their correlations are small enough so as to be neglected.

The estimate of the systematic error associated with the measurement of the charm lifetime is shown in Table 9.8. The systematic errors in τ_c due to the fractions and thrust uncertainty are significantly larger than those for τ_b . This difference comes about for a number of reasons. The C region has more background than the B region, the impact parameters from C decays are not much different from those of B decay in the C region, and the overall impact parameter effect due to τ_c is only one-fourth that due to τ_b .

Table 9.8: Summary of systematic errors affecting τ_c .

Source	$\Delta\tau_c / \tau_c$ (%)
Lepton fractions	13.7
B and C fragmentation	9.5
Two-photon background	2.0
Thrust uncertainty	9.1
Resolution uncertainty	5.3
Total	19.8

Conclusions

10.1 Summary of Lifetime Results

This thesis presents a measurement of the B hadron lifetime using the Mark II detector at the PEP storage ring. The lifetime is determined from a maximum likelihood fit to the impact parameter distribution for a sample of 617 lepton tracks. The leptons are required to have momenta greater than 2 GeV/c and transverse momenta (measured relative to the thrust axis) greater than 1 GeV/c. The result of the fit is:

$$\tau_b = (0.98 \pm 0.12 \pm 0.13) \times 10^{-12} \text{ sec}$$
$$\text{(stat)} \quad \text{(sys)}$$

The fit accounts for the various contributions to the lepton sample from sources other than B hadrons. It also uses a resolution function that is determined from the data. This function accounts for non-Gaussian tails in the experimental resolution.

The systematic error in the B lifetime is dominated by uncertainty in the mean B hadron energy, uncertainty in the fraction of B hadrons in the event sample, and imperfect knowledge of the resolution function.

For consistency, using the same impact parameter analysis technique, measurements are made of the average charm hadron and tau lepton lifetimes.

The average charm lifetime is found to be:

$$\tau_c = (0.74 \pm 0.13 \pm 0.15) \times 10^{-12} \text{ sec} . \quad (10.1)$$

The tau lifetime is found to be:

$$\tau_\tau = (0.293 \pm 0.021 \pm 0.023) \times 10^{-12} \text{ sec} . \quad (10.2)$$

As discussed in Chapter 9, these results are consistent with current world averages for τ_c and τ_τ.

10.2 Inclusive Lepton Results

In a separate analysis, a complete study is made of inclusive leptons produced in hadronic events. This study uses a sample of 2631 electrons and 1230 muons with momenta greater than 2 GeV/c. By means of maximum likelihood fits to the lepton (p, p_t) distributions, the mean value of the bottom fragmentation function and the semi-leptonic charm and bottom branching ratios are determined. The results of this fit are given in Table 10.1. As discussed in Chapter 6, these results are in good agreement with current world averages of these quantities.

Table 10.1: Results from the inclusive lepton analysis.

Quantity	Electron	Muon
BR($c \to l$)	$9.6 \pm 0.7 \pm 1.5$ (%)	$7.8 \pm 0.9 \pm 1.2$ (%)
BR($b \to l$)	$11.2 \pm 0.9 \pm 1.1$ (%)	$11.8 \pm 1.2 \pm 1.0$ (%)
$< z_b >$	$0.85 \pm 0.03 \pm 0.05$	$0.82 \pm 0.04 \pm 0.05$

10.3 Other Results

A method is introduced to determine the primary production point on an event by event basis. It provides a significant statistical improvement in impact parameter resolution for lifetime measurements with large beam sizes.

A study is made of the two-photon process $e^+e^- \rightarrow e^+e^-q\bar{q}$. As outlined in Appendix A, this study finds good agreement in the cross section for this process between the data and the Monte Carlo of Behrends, Daverveldt, and Kleiss.

10.4 B Lifetimes From Around the World

Five other experiments have reported a value for the B hadron lifetime. Three of these experiments accumulated data at the PEP storage ring: DELCO, HRS, and MAC. Two experiments operated at the PETRA storage ring in Hamburg: TASSO and JADE. A summary of these experimental results is given in Table 10.2.

Table 10.2: Summary of published B lifetime results. For each experiment, the lifetime value and its reference are given. The errors given are statistical and systematic, respectively. The HRS group reports only the combined errors.

Experiment	Reference	τ_b Result (ps)
TASSO	[107]	$1.57\ ^{+0.35}_{-0.29} \pm 0.27$
JADE	[108]	$1.80\ ^{+0.50}_{-0.40} \pm 0.40$
DELCO	[109]	$1.17\ ^{+0.27\ +0.17}_{-0.22\ -0.16}$
HRS	[110]	$1.02\ ^{+0.41}_{-0.37}$
MAC	[111]	$1.29 \pm 0.20 \pm 0.21$
MARK II	This work	$0.98 \pm 0.12 \pm 0.13$

The results from the other experiments are taken from published papers or preprints [112,113]. Even though numerous previous results exist, only the latest published value from each experiment is quoted.

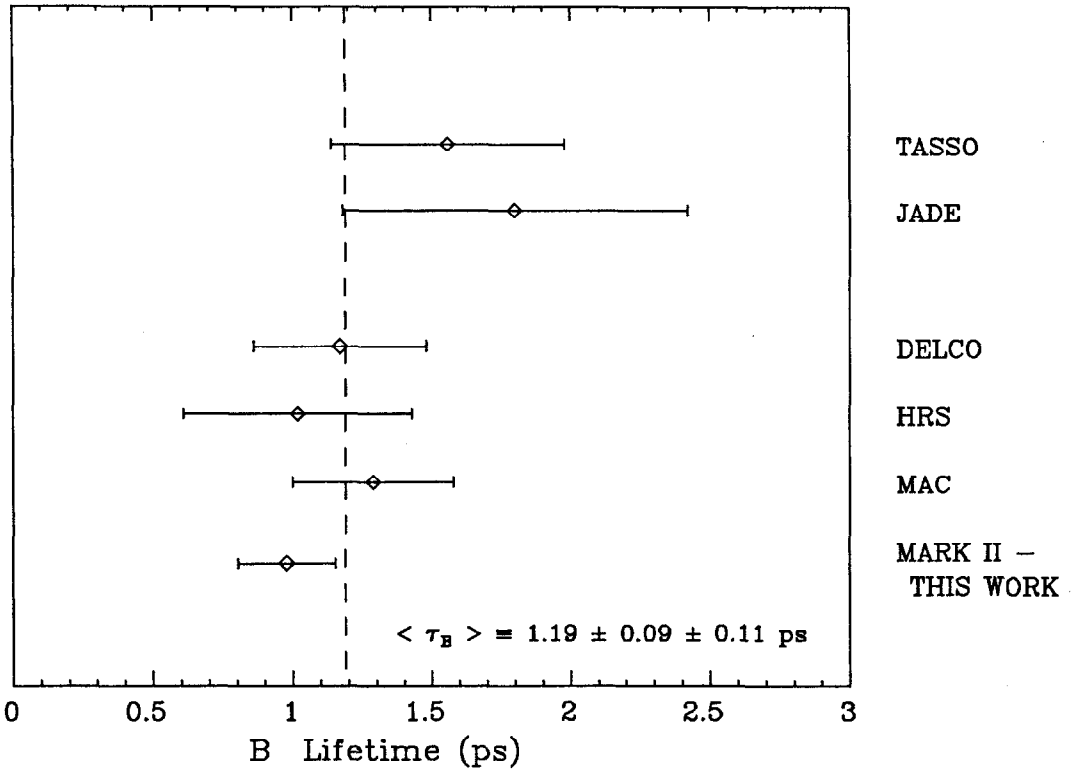

Figure 10.1: B lifetimes from around the world. In this plot the error bars drawn represent the statistical and systematic errors combined in quadrature.

The B lifetime results are presented graphically in Figure 10.1. This figure illustrates that the measurement presented in this thesis is consistent with those from other experiments.

An average lifetime from the world values given in Table 10.2 is:

$$\tau_b = (1.19 \pm 0.09 \pm 0.11) \times 10^{-12} \text{ sec} \quad . \qquad (10.3)$$
$$\text{(World Average)}$$

This world average is determined by weighting each measurement by:

$$\frac{1}{\sqrt{\sigma^2_{\text{stat}} + \sigma^2_{\text{sys}}}} \quad . \qquad (10.4)$$

Since there are common systematic errors between measurements, the systematic error on the average value is simply an estimate.

In Figure 10.2, the world average B lifetime is plotted as a function of

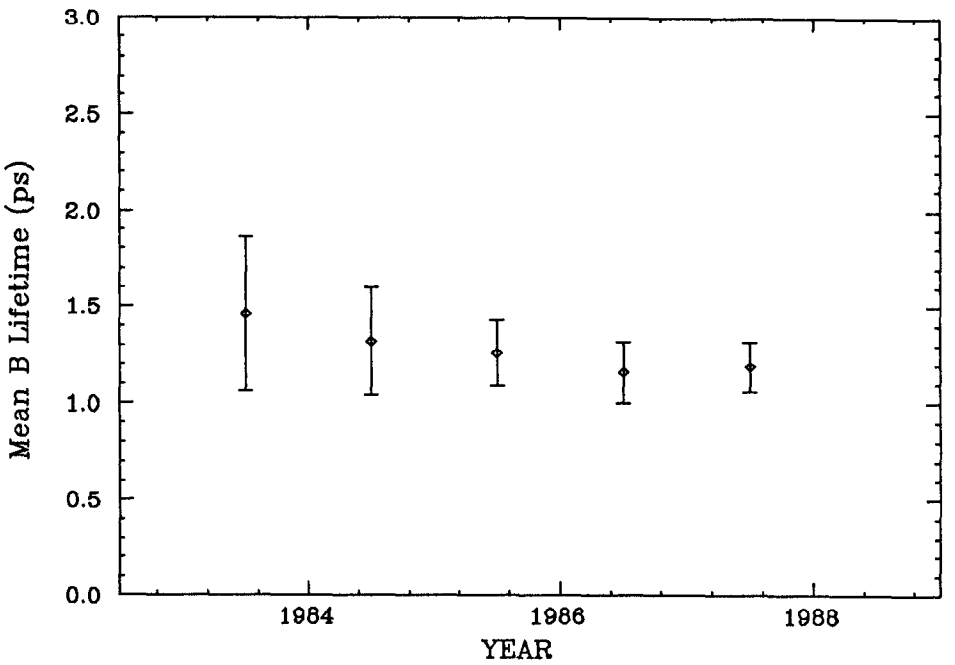

Figure 10.2: World average B lifetime as a function of time.

time [114]. This figure illustrates that there is no significant systematic drift in the average lifetime value over time.

10.5 Constraints on the Standard Model

As outlined in Chapter 1, the B lifetime can be related to two elements of the Kobayashi Maskawa (KM) matrix: $|V_{ub}|$ and $|V_{cb}|$. Inverting the expression for τ_b given in Eqn. 1.28, this relation can be written:

$$2.01\,|V_{ub}|^2 + |V_{cb}|^2 = \frac{(2.35 \times 10^{-14})\,\mathrm{BR}(B \to Xl\nu)}{\tau_b} \quad . \qquad (10.5)$$

Eqn. 10.5 is derived using the free quark model of hadron decay with $m_b = 4.95\ \mathrm{GeV}/c^2$. As discussed in Section 1.3, the value of m_b used is taken from a fit to the lepton spectrum from B decay at the $\Upsilon(4S)$ resonance. Similar expressions to that given in Eqn. 10.5 can be derived for other models of hadron decay, for example, the model of Wirbel, Stech and Bauer (Eqn. 1.24), or the model of Grinstein, Isgur, and Wise (Eqn. 1.26).

Using a B hadron semi-leptonic branching ratio of $12.1 \pm 0.8\,\%$ [80], and the B

lifetime measured in this thesis, Eqn. 10.5 becomes:

$$2.01\,|V_{ub}|^2 + |V_{cb}|^2 \;=\; (2.91 \pm 0.38 \pm 0.46) \times 10^{-3} \quad . \tag{10.6}$$

The statistical error in this relation is determined from the statistical uncertainty on the B lifetime, while the systematic error includes the uncertainty in the branching ratio, as well as the systematic error in the B lifetime. Any error from model uncertainty in the decay calculation is not included in Eqn. 10.6.

The constraints on the matrix elements $|V_{ub}|$ and $|V_{cb}|$ imposed by Eqn. 10.6, are illustrated in Figure 10.3. Also plotted in this figure is the constraint imposed by the limit:

$$0.07 \;<\; \frac{|V_{ub}|}{|V_{cb}|} \;<\; 0.23 \quad , \tag{10.7}$$

taken from Eqn. 1.30 and Eqn. 1.31.

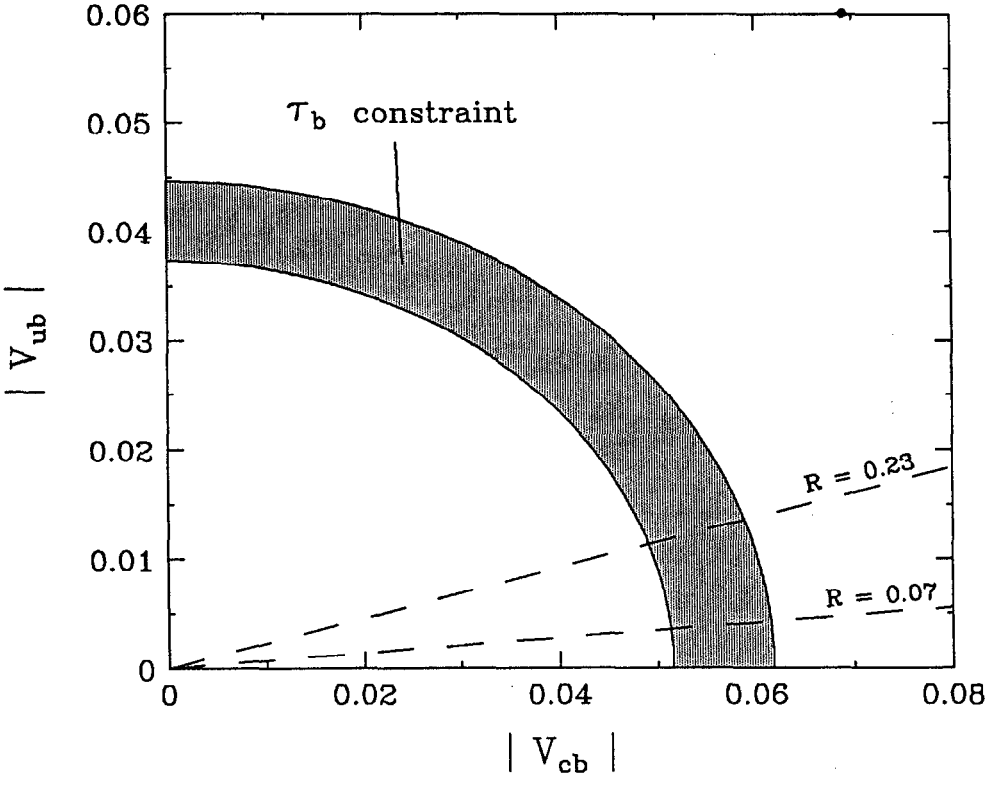

Figure 10.3: Constraints on the KM terms for B decay. The shaded band represents the constraint imposed by the B lifetime measured in this thesis. The dotted lines represent the upper and lower bounds imposed by the ratio $R = |V_{ub}|/|V_{cb}|$.

By setting $|V_{ub}|/|V_{cb}|$ equal to 0.15, one obtains a value for $|V_{cb}|$ of:

$$|V_{cb}| \;=\; 0.054 \pm 0.003 \pm 0.004 \quad . \tag{10.8}$$

The measurement of the B lifetime puts quite stringent bounds on $|V_{cb}|$. Using a value of $|V_{ub}|$ at the upper limit or lower limits of Eqn. 10.7, changes the value of $|V_{cb}|$ by only 3 %.

What have we learned about the overall KM matrix from the constraint imposed on $|V_{cb}|$? Returning to the discussion in Chapter 1, we use Eqns. 1.32 and 1.33 to write:

$$\begin{aligned} |V_{us}| &\sim s_{12} \sim 0.22 \quad ; \\ |V_{cb}| &\sim s_{23} \sim 0.054 \quad ; \\ |V_{ub}| &\sim s_{13} < 0.013 \quad . \end{aligned} \tag{10.9}$$

These relations clearly indicate that the coupling between the second and third generations is much weaker than that between the first and second. The coupling between the first and third generations is weaker still. Therefore, terms of the order $s_{ij}\, s_{jk}$ will be quite small in comparison to the corresponding c_{ij} terms. Using this fact, and setting all c_{ij} terms equal to one, Eqn. 1.33 can be written:

$$V \;=\; \begin{pmatrix} 1 & s_{12} & s_{13}e^{-i\delta} \\ -s_{12} & 1 & s_{23} \\ s_{12}s_{23} - s_{13}e^{i\delta} & -s_{23} & 1 \end{pmatrix} \quad . \tag{10.10}$$

This expression for the KM matrix is clearly a great simplification from our original one (Eqn. 1.8). Eqn. 10.10 is easy to remember and exhibits the smallness of CP violation explicitly (by the s_{13} coefficient of the $e^{i\delta}$ term).

As discussed in Chapter 1, there are other experimental quantities that one would like accommodate within the Standard Model of three quark families (e.g. $B\bar{B}$ mixing and the values of ϵ and ϵ'/ϵ). The scale of these quantities is largely set by the components of the KM matrix $|V_{td}|$ and $|V_{ts}|$. In spite of significant theoretical uncertainties, given the stringent limits on s_{23} imposed by the B lifetime and the weaker limit on s_{13}, there are few parameters in the model left to vary (e.g. δ and m_t). It is possible that following more precise experiments, the model may be hard pressed to explain all of these phenomena with a unitary quark mixing matrix.

Event Backgrounds

There are two sources of non-hadronic background in the inclusive lepton sample. The first one is two-photon hadron production, while the second one is τ pair production.

A.1 Two-Photon Hadron Production

As outlined in Chapter 6, there is a background in the inclusive lepton signal coming from the two-photon process $e^+e^- \rightarrow e^+e^-q\bar{q}$. These events appear when one of the beam electrons scatters into the central detector and the $q\bar{q}$ pair hadronizes. Fortunately, events of this type are easy to remove because of their unique topology. In order to balance transverse momentum, the hadronic shower recoils against the scattered electron. As illustrated in Figure A.1, the resulting topology is often one of an isolated electron opposite a low energy hadron jet.

In this section, the cuts used to reduce the effects of this background are discussed. With the help of a Monte Carlo simulation, we verify that the number of events removed by these cuts in the data agrees with the number expected. We then check to ensure that the remaining two-photon background is a small percentage of the lepton signal.

A.1.1 Cuts to remove two-photon background

In order to remove as much of the background as possible, we impose the set of cuts listed on the next page.

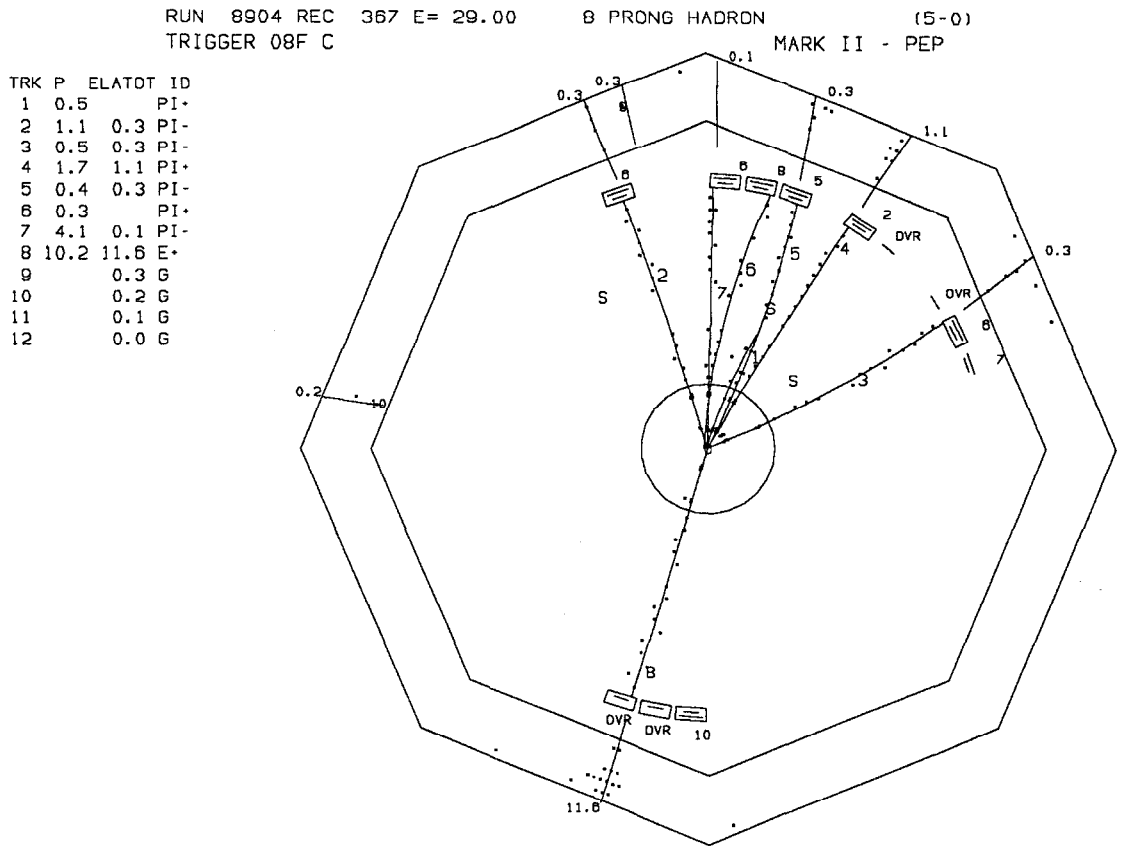

Figure A.1: A two-photon event in the data. In this event the electron is track number 8; it is well isolated and has a momentum of 10.2 GeV/c.

Two-Photon Cuts

Events are rejected if they contain an electron track that satisfies any of the following criteria:

1. $p > 9$ GeV/c.
2. $p_t > 2.5$ GeV/c.
3. $E_{LA} > 9$ GeV/c, where E_{LA} is the energy deposited in the calorimeter.
4. Track is isolated by at least 90° from the nearest charged track in the xy plane.

The cuts are chosen to take advantage of the high energy isolated electron present in most of the two-photon background events. In principle, one could also

use the fact that these events typically have a large amount of missing momentum along the beam axis. Unfortunately, this cut eliminates an unacceptable number of good hadronic events. Applying the above cuts to the data removes a total of 147 electron events. As a control study, the cuts were also applied to the muon sample resulting in 35 events removed.

A.1.2 Two-photon Monte Carlo study

The Monte Carlo program written by Berends, Daverveldt, and Kleiss [115] is used to estimate the background from two-photon processes. This Monte Carlo contains complete lowest order calculations for two-photon produced four lepton final states. The calculations are exact and are therefore valid for large lepton scattering angles. A check on the overall normalization of the program was made by a study of the process $e^+e^- \rightarrow e^+e^-\mu^+\mu^-$ Ref. 95. This study showed that the normalization of the two-photon Monte Carlo is accurate to within 20 %.

The lowest order diagrams for the process $e^+e^- \rightarrow e^+e^-q\bar{q}$ are shown in Figure A.2. The two-photon Monte Carlo is used to generate $eeq\bar{q}$ events by replacing a lepton pair with a quark pair. The quarks are then fragmented using the second order LUND matrix element scheme [68,69].

Table A.1 lists the $eeq\bar{q}$ final states considered. The cross sections listed in this table are calculated in the presence of the following cuts: one electron is required to be scattered by at least 40° with respect to the beam axis and to have momentum greater than 1 GeV/c. The other electron can scatter anywhere (it usually continues along the beam line). No cut is placed on the quark scattering angles. The $eeu\bar{u}$ channel has the largest cross section. The other quark channels are suppressed due to higher mass ($eec\bar{c}$), smaller charge ($eed\bar{d}$), or both ($ees\bar{s}$,$eeb\bar{b}$).

The detected Monte Carlo events are required to pass the hadronic event cuts listed in Chapter 6. In addition, the events are required to have a least one identified lepton with momentum greater than 2 GeV/c. The efficiency for passing these combined cuts is given in the column in Table A.1 labelled "ϵ_{cuts}". This efficiency takes into account the difference in the lepton identification efficiency between the Monte Carlo and data. The $eec\bar{c}$ and $eeb\bar{b}$ channels have larger efficiencies than the lighter quark channels because of the greater amount of energy available in the hadronic system. The final column in Table A.1 lists the number

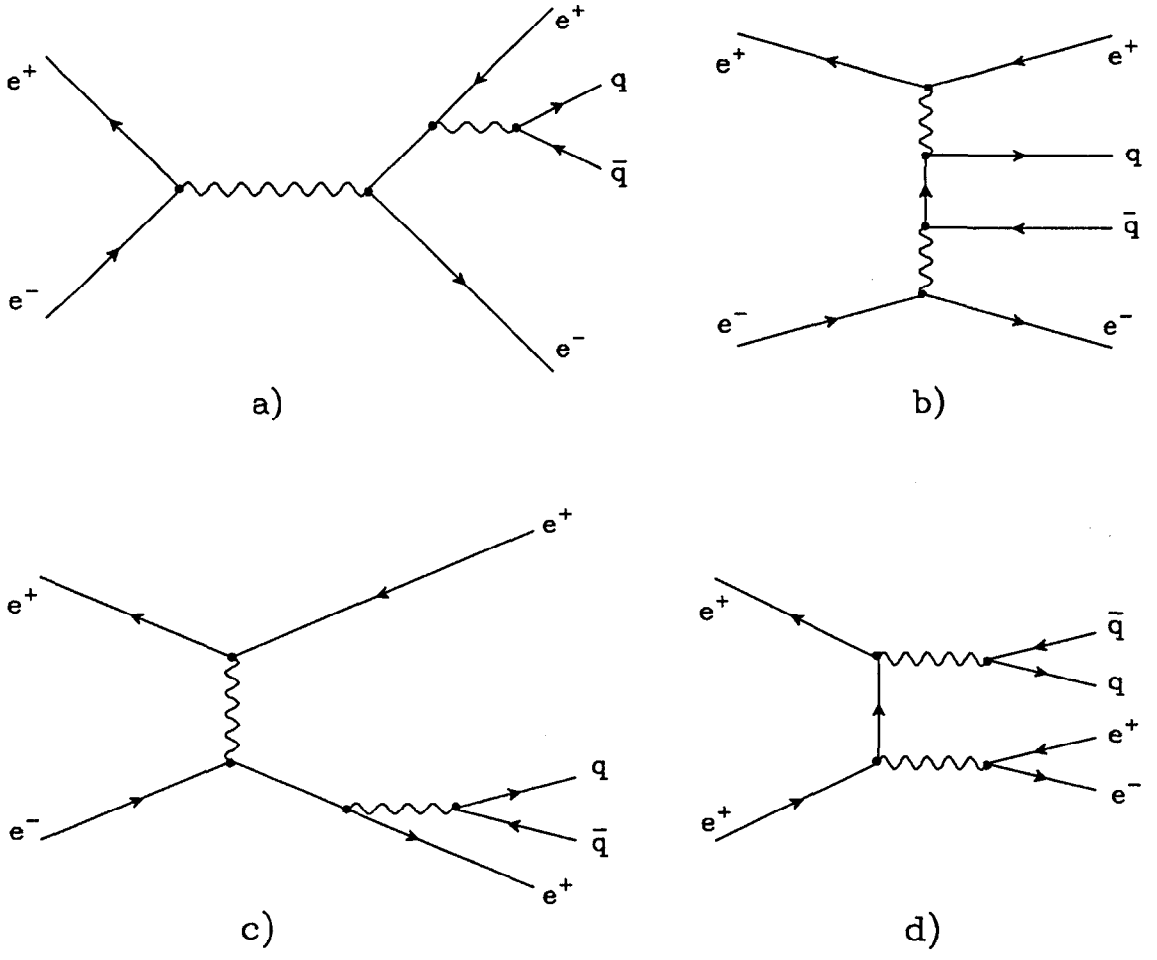

Figure A.2: Diagrams for two-photon hadron production. There are a total of 36 lowest order diagrams for the process $e^+e^- \to e^+e^- q\bar{q}$. These diagrams can be divided into four categories, as illustrated in this figure. For each category, there are numerous permutations allowed on the placement of the photons, quarks and leptons. The categories illustrated are generically referred to as: a) annihilation, b) multi-peripheral, c) bremsstrahlung, and d) conversion.

of events expected in the data from $eeq\bar{q}$ production. The errors in these numbers come from uncertainty in the determination of the cross section, the efficiencies, and the luminosity. Application of the two-photon cuts listed earlier removes most of these events. It is found that these cuts find $eeq\bar{q}$ events with $74 \pm 4\,\%$ efficiency, approximately independent of quark flavor. Using this efficiency, we expect 65.9 ± 10.2 events from two-photon production to be found and removed by the two-photon cuts. The expected number of events remaining in the lepton

Table A.1: Results from $ee q\bar{q}$ Monte Carlo study.

Mode	σ(pb)	ϵ_{cuts} (%)	Exp. # Events
$eeu\bar{u}$	7.48	3.0 ± 0.4	45.8 ± 7.0
$eed\bar{d}$	1.55	2.0 ± 0.5	6.3 ± 3.0
$ees\bar{s}$	1.13	2.4 ± 0.4	5.5 ± 2.4
$eec\bar{c}$	1.44	10.4 ± 0.8	30.6 ± 4.7
$eeb\bar{b}$	0.02	37.7 ± 4.3	1.5 ± 0.5
Total			89.7 ± 9.6

sample from $ee q\bar{q}$ production is 24.2 ± 3.6.

As a check on this prediction, it is important to compare the number of events removed by the two-photon cuts in the data and the number expected from the Monte Carlo. Not all the events removed in the data are expected to come from $ee q\bar{q}$ production. We expect some single-photon hadronic events to fail these cuts as well. In addition, there is a small contribution from τ pair events, as discussed in the following section.

The number of leptons in single-photon hadronic events expected to fail the two-photon cuts is determined using a sample of 100,000 Monte Carlo events. This sample has contributions from non-lepton sources (i.e. mis-identified and punchthrough hadrons).

The number of events from all sources expected to fail the two-photon cuts is given in Table A.2. The total number expected in the electron sample is seen to agree quite well with the number actually observed. The muon sample is included as a consistency check, even though the two-photon cuts are not used on the muons. There is a small contribution to the muon sample from the $\mu\mu q\bar{q}$ final state.

Summary:

The number of events expected in the inclusive lepton sample from two-photon hadron production is shown in Table A.3, along with the percentage of events from this source.

Table A.2: Summary of the events removed by two-photon cuts.

Mode	Electron	Muon
$e^+e^- \rightarrow e^+e^-q\bar{q}$	65.9 ± 10.1	-
$e^+e^- \rightarrow \mu^+\mu^-q\bar{q}$	-	6.9 ± 2.1
$e^+e^- \rightarrow \tau^+\tau^-$	7.5 ± 1.4	4.5 ± 1.1
$e^+e^- \rightarrow e^+e^-\tau^+\tau^-$	1.5 ± 0.4	-
$e^+e^- \rightarrow q\bar{q}$	64.9 ± 4.7	30.8 ± 2.7
Total # Expected	139.8 ± 11.2	42.2 ± 3.6
Total # Observed	147	35

Table A.3: Background from two-photon hadron production. This table lists the expected number and percentage of events in the inclusive lepton sample from two-photon hadron production.

Type	Expected # of Events	Percentage of Events
Electron	24.0	0.9 %
Muon	7.0	0.6 %

A.2 Tau Pair Production

The Feynman diagrams for possible background contributions from tau production are shown in Figure A.3.

In order for τ events to enter the inclusive lepton sample they must contain a lepton and pass the hadronic event cuts listed in Chapter 6. There are three ways in which τ pairs from single-photon annihilation can pass these requirements:

1. One τ decays leptonically and the other τ decays into five (or more) charged tracks. Since the branching ratio for τ into five charged particles is small (0.15 %), this channel does not contribute a great deal to the lepton sample. From Monte Carlo studies, the number of these events expected is 8 (5 electron and 3 muon). The electron events fail the two-photon cuts discussed

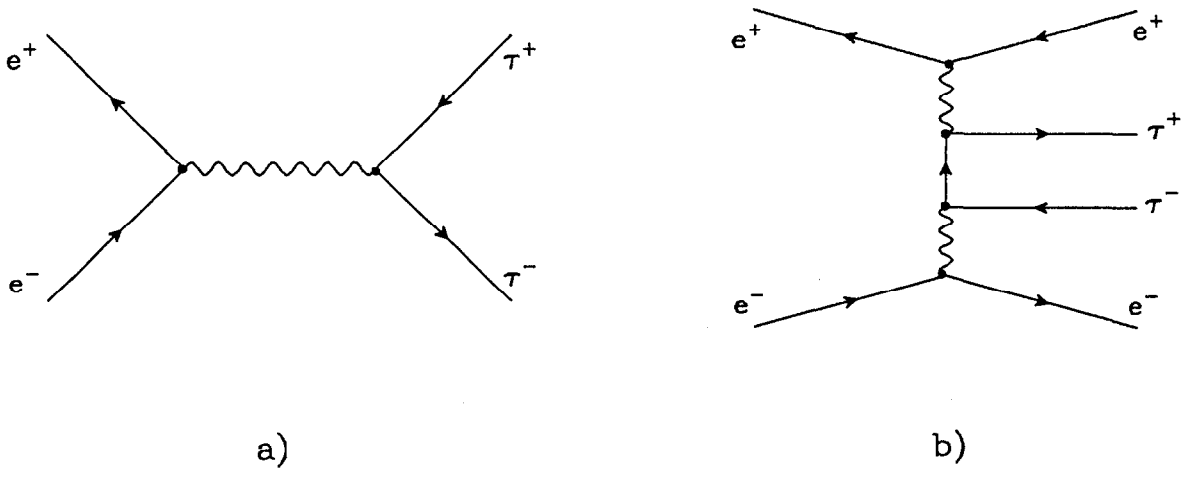

Figure A.3: Diagrams for tau pair production. This figure shows the relevant diagrams for tau pair production from a) single-photon and b) two-photon annihilation.

in the previous section.

2. One τ decays leptonically and the other τ decays into three charged particles plus one or more π^0 's. If a π^0 undergoes Dalitz decay, or produces photons that convert, it is possible to end up with enough charged tracks to satisfy hadronic cuts. For that reason all tracks used in the hadronic event selection must have VC hits and can not come from an identified pair. To estimate the remaining background from this source, a Monte Carlo τ sample equivalent to 4 times the luminosity of the data is used, predicting 4 leptons (2.5 electrons and 1.5 muons) from 1-3 (plus neutrals) τ events in the sample. The electron events fail the two-photon cuts.
3. Both τ's decay into three charged pions and one of the pions is mis-identified as an electron, punches through, or decays to a muon. The amount of this background is estimated from the measured number of 3-3 decays knowing the mis-identification, punchthrough, and decay probabilities. A total of 11 electrons and 4 muons are expected from 3-3 τ's in the lepton sample.

In addition to contributions from τ pairs from single-photon annihilation, the two-photon process $e^+e^- \rightarrow e^+e^-\tau^+\tau^-$ also contributes to the lepton sample when an electron scatters into the detector and there are enough charged tracks in the

τ pair decay to satisfy hadronic cuts. The two-photon Monte Carlo predicts 1.5 events in the electron sample from this process. Events of this type are removed by the two-photon cuts.

Summary:

The number of events expected in the inclusive lepton sample from single and two-photon produced τ pairs is shown in Table A.4, along with the percentage of events from these sources.

Table A.4: Background from tau pair production. This table lists the expected number and percentage of events in the inclusive lepton sample from τ pair production. The electron percentage is lower than the muon because of the two-photon cuts placed on the electron candidates.

Type	Expected # of Events	Percentage of Events
Electron	11.0	0.4 %
Muon	8.5	0.7 %

The Decay Length Method

The method of determining the decay lengths for short-lived particles has been discussed by a number of authors [103]. With the advent of precision vertex detectors, this method (along with impact parameter techniques) has been used in e^+e^- experiments to measure the lifetimes of the D^0, D^+, D_s^+, and B hadrons, and the lifetime of the τ lepton.

In this thesis, the decay length method is used in the algorithm to determine the B production point (see Chapter 7). The sole purpose of this algorithm is to reduce the contribution to the lepton impact parameter error from the horizontal beam size. For completeness, we summarize here the decay length method. Initially, we assume that the particle direction is known perfectly; later, we consider the effect of uncertainty in the particle direction as appropriate in the case of B hadron decays.

B.1 The Decay Length Formulae

Initially, we make a few definitions. As an illustration of these definitions, consider the decay: $\tau \rightarrow \pi\pi\pi\nu$, as shown in Figure B.1 . The τ is produced at the e^+e^- collision point, also named the *primary production point* (x_p, y_p). It travels a distance l and decays at the *decay point* (x_o, y_o). In general, the positions of the primary production point and the decay point are not known. Experimentally, the average *beam position* (x_b, y_b) and the *vertex position* (x_v, y_v) of the three pion tracks are measured. The beam position is determined by minimizing the track

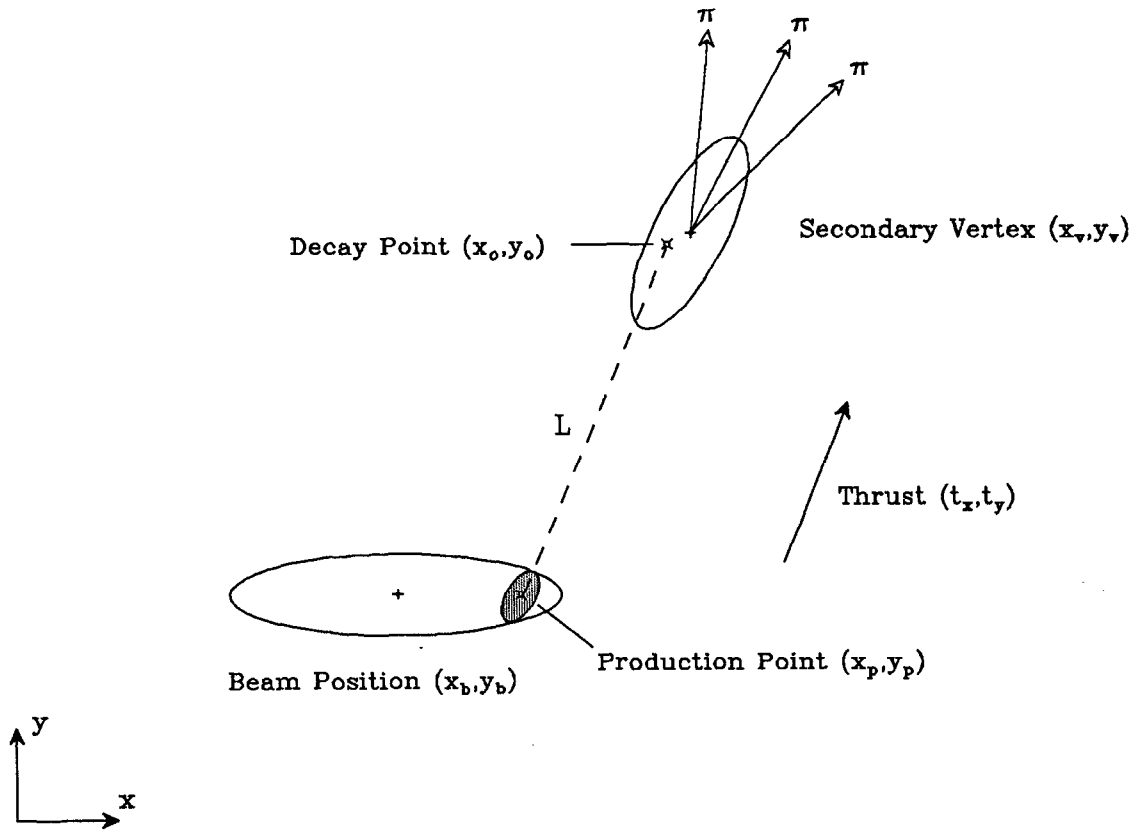

Figure B.1: Measurement of the tau decay length.

distance of closest approach over many events; it has associated with it a beam ellipse, describing the physical spread of the electron and positron beams.

An estimate of the τ direction is provided by the *thrust axis* (t_x, t_y).* This axis can be determined by the overall event thrust direction or from the momentum sum of the three pion tracks. In the following derivation, we make the assumption that the thrust direction is perfectly known, and that it coincides with the τ flight path. The decay length method is derived in the xy plane, although its extension to three dimensions is straightforward.

Define the error associated with the beam position to be the beam error matrix σ_b:

$$\sigma_b \equiv \begin{pmatrix} \sigma_{bxx} & 0 \\ 0 & \sigma_{byy} \end{pmatrix}, \qquad (B.1)$$

the terms in this diagonal matrix are the *squared* x, y beam spreads. Define the

* Note that (t_x, t_y) is normalized: $\sqrt{t_x^2 + t_y^2} = 1$.

error associated with the vertex position to be the vertex error matrix σ_v:

$$\sigma_v \equiv \begin{pmatrix} \sigma_{vxx} & \sigma_{vxy} \\ \sigma_{vxy} & \sigma_{vyy} \end{pmatrix}, \tag{B.2}$$

the terms in this matrix are the *squared* error matrix terms from the secondary vertex fit. For notational ease, it is useful to define the inverse error matrices:

$$B \equiv \sigma_b^{-1} \quad , \quad V \equiv \sigma_v^{-1} \quad . \tag{B.3}$$

The decay length method finds the most probable decay position (x_o, y_o) and the most probable production point (x_p, y_p), given the known beam position and the known vertex position, subject to the directional constraint:

$$x_o = y_p + l \cdot t_x \quad , \quad y_o = y_p + l \cdot t_y \quad . \tag{B.4}$$

To solve this problem, introduce the χ^2 notation:

$$\chi^2 = (x_p - x_b, y_p - y_b)\, B \begin{pmatrix} x_p - x_b \\ y_p - y_b \end{pmatrix} \; + \; (x_o - x_v, y_o - y_v)\, V \begin{pmatrix} x_o - x_v \\ x_o - y_v \end{pmatrix} \tag{B.5}$$

The first term in the χ^2 equation constrains the production point to the beam position given the beam errors B; the second term constrains the decay point to the vertex position given the vertex errors V. For now, assume the beam position to be at $(x_b, y_b) = (0,0)$. Substituting Eqn. B.4 into Eqn. B.5, we then get:

$$\begin{aligned} \chi^2 \; = \quad & x_p^2\, B_{xx} + y_p^2\, B_{yy} + \\ & (l \cdot t_x + x_p - x_v)^2\, V_{xx} \; + \; (l \cdot t_y + y_p - y_v)^2\, V_{yy} + \\ & 2\,(l \cdot t_x + x_p - x_v)\,(l \cdot t_y + y_p - y_v)\, V_{xy} \quad , \end{aligned} \tag{B.6}$$

where $B_{xx}, B_{yy}, V_{xx}, V_{yy}$ and V_{xy} are the appropriate components of the matrices B and V, defined in Eqn. B.3. Minimization of this χ^2 with respect to the three unknowns (x_p, y_p, l) is equivalent to simultaneously solving:

$$\frac{\partial \chi^2}{\partial x_p} \; = \; \frac{\partial \chi^2}{\partial y_p} \; = \; \frac{\partial \chi^2}{\partial l} \; = \; 0 \quad . \tag{B.7}$$

Applying Eqn. B.7 to the χ^2 formula given in Eqn. B.6, and dividing by 2 yields the linear matrix equation:

$$A\,\vec{X} \;=\; \vec{Y}, \tag{B.8}$$

where:

$$\vec{X} = \begin{pmatrix} x_p \\ y_p \\ l \end{pmatrix} \qquad \vec{Y} = \begin{pmatrix} x_v V_{xx} + y_v V_{xy} \\ y_v V_{yy} + x_v V_{xy} \\ x_v(t_x V_{xx} + t_y V_{xy}) + y_v(t_y V_{yy} + t_x V_{xy}) \end{pmatrix}$$

$$A = \begin{pmatrix} B_{xx} + V_{xx} & V_{xy} & t_x V_{xx} + t_y V_{xy} \\ V_{xy} & B_{yy} + V_{yy} & t_y V_{yy} + t_x V_{xy} \\ t_x V_{xx} + t_y V_{xy} & t_y V_{yy} + t_x V_{xy} & t_x^2 V_{xx} + t_y^2 V_{yy} + 2 t_x t_y V_{xy} \end{pmatrix} \tag{B.9}$$

The solution to Eqn. B.8 is obtained by multiplying both sides by the inverse of A. After much algebra, this procedure yields the solution for (x_p, y_p, l), given in the summary on the next page. In these expressions, we now relax the requirement that $(x_b, y_b) = (0,0)$. Any expressions for x or y simply gain an additive offset $(-x_b, -y_b)$ respectively. In addition, we consider the case where the beam error matrix is non-diagonal. The formulae given for this latter situation are useful in determining the decay lengths between two separated vertices.

It is important to note that the matrix A is simply $\frac{1}{2}$ times the matrix of second derivatives of the χ^2 equation. Thus, A is equivalent to the inverse error matrix of the quantities (x_p, y_p, l). After a lot more algebra, the errors in (x_p, y_p, l) are found by inverting A, and are given in simplified form on the next page. Also, note that the formula given for l on the next page is the projected decay length in the x-y plane. To obtain the decay length in three dimensions we need:

$$l_{\mathrm{xyz}} = \frac{l}{\sin\theta} \quad , \tag{B.10}$$

where θ is the dip angle of the particle direction. The proper decay time is then:

$$\tau = \frac{l}{\gamma\beta c \sin\theta} \quad . \tag{B.11}$$

Summary of Decay Length Method

Beam Position at (x_b, y_b), Vertex Position at (x_v, y_v)

Particle Direction in x-y plane is (t_x, t_y)

Beam and Vertex Errors:

$$\sigma_b = \begin{pmatrix} \sigma_{bxx} & 0 \\ 0 & \sigma_{byy} \end{pmatrix} \quad \sigma_v = \begin{pmatrix} \sigma_{vxx} & \sigma_{vxy} \\ \sigma_{vxy} & \sigma_{vyy} \end{pmatrix}$$

Define: $x \equiv x_v - x_b$, $y \equiv y_v - y_b$, and

$$\sigma \equiv \sigma_b + \sigma_v \ , \quad D \equiv t_y^2 \sigma_{xx} + t_x^2 \sigma_{yy} - 2 t_x t_y \sigma_{xy}$$

Decay Length (projected in xy plane:

$$l = \frac{x t_x \sigma_{yy} + y t_y \sigma_{xx} - (x t_y + y t_x) \sigma_{xy}}{D}$$

Production Point:

$$x_p = x_b + \frac{(x t_y^2 - y t_x t_y) \sigma_{bxx}}{D} \qquad y_p = y_b + \frac{(y t_x^2 - x t_x t_y) \sigma_{byy}}{D}$$

Errors:

$$\sigma_{ll} = \frac{\sigma_{xx}\sigma_{yy} - \sigma_{xy}^2}{D}$$

$$\begin{pmatrix} \sigma_{x_p x_p} & \sigma_{x_p y_p} \\ \sigma_{x_p y_p} & \sigma_{y_p y_p} \end{pmatrix} = \begin{pmatrix} \sigma_{bxx} - \frac{t_y^2 \sigma_{bxx}^2}{D} & \frac{t_x t_y \sigma_{bxx} \sigma_{byy}}{D} \\ \frac{t_x t_y \sigma_{bxx} \sigma_{byy}}{D} & \sigma_{byy} - \frac{t_x^2 \sigma_{byy}^2}{D} \end{pmatrix}$$

χ^2 at solution:

$$\chi^2_{\min} = \frac{(x t_y - y t_x)^2}{D}$$

When the beam position error matrix has the non-diagonal form

$$\sigma_b = \begin{pmatrix} \sigma_{bxx} & \sigma_{bxy} \\ \sigma_{bxy} & \sigma_{byy} \end{pmatrix},$$

the expressions given before for the decay length, the decay length error and the minimum χ^2 remain unchanged, but the expressions for the production point coordinates and their errors become:

Production Point:

$$x_p = x_b + \frac{(xt_y^2 - yt_xt_y)\,\sigma_{bxx} + (yt_x^2 - xt_xt_y)\,\sigma_{bxy}}{D}$$
$$y_p = y_b + \frac{(yt_x^2 - xt_xt_y)\,\sigma_{byy} + (xt_y^2 - yt_xt_y)\,\sigma_{bxy}}{D}$$

Errors:

$$\begin{pmatrix} \sigma_{x_px_p} & \sigma_{x_py_p} \\ \sigma_{x_py_p} & \sigma_{y_py_p} \end{pmatrix} = \begin{pmatrix} \sigma_{bxx} + \Delta_{xx} & \sigma_{bxy} + \Delta_{xy} \\ \sigma_{bxy} + \Delta_{xy} & \sigma_{byy} + \Delta_{yy} \end{pmatrix}$$

where

$$\Delta_{xx} = \frac{-(t_y\sigma_{bxx} - t_x\sigma_{bxy})^2}{D} \qquad \Delta_{yy} = \frac{-(t_x\sigma_{byy} - t_y\sigma_{bxy})^2}{D}$$

$$\Delta_{xy} = \frac{(t_x\sigma_{byy} - t_y\sigma_{bxy})\,(t_y\sigma_{bxx} - t_x\sigma_{bxy})}{D}$$

B.2 Uncertainty in the Particle Direction

In the previous section, we made the assumption that the τ direction was perfectly known. In reality, there is always some error in the determination of particle's direction from its decay products. For decays that are fully reconstructed (e.g. $D^0 \to K\pi$), that error is quite small and usually can be ignored. For decays

that contain one or more undetected particles (e.g. $\tau \rightarrow \pi\pi\pi\nu$ or $D^0 \rightarrow K\pi\pi^0$) the error may be non-negligible.

Consider the case of $\tau \rightarrow \pi\pi\pi\nu$ decays at PEP energies. The thrust direction is accurate to the true τ flight path to $\sim$ 3°. (Here we generically refer to any estimate of a particle's direction as the thrust direction.) Therefore, the extrapolation from the decay point back to the production point gains an angular uncertainty of that magnitude. For a τ decay length of 1 mm, this angular uncertainty translates to an error on the production point of $\sim 50\,\mu$m . This error must be added in quadrature with the error on the production point from the beam sizes. In addition, the position of the fitted production point changes as a result of including angular uncertainty; it tends to move toward the beam position. The effect of including uncertainty in the thrust direction is illustrated in Figure B.2.

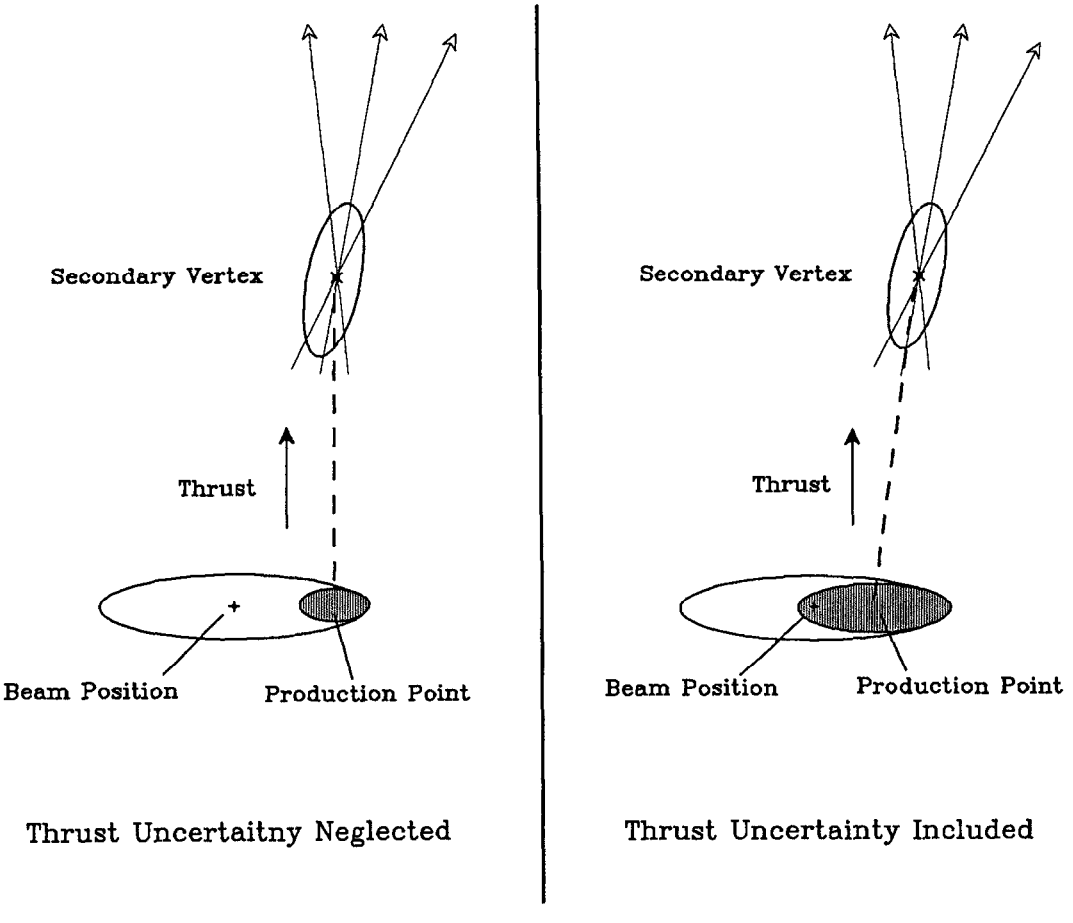

Figure B.2: The effect of including thrust uncertainties.

In this analysis, the thrust axis estimates the B hadron direction with a rms error of $\sim 9^\circ$, considerably larger than in the tau case. Therefore, it is essential to incorporate thrust uncertainty into the decay length formalism.

Since thrust uncertainty is equivalent to an error in azimuthal angle, it is reasonable to implement this uncertainty in the decay length formalism by the addition of a term:

$$\chi^2_{\rm new} \;=\; \chi^2 + \frac{(\phi - \phi_o)^2}{\sigma^2_\phi} \quad , \tag{B.12}$$

where χ^2 is given in Eqn. B.6, ϕ_o is the original azimuthal angle (a constant), σ_ϕ is the error in the thrust direction, and ϕ is the azimuthal angle that we now solve for. In particular, rewriting Eqn. B.4 as:

$$x_o \;=\; y_p + l \cdot \cos\phi \quad , \quad y_o \;=\; y_p + l \cdot \sin\phi \quad , \tag{B.13}$$

Eqn. B.6 becomes:

$$\begin{aligned} \chi^2_{\rm new} \;=\; & x_p^2\, B_{xx} + y_p^2\, B_{yy} + \\ & (l \cdot \cos\phi + x_p - x_v)^2\, V_{xx} \;+\; (l \cdot \sin\phi + y_p - y_v)^2\, V_{yy} \;+ \\ & 2\,(l \cdot \cos\phi + x_p - x_v)\,(l \cdot \sin\phi + y_p - y_v)\, V_{xy} \;+\; \frac{(\phi - \phi_o)^2}{\sigma^2_\phi} \quad . \end{aligned} \tag{B.14}$$

The value of σ_ϕ is taken from the Monte Carlo (Eqn. 3.3). Instead of three unknowns, we now have four (x_p, y_p, l, ϕ). Minimization requires:

$$\frac{\partial \chi^2_{\rm new}}{\partial \phi} \;=\; 0 \quad , \tag{B.15}$$

in addition to the conditions imposed by Eqn. B.7.

Using the same procedure as in the previous section, it is easy to construct a 4x4 matrix equation, analogous to Eqn. B.8. Unfortunately, because of the presence of terms in $\cos\phi$ and $\sin\phi$, the coefficients of the matrix A now depend on the variables (x_p, y_p, l, ϕ), making a linear solution impossible. In this analysis, the χ^2 of Eqn. B.14 is minimized by numerical methods.

The Longest Lived Event

The impact parameter distribution for leptons in the B enhanced region is shown in Figure 7.16. The two leptons with the largest impact parameters in this distribution come from the same event, recorded during the 1982-1983 run. This event is shown in Figure C.1. In one thrust hemisphere, there are two muon candidates that leave clean hits in all four layers of the muon system. In the opposite hemisphere, there is a well isolated electron candidate.

Using the charged tracks in the event, the thrust axis is determined to be:

$$t_x = 0.848 \ , \ t_y = -0.529 \ , \ t_z = 0.017 \ . \qquad (C.1)$$

The low value of t_z indicates that the event lies largely in the plane perpendicular to the beam direction. All three leptons have transverse momentum greater than 1.0 GeV/c, measured relative to the thrust axis. Each lepton passes track quality cuts and appears in the final lifetime sample.

The impact parameter for each track is measured relative to an estimated production point, as discussed in Chapter 7.* These impact parameter values are listed in Table C.1, along with relevant kinematic details about each track.

The two muon candidates balance one another in transverse momentum and have relatively large impact parameters. Their tracks form a good vertex in three

* In this event, the jet vertex in the hemisphere containing the electron track is used to determine the production point.

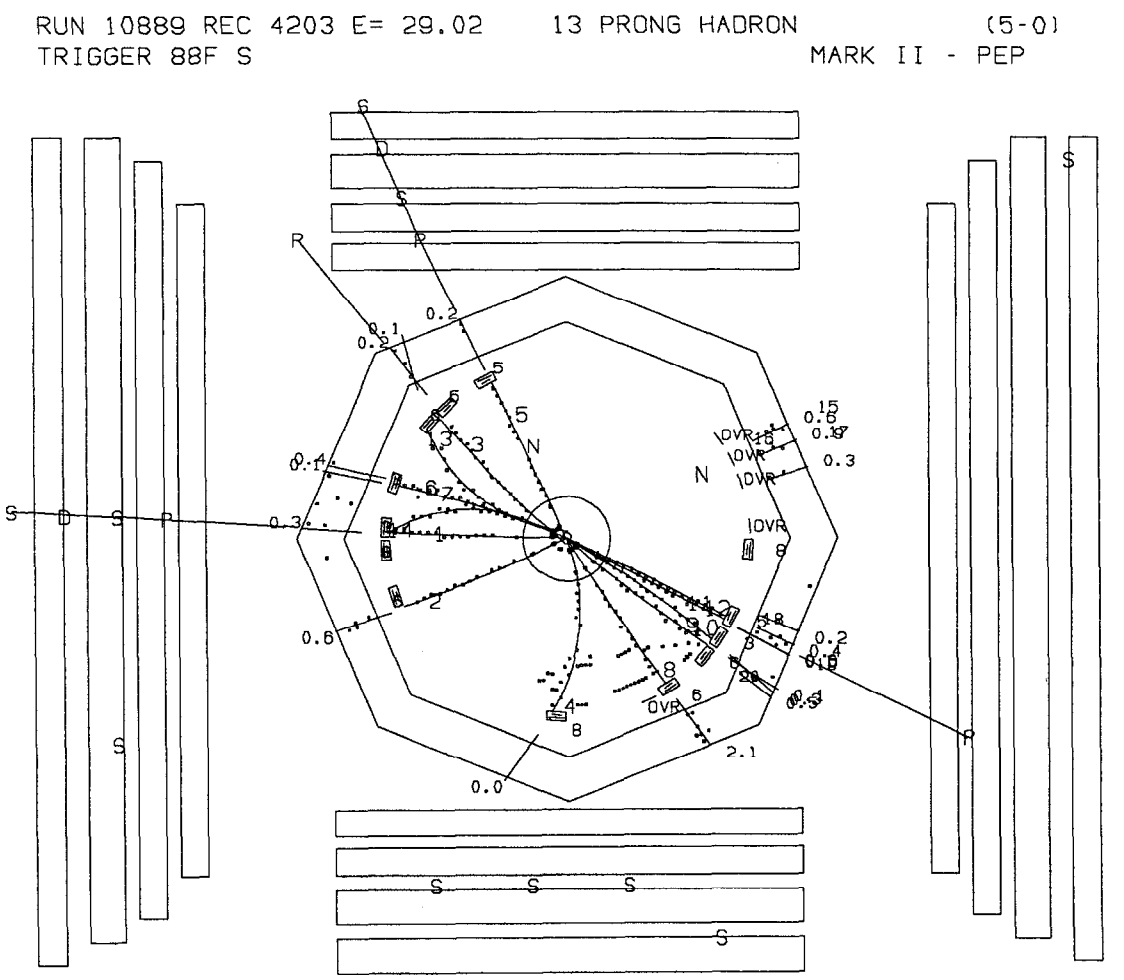

Figure C.1: An interesting event. In this event, track 8 is a high p_t electron, identified by the large amount of energy it deposits in the LA calorimeter. Tracks 1 and 5 are high p_t muons, identified by the hits in the outer muon system.

Table C.1: Track details in the longest lived event.

Track #	Identification	P (GeV/c)	p_t (GeV/c)	δ (mm)
1	μ^+	2.64	1.53	1.993
5	μ^-	2.48	1.56	2.716
8	e^-	2.25	1.11	-0.044

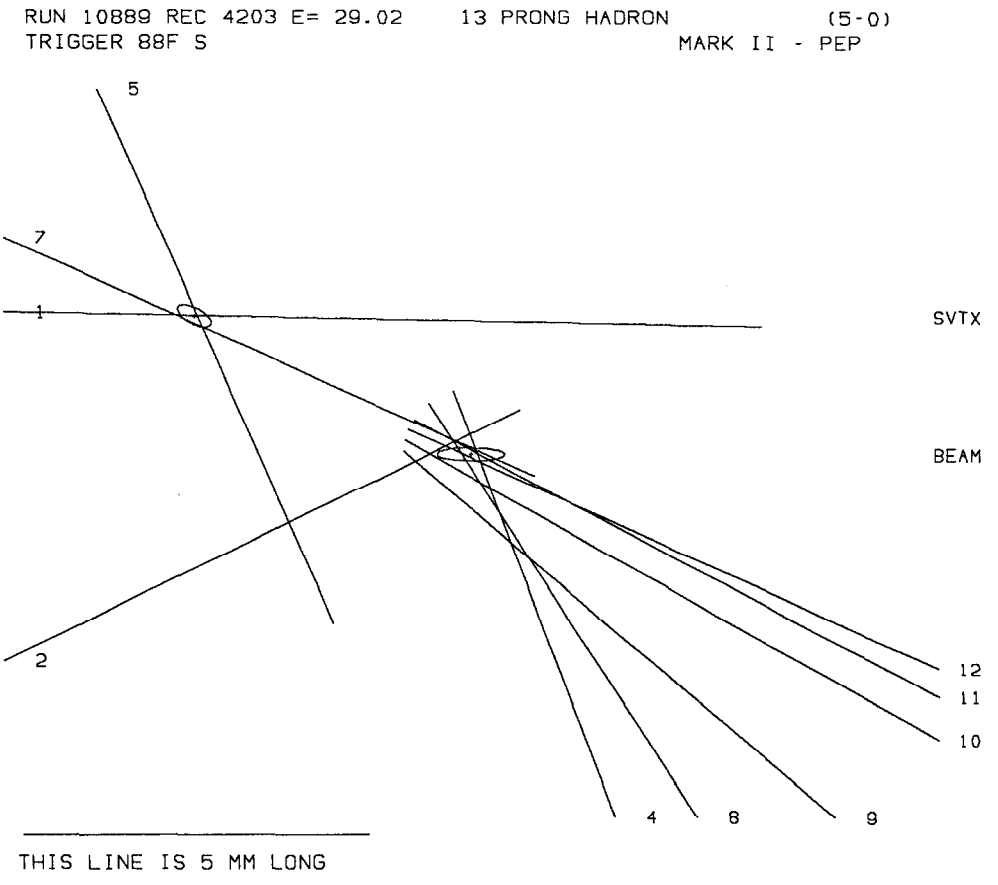

Figure C.2: **Enlarged view of the event. The beam ellipse is drawn in the center of this figure. A separate ellipse is drawn representing the one sigma errors associated with the vertex of tracks 1, 5, and 7.**

dimensions.† As illustrated in Figure C.2, there a 0.5 GeV/c track in the same hemisphere consistent with coming from the same vertex.

Since each of the lepton candidates are well isolated, they have a small probability to be background. Assuming that each candidate is a lepton, this event is interesting because of a number of uncommon occurrences:

1. There are three high p_t leptons in the event.
2. The invariant mass of the dimuon pair is high: 2.78 ± 0.08 GeV/c^2.
3. The decay length of the vertex associated with the dimuon pair (relative to the average beam position) is long: 4.3 mm.

† In this vertex fit there is only one degree of freedom (in the z direction), so the fit provides limited information.

There are 10 events in the lifetime sample that contain two leptons at high transverse momentum. The event of interest is the only one with three leptons at high p_t . After all cuts, the Monte Carlo predicts 9.3 and 0.4 events of these types, respectively. This prediction is therefore consistent with observation.

Because of the large dimuon invariant mass, it is tempting to classify the event as an example of $B \rightarrow \psi X \rightarrow \mu^+\mu^- X$. The branching ratio for $B \rightarrow \psi X$ has been measured at the $\Upsilon(4S)$ resonance to be approximately 1.1 % [116]. Using this branching ratio, the Monte Carlo predicts approximately 5 dilepton events from $B \rightarrow \psi$ decay in the data sample. The dimuon mass here is somewhat too low to be consistent with a ψ. A more likely explanation for this event is the cascade process $B \rightarrow \mu^+ X_c \rightarrow \mu^+\mu^- X$. After all cuts, the Monte Carlo predicts 1.8 events of this type in the invariant mass region between 2.5 and 3.0 GeV/c^2.

The decay length associated with the dimuon vertex is seven times the average B decay length.† In a sample of almost 600 events, however, the probability to observe such a decay length is 55 %. The long decay length observed in this event is therefore not incompatible with the measured lifetime.

From these studies, we conclude that although the event shown here illustrates a number of unusual occurrences in combination, it is is fully consistent with being a cascade $b\bar{b}$ event. Independent of the lifetime, the probability that it is a charm quark event is small (a few percent); the probability that it is a light quark event is vanishingly small. These low probabilities result from the need to explain three high momentum leptons, given the low per track background probabilities. The event is therefore judged to be suitable for inclusion in the lifetime determination.

† This comparison is done assuming the muon tracks originate from a common point. If the tracks come from the cascade process $B \rightarrow \mu^+ X_c \rightarrow \mu^+\mu^- X$, however, their vertex could lead to decay lengths somewhat longer than the B decay length.

REFERENCES

1. J. Friedman and H. Kendall, Ann. Rev. Nucl. Sci. **22**, 203 (1972).

2. J.J. Aubert *et al.*, Phys. Rev. Lett. **34**, 1404 (1974).
   J.E. Augustin *et al.*, Phys. Rev. Lett. **33**, 1406 (1974).

3. S.W. Herb *et al.*, Phys. Rev. Lett. **39**, 252 (1977).
   W.R. Innes *et al.*, Phys. Rev. Lett. **39**, 1240 (1977).

4. S.L. Glashow, Nucl. Phys. **22**, 579 (1961).
   S. Weinberg, Phys. Rev. Lett. **19**, 1264 (1967).
   A. Salam, *Elementary Particle Theory: Relativistic Groups and Analyticity* (8th Nobel Symposium), edited by N. Svartholm (Almqvist and Wiksell, Stockholm, 1968), p. 367.

5. G. Arnison *et al.*, Phys. Lett. **122B**, 103 (1983).
   M. Banner *et al.*, Phys. Lett. **122B**, 476 (1983).
   G. Arnison *et al.*, Phys. Lett. **126B**, 398 (1983).
   P. Bagnaia *et al.*, Phys. Lett. **129B**, 130 (1983).

6. See, for example, talks in *Proceedings of the 1979 International Symposium on Lepton and Photon Interactions at High Energies*, edited by T.B.W. Kirk and H.D.I. Abarbanel (Batavia Il, 1979), pp. 3, 19, 34, 52.

7. H. Harari, *Proceedings of the 12th SLAC Summer Institute on Particle Physics*, edited by P.M. McDonough (Stanford CA, 1984), p. 264.

8. P. Langacker, *Proceedings of the 1985 International Symposium on Lepton and Photon Interactions at High Energies*, edited by M. Konuma and K. Takahashi (Kyoto, 1986), p. 186.

9. Particle Data Group, Phys. Lett. **170B**, 1 (1986).

10. C. Peterson *et al.*, Phys. Rev. **D27** 105 (1983).

11. B. Andersson *et al.*, Phys. Rep. **97**, 33 (1983).
    T. Sjöstrand, Comp. Phys. Comm. **27**, 243 (1982); ibid. **28**, 229 (1983).
    T.D. Gottschalk, Nucl. Phys. **B214**, 201 (1983).
    B.R. Webber and G. Marchesini, Nucl. Phys. **B238**, 1 (1984);
    B.R. Webber, Nucl. Phys. **B238**, 492 (1984).

12. M. Suzuki, Phys. Lett. **71B**, 139 (1977).
    J. D. Bjorken, Phys. Rev. **D17**, 171 (1978).

13. S. Bethke, Z. Phys. **C29**, 175 (1985); S. Bethke, *International Symposium on Production and Decay of Heavy Hadrons* (Heidelberg, 1986), HD-PY 86/07 (1986).

14. W. Bartel *et al.*, Z. Phys. **C33**, 339 (1987).

15. M. Kobayashi and T. Maskawa, Prog. Theor. Phys. **49**, 652 (1973).

16. S.L. Glashow, J. Iliopoulos, and L. Maiani, Phys. Rev. **D2**, 1285 (1970).
N. Cabibbo, Phys. Rev. Lett. **10**, 531 (1963).

17. L. Maiani, Phys. Lett. **62B**, 183 (1976); L. Maiani, *Proceedings of the 1977 International Symposium on Lepton and Photon Interactions at High Energies*, edited by F. Gutbrod, (Hamburg, 1977), p. 867.
L. Wolfenstein, Phys. Rev. Lett. **51**, 1945 (1984).
L.L. Chau and W.Y. Keung, Phys. Rev. Lett. **53**, 1802 (1984).
H. Fritzsch, Phys. Rev. **D32**, 3058 (1985).
H. Harari and M. Leurer, Phys. Lett. **B181**, 123 (1986).

18. G. Altarelli, N. Cabibbo, and L. Maiani, Nucl. Phys. **B88**, 285 (1975).
J. Ellis, M.K. Gaillard, and D.V. Nanopoulos, Nucl. Phys. **B100**, 313 (1975).
J. Ellis, M.K. Gaillard, D.V. Nanopoulos, and S. Rudaz, Nucl. Phys. **B131**, 285 (1977).
N. Cabibbo and L. Maiani, Phys. Lett. **73B**, 418 (1978).

19. W. Bacino *et al.*, Phys. Rev. Lett. **43**, 1073 (1979).

20. B. Guberina, S. Nussinov, R.D. Peccei, and R. Rückl, Phys. Lett. **89B**, 111 (1979).
F.J. Gilman and M.B. Wise, Phys. Rev. **D20**, 20 (1979).
M. Bander, D. Silverman, and A. Soni, Phys. Rev. Lett. **44**, 7 (1980).

21. R. Rückl, Habilitionschrift, Univ. of Munich, CERN 83-1063 (1983).
M. Bauer and B. Stech, Phys. Lett. **152B**, 380 (1985).
A.J. Buras, J.M. Gérard, and R. Rückl, Nucl. Phys. **B268**, 16 (1986).

22. M. Suzuki, Nucl. Phys. **B145**, 420 (1978).
N. Cabibbo and L. Maiani, Phys. Lett. **79B**, 109 (1978).
N. Cabibbo, G. Corbò, and L. Maiani, Nucl. Phys. **B155**, 95 (1979).

23. R.E. Behrends, R.J. Finkelstein, and A. Sirlin, Phys. Rev. **101**, 866 (1956).
S.M. Berman, Phys. Rev. **112**, 627 (1958).
T. Kinoshita and A. Sirlin, Phys. Rev. **113**, 1652 (1959).

24. A. Ali and E. Pitarinen, Nucl. Phys. **B154**, 519 (1979).
G. Corbò, Phys. Lett. **116B**, 298 (1982).
G. Corbò, Nucl. Phys. **B212**, 99 (1983).

25. M.K. Gaillard and B.W. Lee, Phys. Rev. Lett. **33**, 108 (1974).
G. Altarelli and L. Maiani, Phys. Lett. **52B** 351 (1974).

26. F. Gilman, *Proceedings of the 14th SLAC Summer Institute on Particle Physics*, edited by E. Brennan (Stanford CA, 1986), p. 191.

27. J.L. Cortes, X.Y. Pham, and A. Tounsi, Phys. Rev. **D25**, 188 (1982).

28. G. Altarelli *et al.*, Nucl. Phys. **B208**, 365 (1982).

29. E.H. Thorndike, *Proceedings of the 1985 International Symposium on Lepton and Photon Interactions at High Energies*, edited by M. Konuma and K. Takahashi (Kyoto, 1986), p. 406.

30. M. Wirbel, B. Stech, and M. Bauer, Z. Phys. **C29**, 637 (1985).

31. B. Grinstein, M.B. Wise, and N. Isgur, Cal. Tech. preprint CALT-68-1311, 1985 (unpublished).
B. Grinstein, M.B. Wise, and N. Isgur, Phys. Rev. Lett. **56**, 298 (1986).

32. B. Stech, Heidelberg preprint HD-THEP-86-7, 1986 (unpublished).

33. T.Altomari and L. Wolfenstein, Phys. Rev. Lett. **58**, 1583 (1987).

34. See, for example:
P.H. Ginsparg, S.L. Glashow, and M.B. Wise, Phys. Rev. Lett. **50**, 1415 (1983).
L.L. Chau, W.Y. Keung, and M.D. Tran, Phys. Rev. **D27**, 2145 (1983).

35. H. Fritzsch, Phys. Lett. **70B**, 436 (1977).
M. Shin, Phys. Lett. **154B**, 205 (1985).
M. Gronau, V. Gupta, R. Johnson, and J. Schechter, Phys. Rev. **D33**, 3368 (1986).

36. F.J. Gilman and K. Kleinknecht, for the Particle Data Group, Phys. Lett. **170B**, 74 (1986).

37. W. Schmidt-Parzefall, *Proceedings of the 1987 International Conference on Lepton and Photon Interactions at High Energies*, (Hamburg, 1987).

38. W.J. Marciano, *Proceedings of the XXIII International Conference on High Energy Physics*, edited by S.C. Loken (Berkeley CA, 1986), p. 999.

39. M. B. Wise, *Proceedings of the 12th SLAC Summer Institute on Particle Physics*, edited by P.M. McDonough (Stanford CA, 1984), p. 574.

40. F.J. Gilman and M.B. Wise, Phys. Rev. **D27**, 1128 (1983).
F.J. Gilman, *Proceedings of the Aspen Winter Particle Physics Conference*, (Aspen Co, 1986).

41. D. Cundy *et al.*, CERN/SPSC/81-110, SPSC/P174 (Proposal for experiment NA31 at CERN), 1981.
G. Gollin *et al.*, FNAL P731 (Proposal for experiment E731 at FNAL), 1983.
L. Adiels *et al.*, CERN-EP/86-04 (CP violation study at LEAR), 1986.

42. I.I. Bigi, Phys. Lett. **155B**, 125 (1985).
L.L. Chau and W.Y. Keung, UC Davis preprint UCD-87-02, 1987 (unpublished).
H. Harari and J. Nir, SLAC-Pub-4341, 1987 (submitted to Phys. Lett).

43. H. Albrecht *et al.*, DESY Report 87-029, 1987 (unpublished).

44. C. Albajar *et al.*, Phys. Lett. **186B**, 247 (1987).

45. T. Inami and C.S. Lim, Prog. Theor. Phys. **65**, 297 (1981).
P.J. O'Donnell, Phys. Lett. **175B**, 369 (1986).
J.D. Bjorken, *International Symposium for the Fourth Family of Quarks and Leptons*, (Los Angeles CA, 1987), FNAL-Conf-87/83 (1987).

46. I.H. Chiang *et al.*, (Proposal for experiment 787 at the BNL AGS), Sept. 1983.

47. E. Fernandez *et al.*, Phys. Rev. Lett. **51**, 1022 (1983).

48. N. Lockyer *et al.*, Phys. Rev. Lett. **51**, 1316 (1983).

49. V. Barger *et al.*, Phys. Rev. **D16**, 746 (1978).
A. Ali, Z. Phys. **C1**, 25 (1979).
M.J. Puhala *et al.*, Phys. Rev. **D25**, 695 (1982).

50. *PEP Conceptual Design Report*, SLAC-189, LBL-4288, 1976.
Another e^+e^- facility at high energy is the PETRA storage ring located in Hamburg, West Germany. This machine has characteristics similar to those of PEP, operating at center of mass energies somewhat higher than PEP.

51. The Mark II collaboration at PEP consisted of about fifty physicists from SLAC, LBL and Harvard University.

52. R.H. Schindler *et al.*, Phys. Rev. **D24**, 78 (1981); R.H. Schindler, Ph.D. thesis, Stanford University, SLAC-Report-219, 1979.

53. See, for example, D.H. Perkins, *Introduction to High Energy Physics* (Addison-Wesley, Reading MA, 1982), Ch. 2.

54. J.A. Jaros, *Proceedings of the International Conference on Instrumentation for Colliding Beam Physics*, SLAC-Report-250, edited by W. Ash (Stanford CA, 1982), p. 29.

55. D.E. Amidei, Ph.D. thesis, University of California, Berkeley, LBL-17795, 1984.

56. E.L. Cisneros *et al.*, IEEE Trans. Nucl. Sci. **NS-24**, 413 (1977).

57. M. Breidenbach *et al.*, , IEEE Trans. Nucl. Sci **NS-25**, 706 (1978).

58. L.D. Gladney, Ph.D. thesis, Stanford University, SLAC-Report-279, 1985.

59. W. Davies-White *et al.*, Nucl. Instrum. and Methods **160**, 227 (1979).

60. G.S. Abrams *et al.*, IEEE Trans. Nucl. Sci. **NS25** 309 (1978); G.S. Abrams *et al.*, IEEE Trans. Nucl. Sci. **NS27** 59 (1980).

61. M. E. Levi, Ph.D. thesis, Harvard University, 1984.

62. K.G. Hayes, Ph.D. thesis, Stanford University, SLAC-Report-237, 1981.

63. T. Himel, Ph.D. thesis, Stanford University, SLAC-Report-223, 1979; H. Brafman *et al.*, IEEE Trans. Nucl. Sci **NS-25**, 692 (1978).

64. M. Atac, CDF Note No. 146, FN-376, 1982 (unpublished).

65. The most recent and complete references for studies on radiation damage can be found in the *Proceedings of the Workshop on Radiation Damage to Wire Chambers,* edited by J. Kadyk, LBL-21170 (Berkeley CA, 1986).

66. M.C. Ross, Mark II memorandum, Jan. 1983 (unpublished).

67. A.D. Johnson and G. Trilling, LBL Note TG-301, Sept. 1978 (unpublished).

68. T. Sjöstrand, Comp. Phys. Comm. **39**, 347 (1986); T. Sjöstrand and M. Bengtsson, Lund preprint LUTP 86-22, 1986 (unpublished).

69. B. Anderson *et al.*, Phys. Rev. **97**, 33 (1983.

70. A.Y. Petersen *et al.*, SLAC-Pub-4290, 1987, submitted to Phys. Rev. D.

71. R.L. Ford and W.R. Nelson, SLAC-Report-0210, 1978 (unpublished).

72. J.F. Patrick, Ph.D. thesis, University of California, Berkeley, LBL-14585, 1982.

73. P.C. Rowson, Ph.D. thesis, University of California, Berkeley, LBL-20463, 1985.

74. G. Hanson *et al.*, Phys. Rev. Lett. **35**, 1609 (1975).

75. C. Berger *et al.*, Phys. Lett. **35**, 176 (1978).
G. Wolf, *Proceedings of the XXI International Conference on High Energy Physics*, edited by P. Petiau and M. Proneuf (Paris, 1982), p. 525.

76. S.D. Drell, D.J. Levy and T.M. Yan, Phys. Rev. **187**, 2159 (1969) and Phys. Rev. **D1**, 1617 (1970).
N. Cabibbo, G. Parisi and M. Testa, Lett. Nuovo Cimento **4**, 35 (1970).
J.D. Bjorken and S.J. Brodsky, Phys. Rev. **D1**, 1416 (1970).

77. E. Fahri, Phys. Rev. Lett. **39**, 1587 (1977).
A. de Rújula, J. Ellis, E.G. Florates and M.K. Gaillard, Nucl. Phys. **B138**, 386 (1978).
S. Brandt and H.D. Dahmen, Z. Phys. **C1**, 61 (1979).
S.L. Wu and G. Zobernig, Z. Phys, **C2**, 107 (1979).

78. C. Bebek *et al.*, Phys. Rev. Lett. **49**, 610 (1982).
A. Chen *et al.*, Phys. Rev. Lett. **51**, 634 (1983).
P. Avery *et al.*, Phys. Rev. Lett. **51**, 1139 (1983).
H. Albrecht *et al.*, DESY Report 84-043, 1984 (unpublished).
M. Derrick *et al.*, Phys. Rev. Lett. **53**, 1971 (1984).
M. Derrick *et al.*, Phys. Lett. **146B**, 261 (1984).
H. Albrecht *et al.*, Phys. Lett. **150B**, 235 (1985).
T. Bowcock *et al.*, Phys. Rev. Lett. **55**, 923 (1985).

79. J. Adler *et al.*, SLAC-Pub-4291, 1987 (submitted to Physical Review Letters); this paper corrects errors made in a previous measurement: R.M. Baltrusaitis *et al.*, Phys. Rev. Lett. **56**. 2140 (1986).

80. M.G.D. Gilchriese, *Proceedings of the XXIII International Conference on High Energy Physics*, edited by S.C. Loken (Berkeley CA, 1986), p. 196.

81. J. Green *et al.*, Phys. Rev. Lett. **51**, 347 (1983).
S.E. Csorna *et al.*, Phys. Rev. lett. **54**, 1894 (1985).
D. Bortoletto *et al.*, Phys. Rev. **D35**, 19 (1987).

82. M.S. Alam *et al.*, Phys. Rev. Lett. **49**, 357 (1982).
R. Giles *et al.*, Phys. Rev. **D 30**, 2279 (1984).

83. R.M. Baltrusaitis *et al.*, Phys. Rev. Lett. **54**, 1976 (1985).

84. W. Bacino *et al.*, Phys. Rev. Lett. **43**, 1073 (1979).

85. K. Chadwick *et al.*, Phys. Rev. **D27**, 475 (1983).
A. Chen *et al.*, Phys. Rev. Lett. **52**, 1084 (1984).

86. C. Klopfenstein *et al.*, Phys. Lett. **103B**, 444 (1983).
G. Levman *et al.*, Phys. Lett. **141B**, 271 (1984).

87. George Trilling, LBL Note TG-360, 1982 (unpublished).

88. V. Highland, Nucl. Instum. Methods **129**, 497 (1975).

89. P.R. Burchat, Ph.D. thesis, Stanford University, SLAC-Report-292, 1986.

90. MAC: H.N. Nelson, Ph.D thesis, Stanford University, 1987.

91. DELCO: D. Klem, Ph.D. thesis, Stanford University, SLAC-Report-0300, 1986.

92. HRS: C.K. Jung, Ph.D. thesis, Indiana University, 1986.

93. L. Gladney *et al.*, Phys. Rev. **D34**, 2601 (1986).

94. M.E. Nelson, Ph.D. thesis, University of California, Berkeley, LBL-16724, 1983.

95. René Ong, Mark II/SLC Note #177, April 1987 (unpublished).

96. H.M. Schellman, Ph.D. thesis, University of California, Berkeley, LBL-18699, 1984.

97. B. Rossi, *High Energy Particles*, (Prentice-Hall, Englewood Cliffs NJ, 1961) p. 68.

98. R.M. Sternheimer, Phys. Rev. **177**, 485 (1980).

99. A. Weir (private communication).

100. H. Aihara *et al.*, Phys. Rev. Lett. **52**, 577 (1984); D. Saxon, *Proceedings of the International Europhysics Conference on High Energy Physics*, edited by L. Nitti and G. Preperata (Bari, 1985), p. 899.

101. F. James and M. Roos, Comp. Phys. Comm **10**, 343 (1985).

102. H.J. Behrend *et al.*, Z. Phys **C19**, 291 (1983).
B. Aveda *et al.*, Phys. Rev. Lett. **50**, 443 (1983).
E. Fernandez *et al.*, Phys. Rev. Lett. **50**, 2054 (1983).
M. Althoff *et al.*, Z. Phys. **C22**, 219 (1984).
M. Althoff *et al.*, Phys. Lett. **146B**, 443 (1984).
D.E. Koop *et al.*, Phys. Rev. Lett. **52**, 970 (1984).
H. Aihara *et al.*, Phys. Rev. **D31**, 2719 (1985).
H. Aihara *et al.*, Z. Phys. **C28**, 31 (1985).
T. Pal *et al.*, Phys. Rev. **D33**, 2708 (1986).

103. J. Jaros *et al.*, Phys. Rev. Lett., **51**, 955 (1983).
Dan Amidei, Ph.D. Thesis (Ref. 55).
M. Althoff *et al.*, Phys. Lett., **141B**, 264 (1984).
Larry Gladney, Ph.D. Thesis (Ref. 58).
M. Althoff *et al.*, DESY Report 86-027, 1986 (unpublished).
C. Jung *et al.*, Phys. Rev. Lett., **56**, 1775 (1986).
L. Gladney *et al* (Ref. 93).

104. René Ong, Mark II memorandum, Feb. 1987 (unpublished).

105. Christopher Wendt *et al.*, Phys. Rev. Lett. **58**, 1810 (1987).

106. S. Petrera and G. Romano, Nucl. Inst. Meth. **174**, 61 (1980).
R. Hollebeek, Mark II memorandum, Dec. 1982 (unpublished).

107. D. Strom, *Proceedings of the XXIII International Conference on High Energy Physics*, edited by S.C. Loken (Berkeley CA, 1986), p. 806.

108. W. Bartel *et al.*, Z. Phys. **C31**, 349 (1986).

109. D.E. Klem *et al.*, SLAC-PUB-4025, 1986 (submitted to Physics Review D).

110. D. Blockus *et al.*, Argonne preprint ANL-HEP-PR-86-144, 1986 (submitted to Physics Review Letters).

111. W.W. Ash *et al.*, Phys. Rev. Lett. **58**, 640 (1987).

112. The JADE group has recently reported a preliminary result of:
$\tau_b = 1.46 \pm 0.19 \pm 0.30$ ps, (R. Ramcke, private communication).

113. The TASSO group has recently reported a preliminary result of:
$\tau_b = 1.39 \pm 0.10 \pm 0.25$ ps, (S.L. Wu, private communication).

114. The world average lifetime values:
1983: The measurements given in Refs. 48 and 49. Average = 1.46 ± 40 ps.
1984: R. Klanner *Proceedings of the XXII International Conference on High Energy Physics*, edited by A. Meyer and E. Wieczorek (Leipzig, 1984), p. 1989. Average = 1.32 ± 0.27 ps.
1985: E.H. Thorndike, *Proceedings of the 1985 International Symposium on Lepton and Photon Interactions at High Energies*, edited by M. Konuma and K. Takahashi (Kyoto, 1985), p. 406. Average = 1.26 ± 0.17 ps.
1986: M.D. Gilchreise (Ref. 80). Average = 1.16 ± 0.16 ps.
1987: Average = 1.19 ± 0.14 ps.

115. F.A. Berends, P.H. Daverveldt and R. Kleiss, Nucl. Phys. **B253** 441 (1985); P.H. Daverveldt, Ph.D. Thesis, University of Leiden, 1985; F.A. Berends, P.H. Daverveldt and R. Kleiss, Comp. Phys. Comm. **40** 271 (1986).

116. H. Albrecht *et al.*, Phys. Lett. **162B**, 395 (1985).
M. Alam *et al.*, Phys. Rev. **D34**, 3279 (1986).